Parametric approximation of surface clusters driven by isotropic and anisotropic surface energies

JOHN W. BARRETT

Department of Mathematics, Imperial College London, London, SW7 2AZ, U.K.
E-mail: j.barrett@imperial.ac.uk

HARALD GARCKE

NWF I – Mathematik, Universität Regensburg, 93040 Regensburg, Germany
E-mail: harald.garcke@mathematik.uni-regensburg.de

ROBERT NÜRNBERG

Department of Mathematics, Imperial College London, London, SW7 2AZ, U.K.
E-mail: robert.nurnberg@imperial.ac.uk

We present a variational formulation for the evolution of surface clusters in $\mathbb{R}^3$ by mean curvature flow, surface diffusion and their anisotropic variants. We introduce the triple junction line conditions that are induced by the considered gradient flows, and present weak formulations of these flows. In addition, we consider the case where a subset of the boundaries of these clusters are constrained to lie on an external boundary. These formulations lead to unconditionally stable, fully discrete, parametric finite element approximations. The resulting schemes have very good properties with respect to the distribution of mesh points and, if applicable, volume conservation. This is demonstrated by several numerical experiments, including isotropic double, triple and quadruple bubbles, as well as clusters evolving under anisotropic mean curvature flow and anisotropic surface diffusion, including computations for regularized crystalline surface energy densities.

1. Introduction

Equilibrium bubble clusters are stationary solutions of the variational problem in which one seeks a least area way to enclose and separate a number of regions with prescribed volumes. The relevant energy in this case is given as the sum of the total surface area. In this paper we study gradient flows of this energy leading to mean curvature flow and surface diffusion depending on whether we consider the gradient flow with respect to the L^2- or the H^{-1}-inner product. In the case of surface diffusion the enclosed volumes are preserved, and hence stationary solutions are equilibrium bubble clusters; whereas in the case of mean curvature flow the enclosed volumes are not preserved, and bounded initial data will in general vanish in finite time. Hence steady state solutions for surface diffusion are natural candidates for surface area minimizing bubble constellations for fixed given volumes. In geometric measure theory such minimizers are frequently called soap bubble clusters. Intriguingly, although the search for such area minimizing constellations historically has received a lot of attention among mathematicians, only very few things are actually known. For instance,

while it is conjectured that the so-called standard k-bubble is the unique global minimizer among all bubbles enclosing and separating k different volumes for $k \leqslant 4$, the proof for this is only known in the cases $k = 1$ and $k = 2$; see [48] for the proof of the double bubble conjecture. Here we recall that the standard 4-bubble in $\mathbb{R}^3$ is homeomorphic to the barycentric subdivision of a tetrahedron into four smaller tetrahedra, and that the standard $k-1$-bubble is homeomorphic to the result of removing an outer surface from the standard k-bubble, for $k = 2 \rightarrow 4$; see e.g. [3]. Numerical approximations of the standard k-bubble for $k = 2 \rightarrow 4$ can be seen in Figures 5, 14 and 19, below. We remark that all of these conjectured minimizers are spherical clusters, i.e. each surface making up the cluster is either flat or part of a sphere. But in general, the surfaces need only have constant mean curvature, and it was conjectured in [66] that for $k = 6$ a soap bubble cluster enclosing k volumes exists which contains non-spherical surfaces, and in addition that $k = 6$ is the smallest such number. Here we recall that it was proven by Taylor (see [68]) that in a soap bubble cluster each surface has constant mean curvature, that only three surfaces can meet at so-called triple junction lines (at equal angles of 120°), and that only four triple junction lines can meet at so-called quadruple junction points (at equal angles of $\arccos(-1/3) \approx 109°$). Of course, these angles are also well-known in the theory of minimal surfaces; see e.g. [46]. When the total surface area is replaced with a weighted sum of surface areas, local minimizers are called immiscible fluid clusters. Here even less is known, and there is often even a lack of conjectures. We refer to the recent review article [53] for more details on historical developments and open questions in this area.

We now return to the discussion of the gradient flows considered in this paper, i.e. surface diffusion and mean curvature flow. For these geometric flows we impose force balance conditions at points where different surfaces meet, or where a surface meets a fixed external boundary; see [44, 72, 34, 15] and the references therein. For example, in the case of mean curvature flow with equal constant surface energy densities this results in a 120° angle condition at triple junction lines, while a 90° contact angle holds where a surface meets an external boundary. Mean curvature flow is a parabolic equation of second order, whereas surface diffusion leads to a parabolic equation of fourth order. As surface diffusion is of higher order, one would expect that additional boundary conditions have to hold at triple junction and boundary contact lines. Physically motivated boundary conditions have been derived in [36], via formal asymptotics, as a singular limit of a degenerate Cahn–Hilliard system. There it turns out that, besides the angle condition, a flux condition and, in the case of triple junction lines, a condition related to the continuity of the chemical potentials have to be prescribed. Geometrically these triple junction line conditions imply that the derivatives of the mean curvature in the direction of the conormal of the surfaces are equal and that a weighted sum of the mean curvatures of the surfaces has to vanish, respectively, and in this paper we will enforce these triple junction line conditions for the fourth order flow surface diffusion. The last condition is also related to the well-known fact that for an equilibrium bubble cluster the mean curvature of the surface is given as a pressure difference.

In the plane, existence of solutions for mean curvature flow and surface diffusion with triple junction points has been shown in [20] and [36], respectively. For the higher dimensional case it is known that very weak solutions exist for the mean curvature flow. In fact, the theory of Brakke, who in his seminal paper [17] first proved an existence result for the mean curvature flow of so-called varifolds of arbitrary dimension and codimension, also allows one to consider triple junctions. A well-posedness result for classical solutions of the mean curvature flow of surface clusters in $\mathbb{R}^3$ has been shown recently in [25]. To the best of our knowledge, corresponding results for the surface diffusion flow of surface clusters with triple junction lines remain open.

Here we will also study situations in which the energy is proportional to surface area, but now the constant of proportionality might be different on each of the surfaces making up the bubble. This frequently appears in the case of clusters of immiscible fluids, where the energy depends upon which fluids are separated by the surface. Another important situation in applications is the case when the surface energy depends not only on its area but also on its tangent plane (which for hypersurfaces is equivalent to a dependence on the normal). Such energies are called anisotropic, and for highly anisotropic situations equilibrium shapes can be polytopes. In such a case one speaks of crystalline energies. For a good introduction to variational problems involving clusters we refer to the book [54], where also the most relevant references can be found. In addition, we refer to [2, 68, 29, 51, 52, 41, 1, 66, 69] for additional information on variational problems involving surface energies for clusters. Curvature driven surface evolution with triple junction lines and/or boundary contact plays a fundamental role in many applications. For example, grain boundaries are driven by mean curvature flow and surface diffusion is an important transport mechanism in the context of thermal grooving, sintering, epitaxial growth and electromigration; see e.g. [64, 44, 56, 67] and the references therein.

In this paper we study the evolution of surface clusters by mean curvature flow or surface diffusion, and their anisotropic variants, in $\mathbb{R}^3$. In particular, we are interested in the numerical approximation of these geometric evolution laws for surface clusters. This paper generalizes the parametric finite element approximation for the evolution of curve networks in the plane, that was introduced and analysed by the present authors in [7, 6, 9], to the natural analogue in three space dimensions. Of course, in this higher dimensional setting the topology is richer, and, in addition to triple junction lines, quadruple junction points have to be considered. In particular, we will present parametric finite element approximations for second and fourth order geometric evolution equations that are unconditionally stable and that exhibit very good mesh properties due to an intrinsic discrete tangential motion. The latter makes a heuristical remeshing during the evolution unnecessary. A detailed description of this discrete tangential motion and the implied properties for the two-dimensional meshes can be found in [10, §4]. Finally, we will also extend these approximations from isotropic to anisotropic surface energy densities, by utilizing ideas that were introduced by the present authors in [12].

Existing approaches for the numerical approximation of surface clusters include the well-known Surface Evolver by Brakke, [18], where a direct parameterization and a gradient descent method for a given energy are used in order to find certain surface area minimizers. We note that the Surface Evolver has recently been used to numerically study large soap bubble clusters; see e.g. [23] and [50]. A level set approach for the simulation of the evolution of soap bubbles has been considered in [77]. An alternative numerical method for the mean curvature flow of surface clusters has been employed in [62]. On the other hand, phase field methods provide a natural way to approximate curvature flows with triple junction lines and we refer to e.g. [32, 33, 58]. Numerical results for a finite element approximation of a phase field model for multi-component surface diffusion, i.e. surface diffusion with triple junction lines, are given in [59]; while an alternative finite element approximation of the same phase field model will be given in the forthcoming article [14]. Note that most of the existing numerical results are for isotropic surface energies only.

The main contribution of this paper is the inclusion of triple junction lines and boundary lines in the geometric evolution equations considered. We recall that isotropic and anisotropic evolution laws for closed surfaces without boundary have been approximated in previous work

by the authors; see [10, 11, 12]. Here we remark that the variational formulation employed there had been previously introduced for curves in the plane by the authors in [7] (see also [6, 9]) in order to derive numerical approximations for the evolution of closed curves and, crucially, curve networks with triple junction points. Extending these formulations from curve networks in $\mathbb{R}^2$ to surface clusters in $\mathbb{R}^3$ is the subject of this paper. A major characteristic of this variational approach is that all the triple junction conditions are handled naturally in a weak formulation. In particular, for second order flows only one condition and for fourth order flows only two conditions need to be enforced strongly via the trial spaces, while the remaining conditions are enforced weakly through the corresponding test spaces. Of course, conforming finite element approximations inherit this property and setting up the necessary discrete trial and test spaces is straightforward for curves and only slightly more involved for surfaces.

The remainder of the paper is organized as follows. In Section 2 we state the evolution equations for a cluster of surfaces that are of interest in this paper, i.e. mean curvature flow and surface diffusion, together with appropriate weak formulations. The variational structure of the stated geometric evolution equations is discussed in Section 3, and in particular we demonstrate that mean curvature flow and surface diffusion can be interpreted as L^2- and H^{-1}-gradient flows of (weighted) surface area, respectively. Stable, fully discrete finite element approximations, which are based on the weak formulations introduced in Section 2, are introduced in Section 4. Efficient solution methods for the arising systems of algebraic equations are given in Section 5, and numerous numerical simulations are presented in Section 6.

2. Geometric evolution equations for surface clusters

Let us now specify the geometric evolution equations for a cluster of surfaces in more detail. We assume that the surface cluster is connected and consists of $I_S \in \mathbb{N}$, $I_S \geqslant 1$, hypersurfaces with boundaries in $\mathbb{R}^3$, and $I_T \in \mathbb{N}$, $I_T \geqslant 0$, different triple junction lines. In order to parameterize the surfaces we choose a collection of domains $\Omega_i \subset \mathbb{R}^2$, $i = 1 \to I_S$, with piecewise smooth boundaries $\partial \Omega_i$. The surface cluster is then given with the help of parameterizations $\vec{x}_i : \overline{\Omega}_i \times [0, T] \to \mathbb{R}^3$ with $\vec{x}_i(\Omega_i, t) = \Gamma_i(t)$, where the Γ_i, $i = 1 \to I_S$, are the surfaces constituting the evolving cluster. Here and throughout we will often use the shorthand notation $\vec{x}(\Omega, t) = \Gamma(t)$, where $\Omega := (\Omega_1, \ldots, \Omega_{I_S})$ and $\Gamma(t) := (\Gamma_1(t), \ldots, \Gamma_{I_S}(t))$. Note that for the standard double bubble we have $I_S = 3$ with $I_T = 1$, and for the standard triple bubble we have $I_S = 6$ and $I_T = 4$; see e.g. Figures 5 and 14. In the former case two volumes are enclosed by the surface cluster, in the latter three. In these cases, one can choose, for example, all the domains Ω_i, $i = 1 \to I_S$, either as the unit disk in $\mathbb{R}^2$; $\Omega_i = \mathbb{B}^2 := \{\vec{z} \in \mathbb{R}^2 : |\vec{z}| < 1\}$ with boundary $\partial \Omega_i = \mathbb{S}^1 := \partial \mathbb{B}^2$, i.e. the unit circle in $\mathbb{R}^2$, or as the upper half of the unit disk; $\Omega_i = \{\vec{z} \in \mathbb{B}^2 : z_1 > 0\}$ with piecewise smooth boundary $\partial \Omega_i$.

Typically three surfaces meet at line junctions, and in this paper we will restrict ourselves to this case; i.e. we will not allow for four surfaces meeting at a line. In the case that all surfaces have the same isotropic energy such a case would be unstable. But we point out that quadruple junction lines can also be stable, if the energies are not the same; see e.g. [22] and [35]. We note that generalizing the presented formulations and numerical approximations to situations where more than three surfaces meet at a junction line is straightforward.

Fundamental for the following considerations will be the identities

$$\Delta_s \vec{x}_i = \vec{\varkappa}_i \equiv \varkappa_i \vec{\nu}_i, \quad i = 1 \to I_S, \tag{2.1}$$

which for a single surface, with or without boundary, was first used in [26] to design a finite element method for geometric partial differential equations and mean curvature flow; see also [27]. The identity (2.1) is well-known from surface geometry (see e.g. [24]), where ∇_s is the surface (tangential) gradient, $\Delta_s \equiv \nabla_s . \nabla_s$ is the surface Laplacian (Laplace–Beltrami operator), $\vec{x}_i$ is a parameterization of Γ_i, $\vec{\varkappa}_i$ is the mean curvature vector, $\varkappa_i$ is the sum of the principal curvatures and $\vec{\nu}_i$ is a unit normal to Γ_i. Here we use the sign convention that $\varkappa_i$ is positive, if the surface Γ_i is curved in the direction of the normal $\vec{\nu}_i$. In this paper, we will investigate the motion of the surface cluster by mean curvature flow

$$\mathcal{V}_i = \varkappa_i, \quad i = 1 \to I_S, \tag{2.2}$$

where $\mathcal{V}_i := [\vec{x}_i]_t . \vec{\nu}_i$ is the normal velocity of the surface Γ_i; and the motion by surface diffusion

$$\mathcal{V}_i = -\Delta_s \varkappa_i, \quad i = 1 \to I_S. \tag{2.3}$$

In addition to the above differential equations, certain boundary conditions have to be prescribed at the boundaries of the surfaces Γ_i, $i = 1 \to I_S$, and this will be outlined below. We remark that it is also possible to consider a setup, where motion by mean curvature is only prescribed for a subset of the surfaces making up the cluster, while the remaining surfaces move by motion by surface diffusion. This is of relevance e.g. in thermal grooving ([57]), in interface motion in polycrystalline two-phase materials ([21]), in sintering processes ([60]), and in the evolution of boundaries in the electromigration of intergranular voids (see [8]). A parametric finite element approximation of such flows for curve networks in the plane has been considered in [6], while its extension to surface clusters is the subject of the forthcoming article [13]. However, in this paper we will only consider the purely second and fourth order flows (2.2) and (2.3), respectively, as well as their anisotropic counterparts.

In order to describe the necessary conditions that need to hold at triple junction lines, where three surfaces meet, and at quadruple junction points, where four triple junction lines meet, we introduce the following notation. Assume that $\partial \Omega_i$, the boundary of Ω_i, is partitioned into connected pieces $\partial_j \Omega_i$, $j = 1 \to I_P^i$, $I_P^i \geqslant 1$. Then the triple junction lines $\mathcal{T}_k$, $k = 1 \to I_T$, are parameterized with the help of the partitioned boundaries $\partial_j \Omega_i$, $j = 1 \to I_P^i$, $i = 1 \to I_S$. We assume that for each $\mathcal{T}_k$, there exist pairs (s_1^k, p_1^k), (s_2^k, p_2^k) and (s_3^k, p_3^k) with $s_1^k < s_2^k < s_3^k$ such that

$$\mathcal{T}_k(t) := \vec{x}_{s_1^k}(\partial_{p_1^k} \Omega_{s_1^k}, t) = \vec{x}_{s_2^k}(\partial_{p_2^k} \Omega_{s_2^k}, t) = \vec{x}_{s_3^k}(\partial_{p_3^k} \Omega_{s_3^k}, t), \quad k = 1 \to I_T. \tag{2.4a}$$

Note that for a standard double bubble, as in e.g. Figure 5, we simply have $I_T = I_P^i = 1$, $i = 1 \to 3$, and $\mathcal{T}_1$ is defined via $((s_j^1, p_j^1))_{j=1}^3 = ((1, 1), (2, 1), (3, 1))$. For a standard triple bubble, as in e.g. Figure 14, on the other hand, we have $I_T = 4$ and $I_P^i = 2$, $i = 1 \to 6$, meaning that there are four triple junction lines and that the boundary of each surface Γ_i, $i = 1 \to 6$, partitions into two parts, each meeting a different triple junction line. As the flows (2.2) and (2.3) are of second and fourth order, respectively, additional boundary conditions have to be prescribed on the triple junction lines. Throughout this paper we will prescribe equilibrium or force balance conditions at triple junction lines, that have previously been derived in the literature. Physically meaningful conditions for mean curvature flow and surface diffusion of curve networks in the plane can be found in [20] and [36], respectively. Extending these conditions to the present case of surface clusters in $\mathbb{R}^3$ is straightforward, and we obtain the following conditions. In the case of mean curvature flow with isotropic and equal surface energies we require, in addition to the attachment conditions (2.4a), that
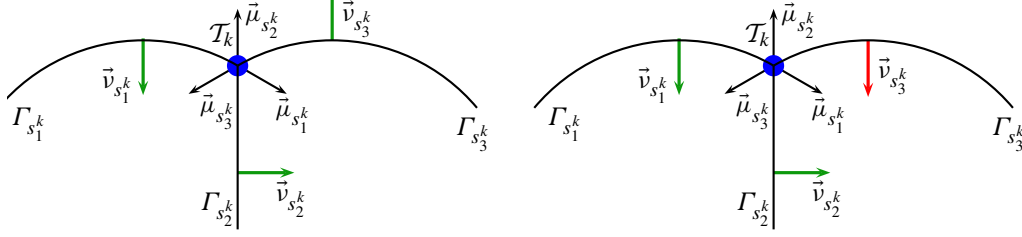
FIG. 1. Sketch of the local orientation of $(\Gamma_{s_1^k}, \Gamma_{s_2^k}, \Gamma_{s_3^k})$ at the triple junction line $\mathcal{T}_k$ (blue in the pdf file). Depicted above is a plane T_k that is perpendicular to $\mathcal{T}_k$. In the example on the left, $o^k := (o_1^k, o_2^k, o_3^k)$ can be chosen as $o^k = (1, 1, 1)$. However, in the example on the right we require $o^k = \pm(1, 1, -1)$.

Young's law

$$\sum_{j=1}^{3} \vec{\mu}_{s_j^k} = \vec{0} \quad \text{on } \mathcal{T}_k, \quad k = 1 \to I_T, \tag{2.4b}$$

is fulfilled, where $\vec{\mu}_i$ denotes the conormal, i.e. the intrinsic outer unit normal to $\partial \Gamma_i$, the boundary of Γ_i, that lies within the tangent plane of Γ_i. The identities (2.4b) are force balance conditions on the triple junction lines $\mathcal{T}_k \subset \mathbb{R}^3$, $k = 1 \to I_T$. In the case of equal isotropic energies, as considered here, the conditions (2.4b) lead to the well known 120° angle condition at triple junction lines. As mentioned above, we need additional boundary conditions for surface diffusion. To formulate these conditions we need to choose an appropriate orientation of the normals along the triple junction lines. Let $\vec{\nu}_i$ be a global normal field on Γ_i. Then we choose at a triple junction point on $\mathcal{T}_k$, $k = 1 \to I_T$, an orientation $o^k := (o_1^k, o_2^k, o_3^k)$, where $o_j^k \in \{-1, 1\}$, such that $(o_j^k \vec{\nu}_{s_j^k}, \vec{\mu}_{s_j^k})$, $j = 1 \to 3$, all have the same orientation in the plane orthogonal to $\mathcal{T}_k$ at that point; see Figure 1. Then the additional boundary conditions are

$$o_1^k \vec{\mu}_{s_1^k} . \nabla_s \varkappa_{s_1^k} = o_2^k \vec{\mu}_{s_2^k} . \nabla_s \varkappa_{s_2^k} = o_3^k \vec{\mu}_{s_3^k} . \nabla_s \varkappa_{s_3^k} \quad \text{on } \mathcal{T}_k, \quad k = 1 \to I_T, \tag{2.4c}$$

$$\sum_{j=1}^{3} o_j^k \varkappa_{s_j^k} = 0 \quad \text{on } \mathcal{T}_k, \quad k = 1 \to I_T; \tag{2.4d}$$

here (2.4c) are flux balance conditions and (2.4d) are chemical potential continuity conditions that need to hold on triple junction lines. The conditions (2.4c,d) are the natural three-dimensional analogues of the junction conditions derived in [36].

We remark that at quadruple junction points no extra conditions need to be prescribed, since the behaviour at quadruple junction points is completely determined by the triple junction line conditions; see [68] or [19] for details. In particular, as a consequence of the 120° angle conditions on the triple junction lines, at a quadruple junction the four triple junction curves meet at equal $\arccos(-1/3)$ angles, where $\arccos(-1/3) \approx 109°$.

In conclusion, motion by mean curvature is given by (2.2) together with (2.4a,b), and surface diffusion is given by (2.3) with (2.4a–d). In Section 3 we show that both of these geometric evolution equations decrease the total surface area

$$E(\Gamma) = |\Gamma| := \sum_{i=1}^{I_S} \int_{\Gamma_i} 1 \, d\mathcal{H}^2, \tag{2.5}$$

where $\mathcal{H}^d$ is the d-dimensional Hausdorff measure in $\mathbb{R}^3$. In addition, the surface diffusion flow is volume preserving, i.e. the volume of each enclosed bubble is preserved; see Remark 3.1 below.

We now introduce weak formulations of these evolution equations. These weak formulations will form the basis of our finite element approximations, which we introduce in Section 4. Let $\widehat{W}(\Gamma) := \times_{i=1}^{I_S} H^1(\Gamma_i, \mathbb{R}) = \{(\chi_1, \ldots, \chi_{I_S}) : \chi_i \in H^1(\Gamma_i, \mathbb{R}), \ i = 1 \to I_S\}$ and

$$\underline{V}(\Gamma) := \left\{(\vec{\chi}_1, \ldots, \vec{\chi}_{I_S}) \in \underset{i=1}{\overset{I_S}{\times}} H^1(\Gamma_i, \mathbb{R}^3) : \vec{\chi}_{s_1^k} = \vec{\chi}_{s_2^k} = \vec{\chi}_{s_3^k} \ \text{on} \ \mathcal{T}_k, \ k = 1 \to I_T \right\}, \quad (2.6a)$$

$$W(\Gamma) := \left\{(\chi_1, \ldots, \chi_{I_S}) \in \widehat{W}(\Gamma) : \sum_{j=1}^{3} o_j^k \chi_{s_j^k} = 0 \ \text{on} \ \mathcal{T}_k, \ k = 1 \to I_T \right\}. \quad (2.6b)$$

Here and throughout, $\Gamma = (\Gamma_1, \ldots, \Gamma_{I_S})$ with $\Gamma_i = \Gamma_i(t) = \vec{x}_i(\Omega_i, t), \ i = 1 \to I_S$; moreover $\vec{x}(\cdot, t) \in \underline{V}(\Omega)$, where

$$\underline{V}(\Omega) := \left\{(\vec{\chi}_1, \ldots, \vec{\chi}_{I_S}) \in \underset{i=1}{\overset{I_S}{\times}} H^1(\Omega_i, \mathbb{R}^3) : \vec{\chi}_{s_1^k}(\partial_{p_1^k}\Omega_{s_1^k}) = \vec{\chi}_{s_2^k}(\partial_{p_2^k}\Omega_{s_2^k}) = \vec{\chi}_{s_3^k}(\partial_{p_3^k}\Omega_{s_3^k}), \right.$$

$$\left. k = 1 \to I_T \right\}.$$

From now on, we will use the shorthand notation $\eta \in W(\Gamma)$ to mean $\eta = (\eta_1, \ldots, \eta_{I_S}) \in W(\Gamma)$, and similarly for other functions and quantities defined on all surfaces $\Gamma_i, \ i = 1 \to I_S$. In addition, for scalar, vector and tensor valued functions $\eta, \chi \in \times_{i=1}^{I_S} L^2(\Gamma_i, Y)$, with $Y = \mathbb{R}, \mathbb{R}^3$ or $\mathbb{R}^{3\times3}$, we define the L^2 inner product $\langle \cdot, \cdot \rangle$ over Γ as follows

$$\langle \eta, \chi \rangle := \sum_{i=1}^{I_S} \int_{\Gamma_i} \eta_i \cdot \chi_i \, d\mathcal{H}^2. \quad (2.7)$$

Following [6, 10], we reformulate (2.2) and (2.3) as

$$[\vec{x}_i]_t \cdot \vec{v}_i = \varkappa_i, \qquad \varkappa_i \vec{v}_i = \Delta_s \vec{x}_i, \quad i = 1 \to I_S, \quad (2.8)$$

$$[\vec{x}_i]_t \cdot \vec{v}_i = -\Delta_s \varkappa_i, \quad \varkappa_i \vec{v}_i = \Delta_s \vec{x}_i, \quad i = 1 \to I_S, \quad (2.9)$$

respectively. Then multiplying the first equation in (2.8) with a test function $\eta \in \widehat{W}(\Gamma)$ and the second equation with a test function $\vec{\chi} \in \underline{V}(\Gamma)$, integrating over Γ and using Green's formula for surfaces, we obtain the following weak formulation for mean curvature flow: Find $\vec{x} \in \underline{V}(\Omega)$ and $\varkappa \in \widehat{W}(\Gamma)$ such that

$$\langle \vec{x}_t, \chi \vec{v} \rangle - \langle \varkappa, \chi \rangle = 0 \quad \forall \chi \in \widehat{W}(\Gamma), \quad (2.10a)$$

$$\langle \varkappa \vec{v}, \vec{\eta} \rangle + \langle \nabla_s \vec{x}, \nabla_s \vec{\eta} \rangle = 0 \quad \forall \vec{\eta} \in \underline{V}(\Gamma). \quad (2.10b)$$

Similarly, for the surface diffusion flow we obtain: Find $\vec{x} \in \underline{V}(\Omega)$ and $\varkappa \in W(\Gamma)$ such that

$$\langle \vec{x}_t, \chi \vec{v} \rangle - \langle \nabla_s \varkappa, \nabla_s \chi \rangle = 0 \quad \forall \chi \in W(\Gamma), \quad (2.11a)$$

$$\langle \varkappa \vec{v}, \vec{\eta} \rangle + \langle \nabla_s \vec{x}, \nabla_s \vec{\eta} \rangle = 0 \quad \forall \vec{\eta} \in \underline{V}(\Gamma). \quad (2.11b)$$

We observe that in the above the conditions (2.4b), and where applicable (2.4c), are formulated weakly, while the remaining conditions are enforced strongly through the trial spaces; recall (2.6a,b).

In the remainder of this section, we outline the generalizations of (2.10a,b) and (2.11a,b) to the case of fully anisotropic surface energies. In this case the isotropic free energy (2.5) is replaced by the anisotropic energy

$$E_\gamma(\Gamma) = |\Gamma|_\gamma := \sum_{i=1}^{I_S} |\Gamma_i|_{\gamma_i} := \sum_{i=1}^{I_S} \int_{\Gamma_i} \gamma_i(\vec{v}_i) \, d\mathcal{H}^2, \qquad (2.12)$$

where $\gamma := (\gamma_1, \ldots, \gamma_{I_S})$ with γ_i, $i = 1 \to I_S$, being positive and absolutely homogeneous functions of degree one; i.e. in particular $\gamma_i : \mathbb{R}^3 \to \mathbb{R}_{\geqslant 0}$ with $\gamma_i(\vec{p}) > 0$ if $\vec{p} \neq \vec{0}$ and

$$\gamma_i(\lambda \vec{p}) = |\lambda| \gamma_i(\vec{p}) \, \forall \vec{p} \in \mathbb{R}^3, \, \forall \lambda \in \mathbb{R} \implies \gamma_i'(\vec{p}) \cdot \vec{p} = \gamma_i(\vec{p}) \, \forall \vec{p} \in \mathbb{R}^3 \setminus \{\vec{0}\}, \qquad (2.13)$$

where γ_i' is the gradient of γ_i. In the isotropic case we have

$$\gamma_i(\vec{p}) = \varsigma_i |\vec{p}| \quad \text{with } \varsigma_i > 0, \quad i = 1 \to I_S, \qquad (2.14)$$

which implies that $\gamma_i(\vec{v}_i) = \varsigma_i$; and so $|\Gamma_i|_{\gamma_i}$ in (2.12) reduces to $\varsigma_i |\Gamma_i|$, the scaled surface area of Γ_i. In the isotropic equal energy density case we have, in addition, $\varsigma_i = 1$, $i = 1 \to I_S$; and so $E_\gamma(\Gamma)$ reduces to $E(\Gamma)$, the surface area of Γ.

Following our recent work in [9, 12], we will restrict ourselves to anisotropic surface energy densities of the form

$$\gamma_i(\vec{p}) = \Big(\sum_{\ell=1}^{L_i} [\gamma_i^{(\ell)}(\vec{p})]^{r_i}\Big)^{1/r_i}, \quad \text{where} \quad \gamma_i^{(\ell)}(\vec{p}) := \sqrt{\vec{p} \cdot G_i^{(\ell)} \vec{p}}, \qquad (2.15)$$

so that

$$\gamma_i'(\vec{p}) = [\gamma_i(\vec{p})]^{1-r_i} \sum_{\ell=1}^{L_i} [\gamma_i^{(\ell)}(\vec{p})]^{r_i-1} [\gamma_i^{(\ell)}]'(\vec{p}),$$

where $r_i \in [1, \infty)$ and $G_i^{(\ell)} \in \mathbb{R}^{3\times3}$, $\ell = 1 \to L_i$, are symmetric and positive definite; $i = 1 \to I_S$. This class of convex anisotropies (2.15) will lead to unconditionally stable numerical approximations; see Section 4 below.
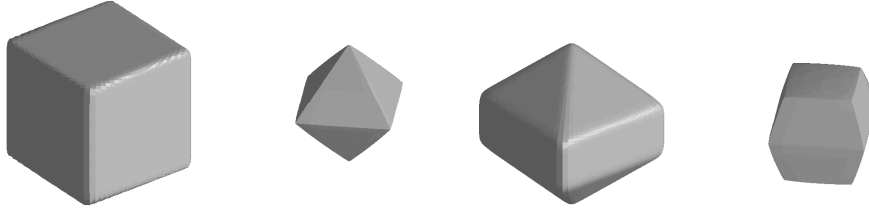
In order to visualize some anisotropies of the form (2.15), we briefly recall the definition of the Wulff shape. For a given anisotropy function γ_i one defines its Frank diagram

$$\mathcal{F}_i := \{\vec{p} \in \mathbb{R}^3 : \gamma_i(\vec{p}) \leqslant 1\}$$

and the corresponding Wulff shape, [76],

$$\mathcal{W}_i := \{\vec{q} \in \mathbb{R}^3 : \gamma_i^*(\vec{q}) \leqslant 1\}, \quad \text{where} \quad \gamma_i^*(\vec{q}) := \sup_{\vec{p} \in \mathbb{R}^3 \setminus \{\vec{0}\}} \frac{\vec{p} \cdot \vec{q}}{\gamma_i(\vec{p})}. \qquad (2.16)$$

As the Wulff shape $\mathcal{W}_i$ is known to be the solution of an isoperimetric problem, i.e. the boundary of $\mathcal{W}_i$ is the minimizer of $| \cdot |_{\gamma_i}$ in the class of all (closed) surfaces enclosing the same volume (see
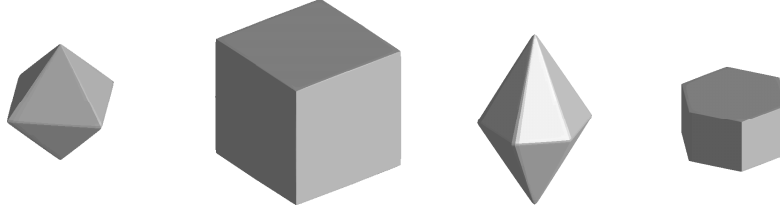
FIG. 2. Frank diagrams and Wulff shapes for different choices of (2.15) with $L_i = 3, 4, r_i = 1$.

FIG. 3. Frank diagrams and Wulff shapes for different choices of (2.15) with $L_i = 3, 6$ and $r_i = 30$.

e.g. [76, 30]), it can be used to visualize the given anisotropy. In Figures 2 and 3 we give the Frank diagrams and Wulff shapes for some anisotropies γ_i of the form (2.15); most of them have already been considered in [12]. Here we briefly state their definitions. Let

$$G_i^{(\ell)} := R(\vec{\theta}_i^{(\ell)})^T \operatorname{diag}(1, \varepsilon_i^2, \varepsilon_i^2) R(\vec{\theta}_i^{(\ell)}), \tag{2.17}$$

where $\operatorname{diag}(a, b, c)$ denotes a diagonal matrix with diagonal entries a, b, c and $R(\vec{\theta}) := R_1(\theta_1) R_2(\theta_2) R_3(\theta_3)$ with

$$R_1(\theta) := \begin{pmatrix} \cos\theta & \sin\theta & 0 \\ -\sin\theta & \cos\theta & 0 \\ 0 & 0 & 1 \end{pmatrix}, \quad R_2(\theta) := \begin{pmatrix} \cos\theta & 0 & \sin\theta \\ 0 & 1 & 0 \\ -\sin\theta & 0 & \cos\theta \end{pmatrix} \quad \text{and} \quad R_3(\theta) := \begin{pmatrix} 1 & 0 & 0 \\ 0 & \cos\theta & \sin\theta \\ 0 & -\sin\theta & \cos\theta \end{pmatrix}$$

being rotation matrices through the given angle θ. For the anisotropies in Figure 2 we have used $r_i = 1$ and $\varepsilon_i = 10^{-2}$ with $(\vec{\theta}_i^{(1)}, \ldots, \vec{\theta}_i^{(L_i)}) = (\vec{0}, (\pi/2, 0, 0), (0, \pi/2, 0))$ and $(\vec{0}, (0, \pi/3, 0), (0, 2\pi/3, 0), (\pi/2, 0, 0))$, respectively. Using the former example but now setting $r_i = 30$ yields the Frank diagram and Wulff shape as on the left of Figure 3. The final displayed anisotropy in Figure 3 can be obtained by choosing $r_i = 30$ and, for (2.17), setting $\varepsilon_i = 10^{-2}$ and $(\vec{\theta}_i^{(1)}, \ldots, \vec{\theta}_i^{(L_i)}) = (\vec{0}, (0, \pi/2, 0), (\pi/4, 0, 0), (-\pi/4, 0, 0), (0, \pi/2, \pi/4), (0, \pi/2, -\pi/4))$.

In order to define anisotropic mean curvature flow and anisotropic surface diffusion, we introduce the Cahn–Hoffman vectors (see [47])

$$\vec{v}_{\gamma,i} := \gamma_i'(\vec{v}_i), \quad i = 1 \to I_S; \tag{2.18a}$$

and define the weighted mean curvatures as

$$\varkappa_{\gamma,i} := -\nabla_s \cdot \vec{v}_{\gamma,i} \quad i = 1 \to I_S. \tag{2.18b}$$

Then the anisotropic versions of mean curvature flow, (2.2), and surface diffusion, (2.3), are given by

$$\mathcal{V}_i = \beta_i(\vec{\nu}_i)\varkappa_{\gamma,i}, \qquad\qquad i = 1 \to I_S, \qquad\qquad (2.19)$$

and

$$\mathcal{V}_i = -\nabla_s \, . \, (\beta_i(\vec{\nu}_i)\nabla_s\varkappa_{\gamma,i}), \quad i = 1 \to I_S; \qquad\qquad (2.20)$$

here $\beta_i : \mathbb{S}^2 \to \mathbb{R}_{>0}$, $i = 1 \to I_S$, are kinetic coefficients, and are assumed to be smooth, even and positive functions defined on the unit sphere $\mathbb{S}^2 \subset \mathbb{R}^3$. For a derivation of these laws in the case of a single closed hypersurface we refer to [4, 38, 72, 71].

Naturally, the triple junction line conditions (2.4a–d) need to be generalized to the anisotropic setting. Here equilibrium conditions in the context of thermodynamics have been derived in e.g. [44, 47], and corresponding boundary conditions for evolution equations have been considered in e.g. [34, 70, 36]. Of course, the attachment conditions (2.4a) still need to hold. In addition, we prescribe the following conditions on the triple junction lines:

$$\sum_{j=1}^3 [\gamma_{s_j^k}(\vec{\nu}_{s_j^k})\vec{\mu}_{s_j^k} - (\gamma'_{s_j^k}(\vec{\nu}_{s_j^k}) \, . \, \vec{\mu}_{s_j^k})\vec{\nu}_{s_j^k}] = \vec{0} \quad \text{on } \mathcal{T}_k, \quad k = 1 \to I_T, \qquad (2.21a)$$

$$o_1^k\vec{\mu}_{s_1^k} \, . \, \beta_{s_1^k}(\vec{\nu}_{s_1^k})\nabla_s\varkappa_{\gamma,s_1^k} = o_2^k\vec{\mu}_{s_2^k} \, . \, \beta_{s_2^k}(\vec{\nu}_{s_2^k})\nabla_s\varkappa_{\gamma,s_2^k} = o_3^k\vec{\mu}_{s_3^k} \, . \, \beta_{s_3^k}(\vec{\nu}_{s_3^k})\nabla_s\varkappa_{\gamma,s_3^k} \quad \text{on } \mathcal{T}_k,$$
$$k = 1 \to I_T, \qquad (2.21b)$$

$$\sum_{j=1}^3 o_j^k\varkappa_{\gamma,s_j^k} = 0 \quad \text{on } \mathcal{T}_k, \quad k = 1 \to I_T. \qquad\qquad (2.21c)$$

We note that in the isotropic case, (2.14), we have $\vec{\nu}_{\gamma,i} = \varsigma_i\vec{\nu}_i$ with $\varkappa_{\gamma,i} = \varsigma_i\varkappa_i$, and hence (2.21a–c) with $\beta = (1, \ldots, 1)$, on recalling that $\vec{\nu}_i \, . \, \vec{\mu}_i = 0$, simplify to $\sum_{j=1}^3 \varsigma_{s_j^k}\vec{\mu}_{s_j^k} = \vec{0}$, $o_1^k\varsigma_{s_1^k}\vec{\mu}_{s_1^k} \, . \, \nabla_s\varkappa_{s_1^k} = o_2^k\varsigma_{s_2^k}\vec{\mu}_{s_2^k} \, . \, \nabla_s\varkappa_{s_2^k} = o_3^k\varsigma_{s_3^k}\vec{\mu}_{s_3^k} \, . \, \nabla_s\varkappa_{s_3^k}$ and $\sum_{j=1}^3 o_j^k\varsigma_{s_j^k}\varkappa_{s_j^k} = 0$ on $\mathcal{T}_k$ for $k = 1 \to I_T$, respectively. Hence we observe that (2.21a–c) collapse to (2.4b–d) in the isotropic equal energy density case.

As in the isotropic case, (2.10a,b) and (2.11a,b), we are able to obtain the following weak formulations; see Section 3 for details. For anisotropic mean curvature flow we obtain: Find $\vec{x} \in \underline{V}(\Omega)$ and $\varkappa_\gamma \in \widehat{W}(\Gamma)$ such that

$$\langle \vec{x}_t, \chi\vec{\nu}\rangle - \langle\beta(\vec{\nu})\varkappa_\gamma, \chi\rangle = 0 \quad \forall\chi \in \widehat{W}(\Gamma), \qquad\qquad (2.22a)$$

$$\langle\varkappa_\gamma\vec{\nu}, \vec{\eta}\rangle + \langle\nabla_s^{\widetilde{G}}\vec{x}, \nabla_s^{\widetilde{G}}\vec{\eta}\rangle_\gamma = 0 \quad \forall\vec{\eta} \in \underline{V}(\Gamma). \qquad\qquad (2.22b)$$

For anisotropic surface diffusion flow we obtain: Find $\vec{x} \in \underline{V}(\Omega)$ and $\varkappa_\gamma \in W(\Gamma)$ such that

$$\langle \vec{x}_t, \chi\vec{\nu}\rangle - \langle\beta(\vec{\nu})\nabla_s\varkappa_\gamma, \nabla_s\chi\rangle = 0 \quad \forall\chi \in W(\Gamma), \qquad\qquad (2.23a)$$

$$\langle\varkappa_\gamma\vec{\nu}, \vec{\eta}\rangle + \langle\nabla_s^{\widetilde{G}}\vec{x}, \nabla_s^{\widetilde{G}}\vec{\eta}\rangle_\gamma = 0 \quad \forall\vec{\eta} \in \underline{V}(\Gamma). \qquad\qquad (2.23b)$$

Here we have introduced the shorthand notation $\langle\nabla_s^{\widetilde{G}}\cdot, \nabla_s^{\widetilde{G}}\cdot\rangle_\gamma$ for the natural cluster analogue of the inner product defined in [12]. This is defined as follows. First, we introduce the symmetric positive

definite matrices $\widetilde{G}_i^{(\ell)}$ with the associated inner products $(\cdot, \cdot)_{\widetilde{G}_i^{(\ell)}}$ on $\mathbb{R}^3$ by

$$\widetilde{G}_i^{(\ell)} := [\det G_i^{(\ell)}]^{1/2} [G_i^{(\ell)}]^{-1} \quad \text{and} \quad (\vec{a}, \vec{b})_{\widetilde{G}_i^{(\ell)}} = \vec{a} \cdot \widetilde{G}_i^{(\ell)} \vec{b} \quad \forall \vec{a}, \vec{b} \in \mathbb{R}^3,$$
$$\ell = 1 \to L_i, \ i = 1 \to I_S.$$

With $\{\vec{p}, \vec{\tau}_1, \vec{\tau}_2\}$ an orthonormal basis for $\mathbb{R}^3$, it follows, on recalling (2.15), that

$$\gamma_i^{(\ell)}(\vec{p}) = [\det B_i^{(\ell)}]^{1/2}, \quad \text{where } B_i^{(\ell)} \in \mathbb{R}^{2 \times 2} \text{ with } [B_i^{(\ell)}]_{jk} = (\vec{\tau}_j, \vec{\tau}_k)_{\widetilde{G}_i^{(\ell)}}, \ j, k = 1 \to 2;$$

see [12, Lemma 2.1]. Secondly, we set

$$H_i^{(\ell)} := [D\vec{x}_i]^T \widetilde{G}_i^{(\ell)} D\vec{x}_i \quad \text{and} \quad [h_i^{(\ell)}]^{jk} := [(H_i^{(\ell)})^{-1}]_{jk}, \quad j, k = 1 \to 2,$$

where $D\vec{x}_i$ denotes the Jacobian matrix. Then

$$\langle \nabla_s^{\widetilde{G}} \vec{\eta}, \nabla_s^{\widetilde{G}} \vec{\chi} \rangle_\gamma := \sum_{i=1}^{I_S} \sum_{\ell=1}^{L_i} \int_{\Gamma_i} \left[\frac{\gamma_i^{(\ell)}(\vec{\nu}_i)}{\gamma_i(\vec{\nu}_i)} \right]^{r_i - 1} (\nabla_s^{\widetilde{G}_i^{(\ell)}} \vec{\eta}_i, \nabla_s^{\widetilde{G}_i^{(\ell)}} \vec{\chi}_i)_{\widetilde{G}_i^{(\ell)}} \gamma_i^{(\ell)}(\vec{\nu}_i) \, d\mathcal{H}^2, \qquad (2.24a)$$

where for all smooth $\vec{\eta}_i, \vec{\chi}_i : \Gamma_i \to \mathbb{R}^3$,

$$(\nabla_s^{\widetilde{G}_i^{(\ell)}} \vec{\eta}_i, \nabla_s^{\widetilde{G}_i^{(\ell)}} \vec{\chi}_i)_{\widetilde{G}_i^{(\ell)}} := \sum_{j=1}^{2} (\partial_{\vec{t}_{i,j}^{(\ell)}} \vec{\eta}_i, \partial_{\vec{t}_{i,j}^{(\ell)}} \vec{\chi}_i)_{\widetilde{G}_i^{(\ell)}}$$

$$= \sum_{j=1}^{2} \sum_{k=1}^{2} [h_i^{(\ell)}]^{jk} (\partial_k [\vec{\eta}_i \circ \vec{x}_i], \partial_j [\vec{\chi}_i \circ \vec{x}_i])_{\widetilde{G}_i^{(\ell)}} \qquad (2.24b)$$

with $\{\vec{t}_{i,1}^{(\ell)}, \vec{t}_{i,2}^{(\ell)}\}$ being an orthonormal basis with respect to the $\widetilde{G}_i^{(\ell)}$ inner product for the tangent plane of Γ_i; see [12, (2.8), (2.11), (2.20)] for further details.

We remark that for equal isotropic energies $\gamma_i(\cdot) = |\cdot|$, $i = 1 \to I_S$, with constant mobilities $\beta = (1, \ldots, 1)$, the formulations (2.22a,b) and (2.23a,b) collapse to their isotropic counterparts (2.10a,b) and (2.11a,b), respectively. We recall that the novel variational formulation in [12] has yielded the first unconditionally stable parametric approximations of anisotropic geometric evolution equations in higher dimensions. Recently, an alternative stable finite element approximation for anisotropic mean curvature flow for closed hypersurfaces in $\mathbb{R}^3$ has been introduced in [61]. For convex anisotropies, on employing a stabilizing term that slightly changes the approximated flow, stability was shown for a fully discrete approximation. However, we stress that this approximation cannot be generalized to the case of surface clusters considered in this paper.

Finally, we will also consider situations in which parts of the boundaries of the surfaces Γ_i, $i = 1 \to I_S$, are constrained to lie on the boundary $\partial\mathcal{D}$ of a domain $\mathcal{D}$. In this case, boundary conditions have to hold on these I_B, $I_B \geqslant 0$, boundary lines. Physically meaningful conditions for curves attached to the boundary of a domain in the plane have been derived in [20] and [36], and here we extend these conditions to the three-dimensional case. To this end, we introduce the following notation. Let the boundary line $\mathcal{B}_k$ be given by the pair (s_k, p_k) such that, similarly to (2.4a),

$$\mathcal{B}_k(t) := \vec{x}_{s_k}(\partial_{p_k} \Omega_{s_k}, t) \subset \partial\mathcal{D}, \quad k = 1 \to I_B. \qquad (2.25)$$

We note that throughout this paper, we assume for simplicity that

$$\bigcup_{k=1}^{I_B} \{(s_k, p_k)\} \cap \bigcup_{k=1}^{I_T} \bigcup_{j=1}^{3} \{(s_j^k, p_j^k)\} = \emptyset, \tag{2.26}$$

i.e. that no triple junction line $\mathcal{T}_k$ is constrained to lie on the boundary $\partial \mathcal{D}$. This still leaves the possibility open that a triple junction line meets the boundary $\partial \mathcal{D}$ at e.g. a single point. In such a case, no extra conditions are needed at these points. In addition, we assume that

$$(i, p) \in \bigcup_{k=1}^{I_B} \{(s_k, p_k)\} \cup \bigcup_{k=1}^{I_T} \bigcup_{j=1}^{3} \{(s_j^k, p_j^k)\}, \quad p = 1 \to I_P^i, \; i = 1 \to I_S;$$

i.e. that each part of the partitioned boundaries $\partial \Omega_i$ is mapped by $\vec{x}$ either to a triple junction line, or to a boundary line. Let $\vec{n}$ be the outer unit normal to $\partial \mathcal{D}$. Then (2.25) can be equivalently formulated as $\vec{x}_{s_k}(\partial_{p_k} \Omega_{s_k}) \subset \partial \mathcal{D}$ at time $t = 0$ together with

$$\vec{n} \cdot \vec{x}_{s_k, t} = 0 \quad \text{on } \mathcal{B}_k, \quad k = 1 \to I_B. \tag{2.27a}$$

In the case of anisotropic curvature flow we require in addition that

$$\vec{n} \cdot \gamma_{s_k}'(\vec{v}_{s_k}) = 0 \quad \text{on } \mathcal{B}_k, \quad k = 1 \to I_B, \tag{2.27b}$$

which collapses to a 90° angle condition, $\vec{n} \cdot \vec{v}_{s_k} = 0$, in the case of isotropic γ_{s_k}. In the case of anisotropic surface diffusion we require, in addition to (2.27b), the no-flux boundary condition

$$\vec{\mu}_{s_k} \cdot \nabla_s \varkappa_{\gamma, s_k} = 0 \quad \text{on } \mathcal{B}_k, \quad k = 1 \to I_B. \tag{2.27c}$$

This condition has been introduced for curves in the plane in [36] in the isotropic case, and was generalized in [9] to the anisotropic case. The condition (2.27c) is the natural generalization of these conditions in the plane to the case of surfaces in $\mathbb{R}^3$.

3. Gradient flow structure and weak formulations

In this section, we will discuss the variational structure of the governing equations for anisotropic mean curvature flow and anisotropic surface diffusion for surface clusters in $\mathbb{R}^3$. In particular, we will show that the former is a weighted L^2-gradient flow of (2.12), while the latter is a weighted H^{-1}-gradient flow of (2.12). We will only consider the general anisotropic situation, and so the isotropic case will just be a specific example of this. First we state a transport theorem for anisotropic energies.

LEMMA 3.1 Let $U_i \subset \mathbb{R}^2$ be open and let $\Omega_i \subset U_i$ be a domain with a piecewise smooth boundary. Let $\vec{x}_i : U_i \times (-\delta_0, \delta_0) \to \mathbb{R}^3$ be a smooth function that parameterizes the evolving hypersurface $(\Gamma_i^\delta)_{|\delta| < \delta_0}$ over Ω_i, i.e. $\Gamma_i^\delta = \vec{x}_i(\Omega_i, \delta)$ for $|\delta| < \delta_0$. Let $\vec{v}_i^\delta$ be a unit normal field to Γ_i^δ, and let $\vec{\mu}_i^\delta$ be the conormal to $\partial \Gamma_i^\delta$. In addition, let $\gamma_i : \mathbb{R}^3 \to \mathbb{R}_{\geqslant 0}$ be a given anisotropy function satisfying (2.13). Then

$$\frac{\mathrm{d}}{\mathrm{d}\delta} \int_{\Gamma_i^\delta} \gamma_i(\vec{v}_i^\delta) \, \mathrm{d}\mathcal{H}^2 = \int_{\Gamma_i^\delta} \mathcal{V}_i^\delta \nabla_s \cdot \gamma_i'(\vec{v}_i^\delta) \, \mathrm{d}\mathcal{H}^2 + \int_{\partial \Gamma_i^\delta} \vec{x}_{i,\delta} \cdot (\gamma_i(\vec{v}_i^\delta)\vec{\mu}_i^\delta - (\gamma_i'(\vec{v}_i^\delta) \cdot \vec{\mu}_i^\delta)\vec{v}_i^\delta) \, \mathrm{d}\mathcal{H}^1,$$

where $\vec{x}_{i,\delta} := \frac{\mathrm{d}}{\mathrm{d}\delta} \vec{x}_i$ and $\mathcal{V}_i^\delta := \vec{x}_{i,\delta} \cdot \vec{v}_i^\delta$ is the normal velocity of Γ_i^δ.

Proof. Using a transport theorem, which can be found for example in [39, (15-31)] and [37, (2.9)], we obtain

$$\frac{\mathrm{d}}{\mathrm{d}\delta} \int_{\Gamma_i^\delta} \gamma_i(\vec{v}_i^\delta) \, \mathrm{d}\mathcal{H}^2 = \int_{\Gamma_i^\delta} (\partial^0 \gamma_i(\vec{v}_i^\delta) - \gamma_i(\vec{v}_i^\delta) \mathcal{V}_i^\delta \varkappa_i^\delta) \, \mathrm{d}\mathcal{H}^2 + \int_{\partial \Gamma_i^\delta} \gamma_i(\vec{v}_i^\delta) \vec{x}_{i,\delta} \cdot \vec{\mu}_i^\delta \, \mathrm{d}\mathcal{H}^1,$$

where ∂^0 is the time derivative following Γ_i^δ (see [39, (15-21)]) and $\varkappa_i^\delta$ is the sum of the principal curvatures of Γ_i^δ. Since $\partial^0 \vec{v}_i^\delta = -\nabla_s \mathcal{V}_i^\delta$ (see [39, (15–24)]), we obtain the desired result by using integration by parts on manifolds (see e.g. [16, Corollary 4]) and the identity $\gamma_i'(\vec{p}) \cdot \vec{p} = \gamma_i(\vec{p})$. Finally we note that the results in [39, 16, 37] remain true for surfaces with piecewise smooth boundaries. $\qquad\square$

Applying the above lemma locally in a situation where the three surfaces $\Gamma_{s_1^k}$, $\Gamma_{s_2^k}$, $\Gamma_{s_3^k}$, with surface energy densities $\gamma_{s_1^k}$, $\gamma_{s_2^k}$, $\gamma_{s_3^k}$, meet at a triple junction line $\mathcal{T}_k$, we see that the condition

$$\sum_{j=1}^3 [\gamma_{s_j^k}(\vec{v}_{s_j^k}) \vec{\mu}_{s_j^k} - (\gamma_{s_j^k}'(\vec{v}_{s_j^k}) \cdot \vec{\mu}_{s_j^k}) \vec{v}_{s_j^k}] = \vec{0} \quad \text{on } \mathcal{T}_k, \tag{3.1}$$

i.e. (2.21a), makes the boundary term on $\mathcal{T}_k$ vanish. It is possible to derive a geometrical interpretation of (3.1). To this end, we remark that the vectors $\vec{v}_{s_j^k}$, $\vec{\mu}_{s_j^k}$, $j = 1 \to 3$, all lie in the plane T_k perpendicular to the triple junction line $\mathcal{T}_k$; see Figure 1. We recall also the choice of (o_1^k, o_2^k, o_3^k) so that $(o_j^k \vec{v}_{s_j^k}, \vec{\mu}_{s_j^k})$, $j = 1 \to 3$, have the same orientation. Noting that $\gamma_i'(\vec{p}_i) \cdot \vec{p} = \gamma_i(\vec{p}) = \gamma_i(-\vec{p}) = -\gamma_i'(-\vec{p}_i) \cdot \vec{p}$, it follows that (3.1) is equivalent to

$$\sum_{j=1}^3 [(\gamma_{s_j^k}'(o_j^k \vec{v}_{s_j^k}) \cdot (o_j^k \vec{v}_{s_j^k})) \vec{\mu}_{s_j^k} - (\gamma_{s_j^k}'(o_j^k \vec{v}_{s_j^k}) \cdot \vec{\mu}_{s_j^k})(o_j^k \vec{v}_{s_j^k})] = \vec{0} \quad \text{on } \mathcal{T}_k. \tag{3.2}$$

Hence on rotating the left hand side of (3.2) by 90° in the plane T_k, we deduce that (3.2), and hence (3.1), are equivalent to

$$\Pi_{|T_k} \sum_{j=1}^3 \gamma_{s_j^k}'(o_j^k \vec{v}_{s_j^k}) = \vec{0} \quad \text{on } \mathcal{T}_k, \tag{3.3}$$

where $\Pi_{|T_k}$ is the orthogonal projection onto the plane T_k. The identity (3.1) can be interpreted as a force balance on the triple junction line $\mathcal{T}_k$; see [44, 47, 31]. It simplifies in the isotropic case, (2.14), to $\sum_{j=1}^3 \varsigma_{s_j^k} \vec{\mu}_{s_j^k} = \vec{0}$, which for equal isotropic surface energies is (2.4b).

Therefore using Lemma 3.1 and recalling (2.18a,b), we deduce that surface clusters, with triple junctions lines, evolving by the anisotropic mean curvature law (2.19) together with the attachment conditions (2.4a) and the boundary conditions (2.21a) fulfill the energy inequality

$$\frac{\mathrm{d}}{\mathrm{d}t} E_\gamma(\Gamma) = \frac{\mathrm{d}}{\mathrm{d}t} \left(\sum_{i=1}^{I_S} \int_{\Gamma_i} \gamma_i(\vec{v}_i) \, \mathrm{d}\mathcal{H}^2 \right) = -\sum_{i=1}^{I_S} \int_{\Gamma_i} \mathcal{V}_i \varkappa_{\gamma,i} \, \mathrm{d}\mathcal{H}^2$$

$$= -\sum_{i=1}^{I_S} \int_{\Gamma_i} \beta_i(\vec{v}_i)(\varkappa_{\gamma,i})^2 \, \mathrm{d}\mathcal{H}^2 = -\sum_{i=1}^{I_S} \int_{\Gamma_i} \frac{1}{\beta_i(\vec{v}_i)} \mathcal{V}_i^2 \, \mathrm{d}\mathcal{H}^2 \leqslant 0. \tag{3.4}$$

This, together with Lemma 3.1, shows that (2.19) with (2.4a), (2.21a) is a (weighted) L^2-gradient flow of $E_\gamma(\Gamma)$.

If we require that parts of the boundaries of Γ remain on $\partial\mathcal{D}$, we need to impose additional conditions. With $\vec{n}$ the outer unit normal to $\partial\mathcal{D}$, we first of all require that $\vec{n} \cdot \vec{x}_{s_k,t} = 0$ on $\mathcal{B}_k \subset \partial\Gamma_{s_k} \cap \partial\mathcal{D}$, i.e. (2.27a), in order to deduce that this part of $\partial\Gamma_{s_k}$ remains on $\partial\mathcal{D}$, for $k = 1 \to I_B$. In addition, for $k = 1 \to I_B$, we require that

$$\vec{x}_{s_k,t} \cdot (\gamma_{s_k}(\vec{\nu}_{s_k})\vec{\mu}_{s_k} - (\gamma'_{s_k}(\vec{\nu}_{s_k}) \cdot \vec{\mu}_{s_k})\vec{\nu}_{s_k}) = 0 \quad \text{on } \mathcal{B}_k \tag{3.5}$$

for all $\vec{n} \cdot \vec{x}_{s_k,t} = 0$ on $\mathcal{B}_k$ in order for the boundary term, arising from applying Lemma 3.1 locally, to vanish. We note that $\vec{\nu}_{s_k}, \vec{\mu}_{s_k}, \vec{n}$ all lie in the plane B_k perpendicular to $\mathcal{B}_k$. In addition, we note that (3.5) is equivalent to the vector $\gamma_{s_k}(\vec{\nu}_{s_k})\vec{\mu}_{s_k} - (\gamma'_{s_k}(\vec{\nu}_{s_k}) \cdot \vec{\mu}_{s_k})\vec{\nu}_{s_k}$ being a multiple of $\vec{n}$, and so a 90° rotation in the plane B_k of this vector yields, similarly to (3.3),

$$\vec{n} \cdot (\Pi_{|B_k} \gamma'_{s_k}(\vec{\nu}_{s_k})) = 0 \quad \text{on } \mathcal{B}_k,$$

where $\Pi_{|B_k}$ is the orthogonal projection onto the plane B_k. Since $\vec{n} \in B_k$, we find that the I_B boundary conditions (3.5) are equivalent to (2.27b). Hence, (3.4) remains valid if parts of $\partial\Gamma_i$ are constrained to lie on $\partial\mathcal{D}$, i.e. if the boundary conditions (2.27a,b) are imposed.

Similarly to (3.4), in the case of surface clusters, with triple junctions lines, evolving by the anisotropic surface diffusion law (2.20), together with the attachment conditions (2.4a) and the boundary conditions (2.21a–c), we deduce that

$$\frac{\mathrm{d}}{\mathrm{d}t} E_\gamma(\Gamma) = \sum_{i=1}^{I_S} \int_{\Gamma_i} \mathcal{V}_i \nabla_s \cdot (\gamma'(\vec{\nu}_i)) \, \mathrm{d}\mathcal{H}^2 = \sum_{i=1}^{I_S} \int_{\Gamma_i} \nabla_s \cdot (\beta_i(\vec{\nu}_i) \nabla_s \varkappa_{\gamma,i}) \varkappa_{\gamma,i} \, \mathrm{d}\mathcal{H}^2$$

$$= -\sum_{i=1}^{I_S} \int_{\Gamma_i} \beta_i(\vec{\nu}_i) |\nabla_s \varkappa_{\gamma,i}|^2 \, \mathrm{d}\mathcal{H}^2 \leqslant 0, \tag{3.6}$$

where the boundary terms which arise from performing integration by parts vanish as (2.21b,c) imply that for $k = 1 \to I_T$,

$$\sum_{j=1}^{3} \varkappa_{\gamma,s_j^k} \beta_{s_j^k}(\vec{\nu}_{s_j^k}) \nabla_s \varkappa_{\gamma,s_j^k} \cdot \vec{\mu}_{s_j^k} = 0 \quad \text{on } \mathcal{T}_k. \tag{3.7}$$

On noting that $\varkappa_{\gamma,i}$ is minus the inverse of the weighted surface Laplacian defined in (2.20) acting on $\mathcal{V}_i$, we see from (3.6) that (2.20) with (2.4a), (2.21a–c) is a (weighted) H^{-1}-gradient flow of $E_\gamma(\Gamma)$. Once again, it is easily seen that (3.6) remains valid if parts of $\partial\Gamma_i$ are constrained to lie on $\partial\mathcal{D}$ if the boundary conditions (2.27a–c) are imposed. Moreover, it is easy to see from (3.6) that stationary solutions of surface diffusion are clusters containing only constant (anisotropic) mean curvature surfaces.

In the remainder of this section, we restrict ourselves to the class of anisotropies (2.15) and derive the weak formulations (2.22a,b) and (2.23a,b). First we compute the first variation of the anisotropic surface energy (2.12). To this end, let

$$\Gamma^\delta(\vec{g}) := \{\vec{z} + \delta\vec{g}(\vec{z}) : \vec{z} \in \Gamma = \vec{x}(\Omega)\} \tag{3.8}$$

for $\delta > 0$ and $\vec{g} \in \underline{V}(\Gamma)$.

LEMMA 3.2 Let E_γ be given by (2.12) with $\gamma = (\gamma_1, \ldots, \gamma_{I_S})$ as in (2.15). Then, on recalling (2.24a,b), for a smooth vector field $\vec{g} \in \underline{V}(\Gamma)$ we have

$$\frac{\mathrm{d}}{\mathrm{d}\delta} E_\gamma(\Gamma^\delta(\vec{g})) \Big|_{\delta=0} = \langle \nabla_s^{\widetilde{G}} \vec{x}, \nabla_s^{\widetilde{G}} \vec{g} \rangle_\gamma. \tag{3.9}$$

Proof. We use the same arguments as in the proofs of [12, Lemma 2.5, Theorem 2.1] to compute the first variation of $\int_{\Gamma_i} \gamma_i(\vec{v}_i) \, \mathrm{d}\mathcal{H}^2$. We note that the arguments applied there to closed surfaces remain true for surfaces Γ_i, $i = 1 \to I_S$, with boundaries $\partial \Gamma_i$. We briefly outline the key steps of the proof.

First, we consider the case of Γ_i, where γ_i is defined by (2.15) with $L_i = 1$. Then combining [12, Lemma 2.5, Lemma 2.2, (2.19b)] with (2.24b) yields

$$\frac{\mathrm{d}}{\mathrm{d}\delta} \int_{\Gamma_i} \gamma_i(\vec{v}_i) \, \mathrm{d}\mathcal{H}^2 \Big|_{\delta=0} = \int_{\Omega_i} \sum_{j=1}^{2} \sum_{k=1}^{2} [h_i^{(1)}]^{jk} (\partial_k \vec{x}_i, \partial_j [\vec{g}_i \circ \vec{x}_i])_{\widetilde{G}_i^{(1)}} [\det H_i^{(1)}]^{1/2} \, \mathrm{d}\mathcal{L}^2$$

$$= \int_{\Gamma_i} (\nabla_s^{\widetilde{G}_i^{(1)}} \vec{x}_i, \nabla_s^{\widetilde{G}_i^{(1)}} \vec{g}_i)_{\widetilde{G}_i^{(1)}} \gamma_i(\vec{v}_i) \, \mathrm{d}\mathcal{H}^2, \tag{3.10}$$

where $\mathcal{L}^d$ denotes the Lebesgue measure in $\mathbb{R}^d$.

The extension of (3.10) to $L_i \geqslant 1$ and $r_i \in [1, \infty)$ follows from combining [12, (2.45), Lemma 2.2, (2.19b)] and (2.24b), and we obtain

$$\frac{\mathrm{d}}{\mathrm{d}\delta} \int_{\Gamma_i} \gamma_i(\vec{v}_i) \, \mathrm{d}\mathcal{H}^2 \Big|_{\delta=0} = \sum_{\ell=1}^{L_i} \int_{\Gamma_i} \left[\frac{\gamma_i^{(\ell)}(\vec{v}_i)}{\gamma_i(\vec{v}_i)} \right]^{r_i - 1} (\nabla_s^{\widetilde{G}_i^{(\ell)}} \vec{x}_i, \nabla_s^{\widetilde{G}_i^{(\ell)}} \vec{g}_i)_{\widetilde{G}_i^{(\ell)}} \gamma_i^{(\ell)}(\vec{v}_i) \, \mathrm{d}\mathcal{H}^2. \tag{3.11}$$

Summing (3.11) for $i = 1 \to I_S$ then yields the desired result (3.9), on recalling the definitions (2.12) and (2.24a). $\qquad \square$

LEMMA 3.3 Let γ be given by (2.15). Then a surface cluster Γ with a parameterization $\vec{x} \in \underline{V}(\Omega) \cap \times_{i=1}^{I_S} C^2(\overline{\Omega}_i, \mathbb{R}^3)$ and a $\varkappa_\gamma \in \widehat{W}(\Gamma)$ fulfill

$$\langle \varkappa_\gamma \vec{v}, \vec{\eta} \rangle + \langle \nabla_s^{\widetilde{G}} \vec{x}, \nabla_s^{\widetilde{G}} \vec{\eta} \rangle_\gamma = 0 \quad \forall \vec{\eta} \in \underline{V}(\Gamma) \tag{3.12}$$

if and only if (2.18a,b) together with the boundary conditions (2.21a) hold.

Proof. We note that combining the results in Lemmas 3.1 and 3.2 for the evolving hypersurfaces $\Gamma^\delta(\vec{g})$ in (3.8) we obtain, on choosing $\vec{x}_\delta = \vec{g}$ in Lemma 3.1,

$$\langle \nabla_s^{\widetilde{G}} \vec{x}, \nabla_s^{\widetilde{G}} \vec{g} \rangle_\gamma = \sum_{i=1}^{I_S} \int_{\Gamma_i} (\vec{g} \cdot \vec{v}_i) \nabla_s . \gamma_i'(\vec{v}_i) \, \mathrm{d}\mathcal{H}^2 + \sum_{i=1}^{I_S} \int_{\partial \Gamma_i} \vec{g} \cdot (\gamma_i(\vec{v}_i) \vec{\mu}_i - (\gamma_i'(\vec{v}_i) . \vec{\mu}_i) \vec{v}_i) \, \mathrm{d}\mathcal{H}^1 \tag{3.13}$$

for all smooth $\vec{g} \in \underline{V}(\Gamma)$.

Now assuming that (3.12) holds, it immediately follows from (3.13) that (2.18a,b) hold. In addition, the integrals on the triple junction lines $\mathcal{T}_k$, $k = 1 \to I_T$, have to vanish and hence the boundary conditions (2.21a) have to hold.

Similarly, if Γ and $\varkappa_\gamma$ fulfill (2.18a,b) and the boundary condition (2.21a), we deduce from (3.13) that (3.12) holds for all smooth $\vec{g} \in \underline{V}(\Gamma)$. The desired result (3.12) then follows from a density argument. $\qquad \square$

We now extend the above to the case when external boundaries are present. To this end, let

$$\underline{V}_\partial(\Gamma) := \{\vec{\chi} \in \underline{V}(\Gamma) : \vec{n} \cdot \vec{\chi}_{s_k} = 0 \text{ on } \mathcal{B}_k, \, k = 1 \to I_B\}.$$

Moreover, similarly to (3.8), let

$$\Gamma_\partial^\delta(\vec{g}) := \{\vec{y}(\vec{z}, \delta) : \vec{z} \in \Gamma = \vec{x}(\Omega), \text{ where } \vec{y}_\delta(\vec{z}, \delta) = \vec{g}(\vec{y}(\vec{z}, \delta)), \, \vec{y}(\vec{z}, 0) = \vec{z} \in \Gamma\} \quad (3.14)$$

for $\delta > 0$ and $\vec{g} \in \underline{V}_\partial(\Gamma)$, with the latter smoothly extended to all of $\mathbb{R}^3$ such that $\vec{n} \cdot \vec{g} = 0$ on $\partial\mathcal{D}$.

LEMMA 3.4   Let E_γ be given by (2.12) with $\gamma = (\gamma_1, \ldots, \gamma_{I_S})$ as in (2.15). In addition, let $\vec{g} \in \underline{V}_\partial(\Gamma)$ be a smooth vector field. Then

$$\frac{\mathrm{d}}{\mathrm{d}\delta} E_\gamma(\Gamma_\partial^\delta(\vec{g})) \bigg|_{\delta=0} = \langle \nabla_s^{\widetilde{G}} \vec{x}, \nabla_s^{\widetilde{G}} \vec{g} \rangle_\gamma. \quad (3.15)$$

Moreover, an evolving family of surface clusters $(\Gamma(t))_{t \geqslant 0}$ with parameterizations $\vec{x}(\cdot, t) \in \underline{V}(\Omega) \cap \times_{i=1}^{I_S} C^2(\overline{\Omega}_i, \mathbb{R}^3)$ satisfying (2.27a) and a $\varkappa_\gamma(\cdot, t) \in \widehat{W}(\Gamma)$ fulfill

$$\langle \varkappa_\gamma \vec{v}, \vec{\eta} \rangle + \langle \nabla_s^{\widetilde{G}} \vec{x}, \nabla_s^{\widetilde{G}} \vec{\eta} \rangle_\gamma = 0 \quad \forall \vec{\eta} \in \underline{V}_\partial(\Gamma) \quad (3.16)$$

if and only if (2.18a,b) together with the triple junction line conditions (2.21a), and the boundary line conditions (2.27b) hold.

Proof. The proof of (3.15) is exactly the same as the one for (3.9), except that the variation is over $\vec{g} \in \underline{V}_\partial(\Gamma)$ as opposed to $\vec{g} \in \underline{V}(\Gamma)$. The equivalence statement follows as in the proof of Lemma 3.3 on recalling the equivalence of the boundary conditions (3.5), $k = 1 \to I_B$, and (2.27b).   □

THEOREM 3.1   Let γ be given by (2.15). Then for a family of evolving surface clusters $(\Gamma(t))_{t \geqslant 0}$, with parameterization $\vec{x}(\cdot, t) \in \underline{V}(\Omega) \cap \times_{i=1}^{I_S} C^2(\overline{\Omega}_i, \mathbb{R}^3)$ and with $I_B = 0$, the weak formulations (2.22a,b) and (2.23a,b) are equivalent to the strong formulations (2.19) with (2.21a) and (2.20) with (2.21a–c), respectively. Similarly, if $I_B > 0$ and $\vec{x}$ satisfies (2.27a), then (3.16) together with (2.22a) or (2.23a) are weak formulations of the corresponding flows when the boundary line conditions (2.27b) and (2.27b,c) are present, respectively.

Proof. The proof for (2.22a,b) follows immediately from Lemma 3.3 and multiplying (2.19) with a test function $\chi \in \widehat{W}(\Gamma)$. Similarly, the proof for (2.23a,b) follows from Lemma 3.3, multiplying (2.20) with a test function $\chi \in W(\Gamma)$ and integrating by parts on noting (2.21b) and (2.6b), similarly to (3.6); recall (3.7). The final statement follows from Lemma 3.4 and the above.   □

REMARK 3.1   Based on (2.23a,b), it is now straightforward to show that anisotropic surface diffusion preserves the enclosed volumes. We illustrate this with an example. Consider a double bubble cluster as shown in Figure 5 below, with $(o_1^1, o_2^1, o_3^1) = (1, 1, 1)$ and $\vec{v}_1$ chosen as the outer normal to the volume enclosed by Γ_1 and Γ_2, which implies that $\vec{v}_2$ is the inner normal to this volume, which we denote by v. Then choosing $\chi = (1, -1, 0) \in W(\Gamma)$ in (2.23a) yields

$$\frac{\mathrm{d}}{\mathrm{d}t} \mathcal{L}^3(v) = \int_{\Gamma_1} [\vec{x}_1]_t \cdot \vec{v}_1 \, \mathrm{d}\mathcal{H}^2 - \int_{\Gamma_2} [\vec{x}_2]_t \cdot \vec{v}_2 \, \mathrm{d}\mathcal{H}^2 = 0,$$

i.e. the volume of v is preserved.

REMARK 3.2 One can also consider volume preserving mean curvature flow as a gradient flow. For the double bubble cluster as shown in Figure 5 below with (o_1^1, o_2^1, o_3^1), $\vec{v}_1$ and $\vec{v}_2$ chosen as in Remark 3.1 above, which implies that $\vec{v}_3$ is the inner normal to the volume enclosed by Γ_2 and Γ_3, then such a flow is given by

$$\mathcal{V}_i = \varkappa_i - \lambda_i \quad \text{on } \Gamma_i, \quad i = 1 \to 3, \tag{3.17}$$

together with (2.4a,b), where $\lambda_i(t) \in \mathbb{R}$ with $\sum_{i=1}^{3} \lambda_i(t) = 0$ are chosen so that $\int_{\Gamma_1} \mathcal{V}_1 \, d\mathcal{H}^2 - \int_{\Gamma_2} \mathcal{V}_2 \, d\mathcal{H}^2 = 0$ and $\int_{\Gamma_2} \mathcal{V}_2 \, d\mathcal{H}^2 - \int_{\Gamma_3} \mathcal{V}_3 \, d\mathcal{H}^2 = 0$ for all $t \geqslant 0$. Obviously, this is easily generalized to more complicated clusters as well as to anisotropic surface energies. It is interesting to note that while stationary solutions of the conserved mean curvature flow are also stationary solutions of the surface diffusion flow, the converse is not necessarily true. This is due to the nonlocal nature of (3.17), and a counterexample involving a nonconnected region is easily constructed. Here the surface diffusion flow would preserve each enclosed volume locally, while the conserved mean curvature flow (3.17) only preserves the total volume of each region, though it is straightforward to adapt (3.17) so that it preserves volumes locally.

4. Parametric finite element approximation

For $i \to I_S$, let Ω_i^h be a triangulation approximating $\overline{\Omega}_i \subset \mathbb{R}^2$, so that $\Omega_i^h = \bigcup_{j=1}^{J_i} \overline{\sigma_j^i}$, where $\{\sigma_j^i\}_{j=1}^{J_i}$ is a family of mutually disjoint open triangles with vertices $\{\vec{q}_k^i\}_{k=1}^{K_i}$. In particular, let $\{\vec{q}_k^i\}_{k=1}^{\overline{K}_i}$ denote the vertices in the interior of Ω_i^h and let $\{\vec{q}_k^i\}_{k=\overline{K}_i+1}^{K_i}$ denote the vertices on $\partial \Omega_i^h$. We set $h := \max_{i=1 \to I_S} \max_{j=1 \to J_i} \operatorname{diam}(\sigma_j^i)$. We introduce the finite element space $\widehat{\underline{V}}^h(\Omega^h) := \{\vec{\chi} \in \times_{i=1}^{I_S} C(\Omega_i^h, \mathbb{R}^3) : \vec{\chi}_i|_{\sigma_j^i} \text{ is linear for } j = 1 \to J_i, \ i = 1 \to I_S\}$. In order to describe the conditions that our discretization needs to satisfy at the triple junction lines, we have to make the following compatibility assumptions. Let $\partial_j \Omega_i^h$ be the polygonal curve approximating $\overline{\partial_j \Omega_i}$, $j = 1 \to I_P^i$, $i = 1 \to I_S$. Then we assume that the endpoints of $\partial_j \Omega_i^h$ and $\overline{\partial_j \Omega_i}$ coincide and that

$$Z_k := \#\{\{\vec{q}_l^{s_1^k}\}_{l=1}^{K_{s_1^k}} \cap \partial_{p_1^k} \Omega_{s_1^k}^h\} = \#\{\{\vec{q}_l^{s_2^k}\}_{l=1}^{K_{s_2^k}} \cap \partial_{p_2^k} \Omega_{s_2^k}^h\} = \#\{\{\vec{q}_l^{s_3^k}\}_{l=1}^{K_{s_3^k}} \cap \partial_{p_3^k} \Omega_{s_3^k}^h\} \tag{4.1}$$

for all $k = 1 \to I_T$. The condition (4.1) simply says that the triangulations of Ω^h need to "match up" at their boundaries, where they meet at triple junction lines. In addition, let

$$\vec{\rho}_j^k : \{1 \to Z_k\} \to \{\{\vec{q}_l^{s_j^k}\}_{l=1}^{K_{s_j^k}} \cap \partial_{p_j^k} \Omega_{s_j^k}^h\}, \quad j = 1 \to 3, \tag{4.2}$$

be a bijective map such that $(\vec{\rho}_j^k(1), \ldots, \vec{\rho}_j^k(Z_k))$ is an ordered sequence of vertices of the polygonal curve $\partial_{p_j^k} \Omega_{s_j^k}^h$, $j = 1 \to 3, k = 1 \to I_T$.

Then we define the natural discrete analogue of $\underline{V}(\Omega)$ by $\underline{V}^h(\Omega^h) := \{\vec{\chi} \in \widehat{\underline{V}}^h(\Omega^h) : \vec{\chi}_{s_1^k}(\vec{\rho}_1^k(l)) = \vec{\chi}_{s_2^k}(\vec{\rho}_2^k(l)) = \vec{\chi}_{s_3^k}(\vec{\rho}_3^k(l)), \ l = 1 \to Z_k, k = 1 \to I_T\}$.

Let $0 = t_0 < t_1 < \cdots < t_{M-1} < t_M = T$ be a partitioning of $[0, T]$ into possibly variable time steps $\tau_m := t_{m+1} - t_m, m = 0 \to M - 1$.
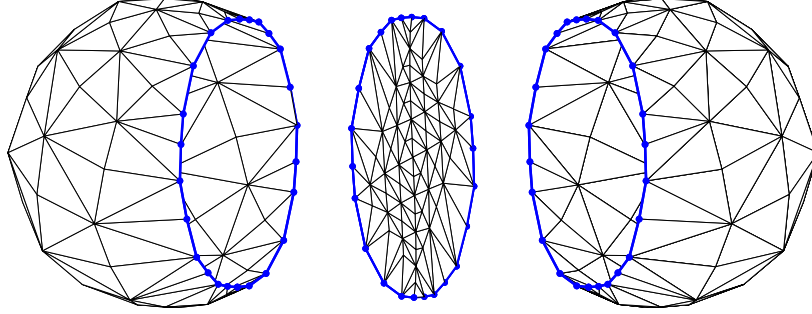
FIG. 4. Example triangulation Γ^m of a triple bubble with polygonal triple junction line $\mathcal{T}_1^m$, where $Z_1 = 24$.

The surfaces Γ_i^m are now given by their parameterizations $\vec{X}_i^m$, $i = 1 \to I_S$, where $\vec{X}^m \in \underline{V}^h(\Omega^h)$. We set $\Gamma^m := \vec{X}^m(\Omega^h)$ and observe that, with the above definitions, the polygonal curves $\mathcal{T}_k^m$ defined by the ordered sequence of vertices $(\vec{X}_{s_1^k}^m(\vec{\rho}_1^k(1)), \ldots,$ $\vec{X}_{s_1^k}^m(\vec{\rho}_1^k(Z_k)))$, $k = 1 \to I_T$, are the triple junction lines of the polyhedral surface cluster Γ^m; see Figure 4 for an example. These will now be used to defined the necessary finite element spaces on Γ^m. Let $\sigma_j^{m,i} := \vec{X}_i^m(\sigma_j^i)$ and similarly $\vec{q}_k^{m,i} := \vec{X}_i^m(\vec{q}_k^i)$. Then we define

$$\underline{\widehat{V}}^h(\Gamma^m) := \left\{ \vec{\chi} \in \underset{i=1}{\overset{I_S}{\times}} C(\Gamma_i^m, \mathbb{R}^3) : \vec{\chi}_i \mid_{\sigma_j^{m,i}} \text{ is linear for } j = 1 \to J_i, \, i = 1 \to I_S \right\}$$
$$=: [\widehat{W}^h(\Gamma^m)]^3, \quad (4.3)$$

where $\widehat{W}^h(\Gamma^m) \subset \times_{i=1}^{I_S} H^1(\Gamma_i^m, \mathbb{R})$ is the space of scalar continuous piecewise linear functions on Γ^m, with $\{\{\phi_k^{m,i}\}_{k=1}^{K_i}\}_{i=1}^{I_S}$ denoting the standard basis of $\widehat{W}^h(\Gamma^m)$, i.e. $\phi_l^{m,i}(\vec{q}_k^{m,i}) = \delta_{kl}$ for all $k, l = 1 \to K_i$, $i = 1 \to I_S$. Then $\underline{V}^h(\Gamma^m)$ and $W^h(\Gamma^m)$, the natural discrete analogues of $\underline{V}(\Gamma)$ and $W(\Gamma)$, are defined by

$$\underline{V}^h(\Gamma^m) := \{\vec{\chi} \in \underline{\widehat{V}}^h(\Gamma^m) : \vec{\chi}_{s_1^k} = \vec{\chi}_{s_2^k} = \vec{\chi}_{s_3^k} \text{ on } \mathcal{T}_k^m, \, k = 1 \to I_T\}, \quad (4.4a)$$

$$W^h(\Gamma^m) := \left\{ \chi \in \widehat{W}^h(\Gamma^m) : \sum_{j=1}^{3} o_j^k \chi_{s_j^k} = 0 \text{ on } \mathcal{T}_k^m, \, k = 1 \to I_T \right\}. \quad (4.4b)$$

For notational convenience we will often not distinguish whether a surface is parameterized over Ω^h or over Γ^m. For instance, we will use $\vec{X}^m$ also to denote the identity $\text{id} \mid_{\Gamma^m} \in \underline{V}^h(\Gamma^m)$ on Γ^m and similarly use the symbol $\vec{X}^{m+1}$ also to denote the parameterization of Γ^{m+1} over Γ^m, i.e. formally $\Gamma^{m+1} = \vec{X}^{m+1}(\Gamma^m)$.

Similarly to (2.7), we introduce the L^2 inner product $\langle \cdot, \cdot \rangle_m$ over the current polyhedral surface cluster Γ^m, which is described by the vector function $\vec{X}^m$, as follows:

$$\langle u, v \rangle_m := \sum_{i=1}^{I_S} \int_{\Gamma_i^m} u_i \cdot v_i \, d\mathcal{H}^2. \quad (4.5)$$

If u, v are piecewise continuous, with possible jumps across the edges of $\{\sigma_j^{m,i}\}_{j=1}^{J_i}$, $i = 1 \to I_S$, we introduce the mass lumped inner product $\langle \cdot, \cdot \rangle_m^h$ as

$$\langle u, v \rangle_m^h := \sum_{i=1}^{I_S} \frac{1}{3} \sum_{j=1}^{J_i} |\sigma_j^{m,i}| \sum_{k=0}^{2} \lim_{\sigma_j^{m,i} \ni \vec{p} \to \vec{q}_{j_k}^{m,i}} (u_i . v_i)(\vec{p}),$$

where $\{\vec{q}_{j_k}^{m,i}\}_{k=0}^2$ are the vertices of $\sigma_j^{m,i}$. Here $|\sigma_j^{m,i}| = \frac{1}{2}|(\vec{q}_{j_1}^{m,i} - \vec{q}_{j_0}^{m,i}) \wedge (\vec{q}_{j_2}^{m,i} - \vec{q}_{j_0}^{m,i})|$ is the measure of $\sigma_j^{m,i}$. In addition, we introduce the unit normal $\vec{v}_i^m$ to Γ_i^m:

$$\vec{v}_{i,j}^m := \vec{v}_i^m|_{\sigma_j^{m,i}} := \frac{(\vec{q}_{j_1}^{m,i} - \vec{q}_{j_0}^{m,i}) \wedge (\vec{q}_{j_2}^{m,i} - \vec{q}_{j_0}^{m,i})}{|(\vec{q}_{j_1}^{m,i} - \vec{q}_{j_0}^{m,i}) \wedge (\vec{q}_{j_2}^{m,i}) - \vec{q}_{j_0}^{m,i})|},$$

where we have assumed that the vertices $\{\vec{q}_{j_k}^{m,i}\}_{k=0}^2$ are ordered with the same orientation for all $\sigma_j^{m,i}$, $j = 1 \to J_i$. Finally, we set $|\cdot|_m^2 := \langle \cdot, \cdot \rangle_m$ and $|\cdot|_{m,h}^2 := \langle \cdot, \cdot \rangle_m^h$.

Then we introduce the following parametric finite element approximations of (2.10a,b) and (2.11a,b): Find $\vec{X}^{m+1} \in \underline{V}^h(\Gamma^m)$ and $\kappa^{m+1} \in \widehat{W}^h(\Gamma^m)$ such that

$$\left\langle \frac{\vec{X}^{m+1} - \vec{X}^m}{\tau_m}, \chi \vec{v}^m \right\rangle_m^h - \langle \kappa^{m+1}, \chi \rangle_m^h = 0 \quad \forall \chi \in \widehat{W}^h(\Gamma^m), \tag{4.6a}$$

$$\langle \kappa^{m+1} \vec{v}^m, \vec{\eta} \rangle_m^h + \langle \nabla_s \vec{X}^{m+1}, \nabla_s \vec{\eta} \rangle_m = 0 \quad \forall \vec{\eta} \in \underline{V}^h(\Gamma^m). \tag{4.6b}$$

Find $\vec{X}^{m+1} \in \underline{V}^h(\Gamma^m)$ and $\kappa^{m+1} \in W^h(\Gamma^m)$ such that

$$\left\langle \frac{\vec{X}^{m+1} - \vec{X}^m}{\tau_m}, \chi \vec{v}^m \right\rangle_m^h - \langle \nabla_s \kappa^{m+1}, \nabla_s \chi \rangle_m = 0 \quad \forall \chi \in W^h(\Gamma^m), \tag{4.7a}$$

$$\langle \kappa^{m+1} \vec{v}^m, \vec{\eta} \rangle_m^h + \langle \nabla_s \vec{X}^{m+1}, \nabla_s \vec{\eta} \rangle_m = 0 \quad \forall \vec{\eta} \in \underline{V}^h(\Gamma^m). \tag{4.7b}$$

Following the novel approximations introduced in [12], we can generalize the above schemes to their anisotropic counterparts. On recalling (2.22a,b) and (2.23a,b) we introduce the following fully practical parametric finite element approximations: Find $\vec{X}^{m+1} \in \underline{V}^h(\Gamma^m)$ and $\kappa_\gamma^{m+1} \in \widehat{W}^h(\Gamma^m)$ such that

$$\left\langle \frac{\vec{X}^{m+1} - \vec{X}^m}{\tau_m}, \chi \vec{v}^m \right\rangle_m^h - \langle \beta(\vec{v}^m) \kappa_\gamma^{m+1}, \chi \rangle_m^h = 0 \quad \forall \chi \in \widehat{W}^h(\Gamma^m), \tag{4.8a}$$

$$\langle \kappa_\gamma^{m+1} \vec{v}^m, \vec{\eta} \rangle_m^h + \langle \nabla_s^{\widetilde{G}} \vec{X}^{m+1}, \nabla_s^{\widetilde{G}} \vec{\eta} \rangle_{\gamma,m} = 0 \quad \forall \vec{\eta} \in \underline{V}^h(\Gamma^m). \tag{4.8b}$$

Find $\vec{X}^{m+1} \in \underline{V}^h(\Gamma^m)$ and $\kappa_\gamma^{m+1} \in W^h(\Gamma^m)$ such that

$$\left\langle \frac{\vec{X}^{m+1} - \vec{X}^m}{\tau_m}, \chi \vec{v}^m \right\rangle_m^h - \langle \beta(\vec{v}^m) \nabla_s \kappa_\gamma^{m+1}, \nabla_s \chi \rangle_m = 0 \quad \forall \chi \in W^h(\Gamma^m), \tag{4.9a}$$

$$\langle \kappa_\gamma^{m+1} \vec{v}^m, \vec{\eta} \rangle_m^h + \langle \nabla_s^{\widetilde{G}} \vec{X}^{m+1}, \nabla_s^{\widetilde{G}} \vec{\eta} \rangle_{\gamma,m} = 0 \quad \forall \vec{\eta} \in \underline{V}^h(\Gamma^m). \tag{4.9b}$$

Here $\langle \nabla_s^{\widetilde{G}} \cdot , \nabla_s^{\widetilde{G}} \cdot \rangle_{\gamma,m}$ is the discrete inner product defined by

$$\langle \nabla_s^{\widetilde{G}} \vec{\eta}, \nabla_s^{\widetilde{G}} \vec{\chi} \rangle_{\gamma,m} := \sum_{i=1}^{I_S} \sum_{\ell=1}^{L_i} \int_{\Gamma_i^m} \left[\frac{\gamma_i^{(\ell)}(\vec{v}_i^{m+1})}{\gamma_i(\vec{v}_i^{m+1})} \right]^{r_i - 1} (\nabla_s^{\widetilde{G}_i^{(\ell)}} \vec{\eta}_i, \nabla_s^{\widetilde{G}_i^{(\ell)}} \vec{\chi}_i)_{\widetilde{G}_i^{(\ell)}} \gamma_i^{(\ell)}(\vec{v}_i^m) \, d\mathcal{H}^2. \qquad (4.10)$$

Note that (4.10) is a natural discrete analogue of (2.24a); see [12] for details. The particular choice of normals from the old surface cluster, Γ^m, and the new cluster, Γ^{m+1}, ensures that the solutions to (4.8a,b) and (4.9a,b) are unconditionally stable; see Theorem 4.2 below. Note that this particular choice leads in general to a nonlinear system for $(\vec{X}^{m+1}, \kappa_\gamma^{m+1})$. However, the simpler case $r = (1, \ldots, 1)$ leads to a linear system for $(\vec{X}^{m+1}, \kappa_\gamma^{m+1})$. Finally, observe that in the isotropic case, $\gamma = (|\cdot|, \ldots, |\cdot|)$, the anisotropic schemes above collapse to their isotropic equivalents (4.6a,b) and (4.7a,b), respectively.

REMARK 4.1 The schemes (4.6a,b), (4.7a,b) as well as (4.8a,b) and (4.9a,b) are the natural extensions to surface clusters of the finite element approximations for the isotropic and anisotropic evolution of curve networks in the plane considered in [7, 6] and [9], respectively. Here it should be noted that in the formulations in the former two papers, for the case of isotropic surface energies (2.14) with $\beta = (1, \ldots, 1)$, the analogue of (4.4b) features the constraints $\sum_{j=1}^{3} \varsigma_j o_j^k \chi_{s_j^k} = 0$, while in place of (4.5) the inner product $\langle \cdot, \cdot \rangle_{\widetilde{m}} := \langle \varsigma \cdot, \cdot \rangle_m$ is used throughout. It is easy to see that this yields an equivalent reformulation of the natural two-dimensional analogues of (4.8a,b) and (4.9a,b), previously introduced in [9], for the isotropic case (2.14) with $\beta = (1, \ldots, 1)$.

Finally, the schemes (4.8a,b) and (4.9a,b) can easily be extended to the case when boundary intersections are present. Let $\partial \mathcal{D}$ be given by a function $F \in C^1(\mathbb{R}^3)$ such that

$$\partial \mathcal{D} = \{ \vec{z} \in \mathbb{R}^3 : F(\vec{z}) = 0 \} \quad \text{and} \quad |\nabla F(\vec{z})| = 1 \quad \forall \vec{z} \in \partial \mathcal{D},$$

and let the discrete analogue of $\underline{V}_\partial(\Gamma)$ be defined as

$$\underline{V}_\partial^h(\Gamma^m) := \{ \vec{\chi} \in \underline{V}^h(\Gamma^m) : \nabla F(\vec{q}) \cdot \vec{\chi}_{s_k}(\vec{q}) = 0 \quad \forall \vec{q} \in \mathcal{B}_k^m, \ k = 1 \to I_B \}, \qquad (4.11)$$

where $\mathcal{B}_k^m := \{ \vec{q}_l^{m,s_k} \}_{l=1}^{K_{s_k}} \cap \vec{X}_{s_k}^m(\partial_{p_k} \Omega_{s_k}^h)$. Then we introduce the following approximations: Find $\delta \vec{X}^{m+1} \in \underline{V}_\partial^h(\Gamma^m)$ and $\kappa_\gamma^{m+1} \in \widehat{W}^h(\Gamma^m)$, where $\vec{X}^{m+1} := \vec{X}^m + \delta \vec{X}^{m+1}$, such that

$$\left\langle \frac{\delta \vec{X}^{m+1}}{\tau_m}, \chi \vec{v}^m \right\rangle_m^h - \langle \beta(\vec{v}^m) \kappa_\gamma^{m+1}, \chi \rangle_m^h = 0 \quad \forall \chi \in \widehat{W}^h(\Gamma^m), \qquad (4.12a)$$

$$\langle \kappa_\gamma^{m+1} \vec{v}^m, \vec{\eta} \rangle_m^h + \langle \nabla_s^{\widetilde{G}} \vec{X}^{m+1}, \nabla_s^{\widetilde{G}} \vec{\eta} \rangle_{\gamma,m} = 0 \quad \forall \vec{\eta} \in \underline{V}_\partial^h(\Gamma^m). \qquad (4.12b)$$

Find $\delta \vec{X}^{m+1} \in \underline{V}_\partial^h(\Gamma^m)$ and $\kappa_\gamma^{m+1} \in W^h(\Gamma^m)$, where $\vec{X}^{m+1} := \vec{X}^m + \delta \vec{X}^{m+1}$, such that

$$\left\langle \frac{\delta \vec{X}^{m+1}}{\tau_m}, \chi \vec{v}^m \right\rangle_m^h - \langle \beta(\vec{v}^m) \nabla_s \kappa_\gamma^{m+1}, \nabla_s \chi \rangle_m = 0 \quad \forall \chi \in W^h(\Gamma^m), \qquad (4.13a)$$

$$\langle \kappa_\gamma^{m+1} \vec{v}^m, \vec{\eta} \rangle_m^h + \langle \nabla_s^{\widetilde{G}} \vec{X}^{m+1}, \nabla_s^{\widetilde{G}} \vec{\eta} \rangle_{\gamma,m} = 0 \quad \forall \vec{\eta} \in \underline{V}_\partial^h(\Gamma^m). \qquad (4.13b)$$

We note that the constraint $\delta \vec{X}^{m+1} \in \underline{V}_\partial^h(\Gamma^m)$ weakly approximates (2.25), as it is a linearized approximation of these constraints. In particular, for curved boundaries $\partial \mathcal{D}$ the equations

$$F(\vec{X}_{s_k}^{m+1}) = 0 \quad \text{on } \partial_{p_k} \Omega_{s_k}^h, \quad k = 1 \to I_B, \qquad (4.14)$$

are only approximately satisfied; see e.g. [6] for more details in the planar isotropic case. As a remedy, one could employ a projection step that orthogonally projects $\vec{X}^{m+1}$ onto $\partial\mathcal{D}$ at every time step, which would have the advantage of satisfying (4.14) exactly throughout the evolution. But in general this would result in a loss of our stability bound (see Theorem 4.4 below); hence our preference for the stated approximations.

On noting that $\underline{V}^h_\partial(\Gamma^m) \equiv \underline{V}^h(\Gamma^m)$ if $I_B = 0$, it follows that the schemes (4.12a,b) and (4.13a,b) collapse to (4.8a,b) and (4.9a,b) in this case.

Before we can proceed to prove existence and uniqueness to these approximations, we have to make the following very mild assumption on the triangulations at each time level:

($\mathcal{A}$) We assume for $m = 0 \to M$ and $i = 1 \to I_S$ that $|\det[D\vec{X}^m_i]^T[D\vec{X}^m_i]| > 0$ almost everywhere in Ω^h_i, so that $|\sigma^{m,i}_j| = |\vec{X}^m_i(\sigma^i_j)| > 0$, $j = 1 \to J_i$.

For $k = 1 \to K_i$, let $\Xi^{m,i}_k := \{\sigma^{m,i}_j : \vec{q}^{m,i}_k \in \overline{\sigma^{m,i}_j}\}$ and set

$$\Lambda^{m,i}_k := \bigcup_{\sigma^{m,i}_j \in \Xi^{m,i}_k} \overline{\sigma^{m,i}_j} \quad \text{and} \quad \vec{\omega}^m_{i,k} := \frac{1}{|\Lambda^{m,i}_k|} \sum_{\sigma^i_j \in \Xi^{m,i}_k} |\sigma^{m,i}_j| \, \vec{v}^m_{i,j}.$$

Then we assume further that for each $i = 1 \to I_S$ there exists a $k \in \{1, \ldots, \overline{K}_i\}$ such that $\vec{\omega}^m_{i,k} \neq \vec{0}$. Moreover, we require that $\dim U^m = 3$, $m = 0 \to M - 1$, where $U^m := \text{span}\{\{\vec{\omega}^m_{i,k}\}^{\overline{K}_i}_{k=1}\}^{I_S}_{i=1} \cup \{\{\nabla F(\vec{q})\}_{\vec{q} \in \mathcal{B}^m_k}\}^{I_B}_{k=1}$.

We stress that ($\mathcal{A}$) is a very weak assumption. It merely states that (a) the triangles of the polyhedral surface cluster Γ^m have positive area, (b) on each of the surfaces Γ^m_i, $i = 1 \to I_S$, at least one inner vertex normal $\vec{\omega}^m_{i,k}$ is nonzero, and (c) among all the inner vertex normals $\vec{\omega}^m_{i,k}$ and all the boundary constraint vectors $\nabla F(\vec{q})$ there are three linearly independent vectors. The latter condition is only violated in very pathological cases, e.g. when all the surfaces overlap identically on a flat external boundary, and it never occurred in practice.

THEOREM 4.1 Let the assumption ($\mathcal{A}$) hold. Then there exist unique solutions $(\vec{X}^{m+1}, \kappa^{m+1}) \in \underline{V}^h(\Gamma^m) \times \widehat{W}^h(\Gamma^m)$ to the system (4.6a,b); and $(\vec{X}^{m+1}, \kappa^{m+1}) \in \underline{V}^h(\Gamma^m) \times W^h(\Gamma^m)$ to (4.7a,b).

Proof. This follows directly from Theorem 4.3 below. □

THEOREM 4.2 Let the assumptions ($\mathcal{A}$) hold, and $\{(\vec{X}^m, \kappa^m)\}^M_{m=1}$ be the unique solution to (4.7a,b). Then for $k = 1 \to M$ we have

$$|\Gamma^k| + \sum^{k-1}_{m=0} \tau_m |\nabla_s \kappa^{m+1}|^2_m \leqslant |\Gamma^0|. \tag{4.15a}$$

Similarly, the unique solution to (4.6a,b) satisfies, for $k = 1 \to M$,

$$|\Gamma^k| + \sum^{k-1}_{m=0} \tau_m |\kappa^{m+1}|^2_{m,h} \leqslant |\Gamma^0|. \tag{4.15b}$$

Proof. Clearly, the result directly follows from Theorem 4.4 below. For the benefit of the reader, we also give a separate proof for the isotropic case. We first consider (4.15a). Choosing $\chi = \kappa^{m+1} \in$

$W^h(\Gamma^m)$ in (4.7a) and $\vec{\eta} = \frac{\vec{X}^{m+1} - \vec{X}^m}{\tau_m} \in \underline{V}^h(\Gamma^m)$ in (4.7b) yields

$$\langle \nabla_s \vec{X}^{m+1}, \nabla_s(\vec{X}^{m+1} - \vec{X}^m)\rangle_m + \tau_m |\nabla_s \kappa^{m+1}|_m^2 = 0. \tag{4.16}$$

It follows from Lemma 2.1 in [10], on noting that $\vec{X}^m \equiv \vec{\mathrm{id}}$ on Γ^m, that

$$\langle \nabla_s \vec{X}^{m+1}, \nabla_s(\vec{X}^{m+1} - \vec{X}^m)\rangle_m = \tfrac{1}{2}[|\nabla_s \vec{X}^{m+1}|_m^2 - |\nabla_s \vec{X}^m|_m^2 + |\nabla_s(\vec{X}^{m+1} - \vec{X}^m)|_m^2]$$
$$\geqslant |\Gamma^{m+1}| - |\Gamma^m| + \tfrac{1}{2}|\nabla_s(\vec{X}^{m+1} - \vec{X}^m)|_m^2. \tag{4.17}$$

Combining (4.16) and (4.17) yields

$$|\Gamma^{m+1}| - |\Gamma^m| + \tau_m |\nabla_s \kappa^{m+1}|_m^2 + \tfrac{1}{2}|\nabla_s(\vec{X}^{m+1} - \vec{X}^m)|_m^2 \leqslant 0. \tag{4.18}$$

Summing (4.18) for $m = 0 \to k - 1$ yields the desired result. The steps of the proof of (4.15b) are exactly the same. $\qquad\square$

THEOREM 4.3 Let the assumption $(\mathcal{A})$ hold and let $r = (1, \ldots, 1)$. Then there exist unique solutions $(\vec{X}^{m+1}, \kappa_\gamma^{m+1}) \in \underline{V}^h(\Gamma^m) \times \widehat{W}^h(\Gamma^m)$ to the system (4.8a,b); and $(\vec{X}^{m+1}, \kappa_\gamma^{m+1}) \in \underline{V}^h(\Gamma^m) \times W^h(\Gamma^m)$ to (4.9a,b). Moreover, there exist unique solutions $(\delta\vec{X}^{m+1}, \kappa_\gamma^{m+1}) \in \underline{V}_\partial^h(\Gamma^m) \times \widehat{W}^h(\Gamma^m)$ to the system (4.12a,b); and $(\delta\vec{X}^{m+1}, \kappa_\gamma^{m+1}) \in \underline{V}_\partial^h(\Gamma^m) \times W^h(\Gamma^m)$ to (4.13a,b).

Proof. As (4.8a,b) is linear, existence follows from uniqueness. To investigate the latter, we consider the system: Find $\{\vec{X}, \kappa_\gamma\} \in \underline{V}^h(\Gamma^m) \times \widehat{W}^h(\Gamma^m)$ such that

$$\langle \vec{X}, \chi \vec{\nu}^m \rangle_m^h - \tau_m \langle \beta(\vec{\nu}^m)\kappa_\gamma, \chi \rangle_m^h = 0 \quad \forall \chi \in \widehat{W}^h(\Gamma^m), \tag{4.19a}$$

$$\langle \kappa_\gamma \vec{\nu}^m, \vec{\eta} \rangle_m^h + \sum_{i=1}^{I_S} \sum_{\ell=1}^{L_i} \int_{\Gamma_i^m} (\nabla_s^{\widetilde{G}_i^{(\ell)}} \vec{X}_i, \nabla_s^{\widetilde{G}_i^{(\ell)}} \vec{\eta}_i)_{\widetilde{G}_i^{(\ell)}} \gamma_i^{(\ell)}(\vec{\nu}_i^m)\, \mathrm{d}\mathcal{H}^2 = 0 \quad \forall \vec{\eta} \in \underline{V}^h(\Gamma^m). \tag{4.19b}$$

Choosing $\chi = \kappa_\gamma \in \widehat{W}^h(\Gamma^m)$ in (4.19a) and $\vec{\eta} = \vec{X} \in \underline{V}^h(\Gamma^m)$ in (4.19b) yields

$$\sum_{i=1}^{I_S} \sum_{\ell=1}^{L_i} \int_{\Gamma_i^m} (\nabla_s^{\widetilde{G}_i^{(\ell)}} \vec{X}_i, \nabla_s^{\widetilde{G}_i^{(\ell)}} \vec{X}_i)_{\widetilde{G}_i^{(\ell)}} \gamma_i^{(\ell)}(\vec{\nu}_i^m)\, \mathrm{d}\mathcal{H}^2 + \tau_m \langle \beta(\vec{\nu}^m)\kappa_\gamma, \kappa_\gamma \rangle_m^h = 0. \tag{4.20}$$

It follows from (4.20), (2.24b), the positive definiteness of $\widetilde{G}_i^{(\ell)}$, $\ell = 1 \to L_i$, $i = 1 \to I_S$, and the positivity of β that $\kappa_\gamma = (0, \ldots, 0)$ and, on noting $\vec{X} \in \underline{V}^h(\Gamma^m)$ and the connectedness of Γ^m, that $\vec{X}_i \equiv \vec{X}^c \in \mathbb{R}^3$, $i = 1 \to I_S$. Hence it follows that

$$\langle \vec{X}^c, \chi \vec{\nu}^m \rangle_m^h = 0 \quad \forall \chi \in \widehat{W}^h(\Gamma^m). \tag{4.21}$$

Choosing $\chi = (0, \ldots, 0, \phi_k^{m,i}, 0, \ldots, 0)$ in (4.21) yields

$$\vec{X}^c \cdot \vec{\omega}_{i,k}^m = 0, \quad k = 1 \to \overline{K}_i, \, i = 1 \to I_S. \tag{4.22}$$

It follows from assumption $(\mathcal{A})$ that $\vec{X}^c = \vec{0}$. Hence we have shown that there exists a unique solution $(\vec{X}^{m+1}, \kappa_\gamma^{m+1}) \in \underline{V}^h(\Gamma^m) \times \widehat{W}^h(\Gamma^m)$ to (4.8a,b).

The corresponding proof for the system (4.9a,b) is similar with only a minor modification. In particular, following the same argument we obtain (4.20) with the second term replaced by $\tau_m \langle \beta(\vec{v}^m) \nabla_s \kappa_\gamma, \nabla_s \kappa_\gamma \rangle_m$, which implies that $\kappa_{\gamma,i} \equiv \kappa_i^c \in \mathbb{R}$ and $\vec{X}_i \equiv \vec{X}^c \in \mathbb{R}^3$, $i = 1 \to I_S$. Hence

$$\langle \kappa^c \vec{\nu}^m, \vec{\eta} \rangle_m^h = 0 \quad \forall \vec{\eta} \in \underline{V}^h(\Gamma^m). \tag{4.23}$$

For a fixed $i = 1 \to I_S$, choosing $\vec{\eta} = (0, \ldots, 0, \vec{z}\phi_k^{m,i}, 0, \ldots, 0)$, $k = 1 \to \overline{K}_i$, in (4.23) implies, on assuming $\kappa_i^c \neq 0$, that for $k = 1 \to \overline{K}_i$

$$\vec{\omega}_{i,k}^m \cdot \vec{z} = 0 \; \forall \vec{z} \in \mathbb{R}^3 \; \Rightarrow \; \vec{\omega}_{i,k}^m = \vec{0}.$$

However, this contradicts assumption $(\mathcal{A})$ and hence $\kappa_i^c = 0$, $i = 1 \to I_S$, i.e. $\kappa_\gamma = (0, \ldots, 0)$. Now $\vec{X} = (\vec{0}, \ldots, \vec{0})$ follows as before, and so there exists a unique solution $(\vec{X}^{m+1}, \kappa_\gamma^{m+1}) \in \underline{V}^h(\Gamma^m) \times W^h(\Gamma^m)$ to (4.9a,b).

Finally, the proofs for (4.12a,b) and (4.13a,b) are virtually identical with $\underline{V}^h(\Gamma^m)$ replaced by $\underline{V}_\partial^h(\Gamma^m)$. Here we note that in addition to (4.22), it follows from $\vec{X} \in \underline{V}_\partial^h(\Gamma^m)$ that $\vec{X}^c \cdot \nabla F(\vec{q}) = 0$ for $\vec{q} \in \mathcal{B}_k^m$, $k = 1 \to I_B$, and so it follows from assumption $(\mathcal{A})$ that $\vec{X}^c = \vec{0}$. Hence there exist unique solutions to (4.12a,b) and (4.13a,b). □

THEOREM 4.4   Let the assumption $(\mathcal{A})$ hold, and let $\{(\vec{X}^m, \kappa_\gamma^m)\}_{m=1}^M$ be a solution to (4.9a,b) or (4.13a,b). Then for $k = 1 \to M$ we have

$$|\Gamma^k|_\gamma + \sum_{m=0}^{k-1} \tau_m \langle \beta(\vec{v}^m) \nabla_s \kappa_\gamma^{m+1}, \nabla_s \kappa_\gamma^{m+1} \rangle_m \leqslant |\Gamma^0|_\gamma. \tag{4.24a}$$

Similarly, the solutions to (4.8a,b) and (4.12a,b) satisfy, for $k = 1 \to M$,

$$|\Gamma^k|_\gamma + \sum_{m=0}^{k-1} \tau_m \langle \beta(\vec{v}^m) \kappa_\gamma^{m+1}, \kappa_\gamma^{m+1} \rangle_m^h \leqslant |\Gamma^0|_\gamma. \tag{4.24b}$$

Proof. As the four proofs are almost identical, it is sufficient to show (4.24a) for the approximation (4.9a,b). Choosing $\chi = \kappa_\gamma^{m+1} \in W^h(\Gamma^m)$ in (4.9a) and $\vec{\eta} = (\vec{X}^{m+1} - \vec{X}^m)/\tau_m \in \underline{V}^h(\Gamma^m)$ in (4.9b) yields

$$\langle \nabla_s^{\widetilde{G}} \vec{X}^{m+1}, \nabla_s^{\widetilde{G}}(\vec{X}^{m+1} - \vec{X}^m) \rangle_{\gamma,m} + \tau_m \langle \beta(\vec{v}^m) \nabla_s \kappa_\gamma^{m+1}, \nabla_s \kappa_\gamma^{m+1} \rangle_m = 0. \tag{4.25}$$

It follows from [12, Lemma 3.1], similarly to the proof of Theorem 3.2 in [12], on noting that $\vec{X}^m \equiv \text{id}$ on Γ^m, that

$$\langle \nabla_s^{\widetilde{G}} \vec{X}^{m+1}, \nabla_s^{\widetilde{G}}(\vec{X}^{m+1} - \vec{X}^m) \rangle_{\gamma,m} \geqslant |\Gamma^{m+1}|_\gamma - |\Gamma^m|_\gamma. \tag{4.26}$$

Combining (4.25) and (4.26) yields

$$|\Gamma^{m+1}|_\gamma - |\Gamma^m|_\gamma + \tau_m \langle \beta(\vec{v}^m) \nabla_s \kappa_\gamma^{m+1}, \nabla_s \kappa_\gamma^{m+1} \rangle_m \leqslant 0. \tag{4.27}$$

Summing (4.27) for $m = 0 \to k - 1$ yields the desired result (4.24a). □

REMARK 4.2 Similarly to the semidiscrete approximations considered in e.g. [10, 12], it is possible to derive certain properties for semidiscrete continuous-in-time versions of the finite element approximations considered in this paper. Firstly, one can show that these semidiscrete variants of our schemes maintain "good mesh properties". For instance, assuming that the spatially discrete cluster $\Gamma^h(t)$ is the solution to the semidiscrete variant of (4.7a,b), each surface $\Gamma_i^h(t)$, $i = 1 \rightarrow I_S$, is a *conformal polyhedral surface*; see [10, §4] for details. Such surfaces are characterized by the fact that the two popular notions of discrete vertex normals, given by the directions of steepest descent of area and volume, respectively, coincide; which in turn means that the triangulation cannot be bad. Related properties can be derived for anisotropic surface energies. Moreover, the semidiscrete versions of (4.7a,b) and (4.9a,b) maintain the enclosed volumes exactly. To illustrate this, we use the same example as in Remark 3.1 and find, on choosing $\chi = (1, -1, 0) \in W^h(\Gamma^h(t))$ in the semidiscrete version of (4.9a), where all integration is over the current cluster $\Gamma^h(t)$, parameterized by $\vec{X}(t) \in \underline{V}^h(\Omega^h)$, with normals $\vec{v}^h$, that

$$0 = \int_{\Gamma_1^h} [\vec{X}_1]_t \cdot \vec{v}_1^h \, d\mathcal{H}^2 - \int_{\Gamma_2^h} [\vec{X}_2]_t \cdot \vec{v}_2^h \, d\mathcal{H}^2 = \frac{d}{dt} \mathcal{L}^3(v^h),$$

where v^h denotes the volume enclosed by the two polyhedral surfaces Γ_1^h and Γ_2^h. We remark that in practice these properties are (approximately) inherited by our fully discrete schemes. As a result, no heuristic redistribution of mesh points is necessary in practice. Moreover, in all of our numerical experiments, the maximum observed relative volume loss for (4.7a,b) and (4.9a,b) was always less than 1%.

REMARK 4.3 Our fully practical finite element approximation of the volume preserving mean curvature flow (3.17) for the double bubble in Figure 5 below is: Find $\vec{X}^{m+1} \in \underline{V}^h(\Gamma^m)$, $\kappa^{m+1} \in \widehat{W}^h(\Gamma^m)$ and $\lambda_i^{m+1} \in \mathbb{R}$, $i = 1 \rightarrow 3$, with $\lambda^{m+1} \in W^h(\Gamma^m)$, such that

$$\left\langle \frac{\vec{X}^{m+1} - \vec{X}^m}{\tau_m}, \chi \vec{v}^m \right\rangle_m^h - \langle \kappa^{m+1} - \lambda^{m+1}, \chi \rangle_m^h = 0 \quad \forall \chi \in \widehat{W}^h(\Gamma^m), \tag{4.28a}$$

$$\langle \kappa^{m+1} \vec{v}^m, \vec{\eta} \rangle_m^h + \langle \nabla_s \vec{X}^{m+1}, \nabla_s \vec{\eta} \rangle_m = 0 \quad \forall \vec{\eta} \in \underline{V}^h(\Gamma^m), \tag{4.28b}$$

where

$$\int_{\Gamma_1^m} (\kappa_1^{m+1} - \lambda_1^{m+1}) \, d\mathcal{H}^2 = \int_{\Gamma_2^m} (\kappa_2^{m+1} - \lambda_2^{m+1}) \, d\mathcal{H}^2 = \int_{\Gamma_3^m} (\kappa_3^{m+1} - \lambda_3^{m+1}) \, d\mathcal{H}^2. \tag{4.28c}$$

As (4.28a–c) requires a linear system to be solved at each time level, existence and uniqueness results are easily established. Moreover, on noting that $\langle \kappa^{m+1} - \lambda^{m+1}, \lambda^{m+1} \rangle_m^h = 0$, the analogue of (4.15b) holds, i.e. for $k = 1 \rightarrow M$,

$$|\Gamma^k| + \sum_{m=0}^{k-1} \tau_m |\kappa^{m+1} - \lambda^{m+1}|_{m,h}^2 \leqslant |\Gamma^0|. \tag{4.29}$$

Here we remark that a simpler linear system, that in practice is as easy to solve as (4.6a,b), can be obtained by replacing κ_i^{m+1} in (4.28c) with κ_i^m. But for this simpler scheme no stability can be established, i.e. (4.29) does not hold. The corresponding approximation for a single surface enclosing a single volume was employed and introduced by the authors in [10]. Similarly to Remark 4.2, it can be shown that a semidiscrete variant of (4.28a–c) conserves volume, while the fully discrete approximation (4.28a–c) will do so only approximately.

5. Solution of the discrete systems

Let $K := \sum_{i=1}^{I_S} K_i$ and, for later reference, $J := \sum_{i=1}^{I_S} J_i$. In addition, for any number $n \in \mathbb{N}$, let $Id_n \in \mathbb{R}^{n \times n}$ be the identity matrix, and similarly for $\vec{Id}_n \in (\mathbb{R}^{d \times d})^{n \times n}$. We define the orthogonal projection $\vec{\mathcal{P}} : (\mathbb{R}^3)^K \to \mathbb{X}$ onto the Euclidean space associated with $\underline{V}^h(\Gamma^m)$, and similarly $\mathcal{K} : \mathbb{R}^K \to \mathbb{X}$ the orthogonal projection onto the Euclidean space associated with $W^h(\Gamma^m)$. In particular, we have

$$\vec{\mathcal{P}} = \vec{Id}_K - \vec{\mathcal{Q}}\vec{\mathcal{Q}}^T \quad \text{and} \quad \mathcal{K} = Id_K - QQ^T, \tag{5.1}$$

where the columns of $\vec{\mathcal{Q}}$ and Q form an orthonormal basis of the orthogonal complements $\mathbb{X}^\perp$ in $(\mathbb{R}^3)^K$ and $\mathbb{X}^\perp$ in $\mathbb{R}^K$, respectively. The two projections $\mathcal{K}$ and $\vec{\mathcal{P}}$ will be crucial in the construction of fully practical solution methods for the finite element approximations introduced in Section 4. For instance, with the help of these two projections it will be sufficient throughout to work with the bases of the simple product finite element spaces $\widehat{W}^h(\Gamma^m)$ and $\widehat{\underline{V}}^h(\Gamma^m)$ (recall (4.3)), rather than having to work with the highly nontrivial trial and test spaces $W^h(\Gamma^m)$ and $\underline{V}^h(\Gamma^m)$ directly. This construction is similar to e.g. the standard technique used for an ODE with periodic boundary conditions. The analogous approach by the authors for the treatment of the evolution of curve networks in the plane can be found in e.g. [7].

REMARK 5.1 Before we introduce the linear systems satisfied by the coefficient vectors of our finite element solutions, where we note that the nonlinear approximations will be iteratively solved with the help of linear auxiliary problems, we remark on some practical issues related to the crucial projections $\mathcal{K}$ and $\vec{\mathcal{P}}$.

A valid strategy for the computation of e.g. $\vec{\mathcal{P}}$ (recall (5.1)) is to construct the columns of $\vec{\mathcal{Q}}$ directly by finding an orthonormal basis of $\mathbb{X}^\perp$. This can be achieved for instance by starting with a set of not necessarily linearly independent vectors that span $\mathbb{X}^\perp$ and then performing an orthogonalization procedure such as Gram–Schmidt. A possible set of such spanning vectors can be easily found on recalling (4.4a), and one advantage of this strategy is that no explicit a priori knowledge about the location of possible quadruple junction points is needed.

However, this approach soon becomes very inefficient, as the matrix $\vec{\mathcal{Q}}$ can be large in practice. On recalling (4.2) we note that the number of columns in $\vec{\mathcal{Q}}$ will be close to $6Z$, where $Z := \sum_{k=1}^{I_T} Z_k$. In fact, if $I_{QJ} \geq 0$ denotes the number of quadruple junction points, then one can show that $\dim(\mathbb{X}^\perp) = 6Z - 9I_{QJ}$. For example, for the experiment in Figure 18 below, we have $6Z = 1584$ and $\dim(\mathbb{X}^\perp) = 6Z - 36 = 1548$, while $3K = 21915$, meaning that $\vec{\mathcal{Q}}$ is a 21915×1548 matrix. Clearly, computing and applying the projection $\vec{\mathcal{P}}$ in this way is computationally expensive, especially because these projections have to be evaluated many times during the course of the employed iterative solution methods; see §5.1 below.

A better and far more efficient treatment is the following, where we assume that information about the I_{QJ} quadruple junction points and their location is available. In particular, we assume that for each quadruple junction point we are given a quadruple (j_1, j_2, j_3, j_4) identifying the four triple junction lines $\mathcal{T}_{j_i}$, $i = 1 \to 4$, that meet there. In addition, for the discretizations we are given for each line $\mathcal{T}_{j_i}$ the index l_{j_i} such that $\vec{X}_{s_k^{j_i}}^m(\vec{\rho}_k^{j_i}(l_{j_i}))$, $k = 1 \to 3$, is the quadruple junction point of Γ^m at which the discretizations $\mathcal{T}_{j_i}^m$ of $\mathcal{T}_{j_i}$, $i = 1 \to 4$, meet; recall (4.4a). It is not difficult to see that the action of $\vec{\mathcal{P}}$ is equivalent to several independent *local* projections, that each involve only very few vertices. In particular, a suitable permutation of its rows and columns, which first separates the coordinates and then groups together indices from different surfaces associated with the same

point on a triple junction line or with the same quadruple junction point, transforms $\vec{\mathcal{P}}$ into a block diagonal form, with only three types of blocks on the diagonal. These blocks are

$$(1)\,, \quad \tfrac{1}{3}\begin{pmatrix} 1 & 1 & 1 \\ 1 & 1 & 1 \\ 1 & 1 & 1 \end{pmatrix}, \quad \tfrac{1}{6}\begin{pmatrix} 1 & 1 & 1 & 1 & 1 & 1 \\ 1 & 1 & 1 & 1 & 1 & 1 \\ 1 & 1 & 1 & 1 & 1 & 1 \\ 1 & 1 & 1 & 1 & 1 & 1 \\ 1 & 1 & 1 & 1 & 1 & 1 \\ 1 & 1 & 1 & 1 & 1 & 1 \end{pmatrix}, \tag{5.2}$$

for vertices lying in the interior of a surface, vertices on a triple junction line that do not correspond to quadruple junction points and vertices that correspond to quadruple junction points, respectively. For the latter case we note that at a quadruple junction point exactly six distinct surfaces meet. Applying the local projections (5.2) is now straightforward and very efficient.

A similar approach can be applied to the projection $\mathcal{K}$. Once again we note that the constraints in (4.4b) mean that $\mathcal{K}$ is equivalent to several independent local projections. We leave the details to the interested reader but note that in diagonalized form the blocks of $\mathcal{K}$ may be of the form e.g.

$$(1)\,, \quad \tfrac{1}{3}\begin{pmatrix} 2 & -1 & -1 \\ -1 & 2 & -1 \\ -1 & -1 & 2 \end{pmatrix} \tag{5.3a}$$

for vertices lying in the interior of a surface and vertices on a triple junction line, say $\mathcal{T}_k^m$ with $o^k = (1, 1, 1)$, that do not correspond to quadruple junction points, respectively, and of the form e.g.

$$\tfrac{1}{4}\begin{pmatrix} 2 & 1 & 1 & -1 & 1 & 0 \\ 1 & 2 & 1 & 0 & -1 & 1 \\ 1 & 1 & 2 & 1 & 0 & -1 \\ -1 & 0 & 1 & 2 & -1 & -1 \\ 1 & -1 & 0 & -1 & 2 & -1 \\ 0 & 1 & -1 & -1 & -1 & 2 \end{pmatrix}, \quad \tfrac{1}{8}\begin{pmatrix} 4 & 2 & 2 & -2 & -2 & 0 \\ 2 & 3 & 3 & 1 & 1 & 0 \\ 2 & 3 & 3 & 1 & 1 & 0 \\ -2 & 1 & 1 & 3 & 3 & 0 \\ -2 & 1 & 1 & 3 & 3 & 0 \\ 0 & 0 & 0 & 0 & 0 & 0 \end{pmatrix}, \tag{5.3b}$$

for vertices that correspond to quadruple junction points; here similar blocks with slightly different signs are obtained for different choices of (o_1^k, o_2^k, o_3^k), $k = 1 \to I_T$. In particular, the examples in (5.3b) are induced by the choices

$$\begin{pmatrix} 1 & 0 & -1 & 1 & 0 & 0 \\ -1 & 1 & 0 & 0 & 1 & 0 \\ 0 & -1 & 1 & 0 & 0 & 1 \\ 0 & 0 & 0 & 1 & 1 & 1 \end{pmatrix} \quad \text{and} \quad \begin{pmatrix} 1 & -1 & 0 & 1 & 0 & 0 \\ 1 & 0 & -1 & 0 & 1 & 0 \\ 0 & 0 & 0 & -1 & 1 & 1 \\ 0 & 1 & -1 & 0 & 0 & 1 \end{pmatrix} \tag{5.4}$$

for the orientation coefficients o^{j_i}, $i = 1 \to 4$, for the six surfaces meeting at the four triple junction lines, respectively. That is, the i-th row of the matrices in (5.4) denotes the coefficients $o^{j_i} \in \{-1, 1\}$ that the six surfaces have in the description of the triple junction line $\mathcal{T}_{j_i}$, or a zero if the corresponding surface does not touch this triple junction line. Similarly to (5.2), applying the local projections (5.3a,b) is straightforward.

In order to give a matrix formulation for (4.6a,b) we introduce the matrices $M^i \in \mathbb{R}^{K_i \times K_i}$, $\vec{N}^i \in (\mathbb{R}^3)^{K_i \times K_i}$, $A^i \in \mathbb{R}^{K_i \times K_i}$ and $\vec{A}^i \in (\mathbb{R}^{d \times d})^{K_i \times K_i}$, $i = 1 \to I_S$, defined by

$$M_{kl}^i := \int_{\Gamma_i^m} \pi_i^m [\phi_k^{m,i} \phi_l^{m,i}] \, \mathrm{d}\mathcal{H}^2, \qquad \vec{N}_{kl}^i := \int_{\Gamma_i^m} \pi_i^m [\phi_k^{m,i} \phi_l^{m,i}] \vec{v}_i^m \, \mathrm{d}\mathcal{H}^2,$$

$$A_{kl}^i := \int_{\Gamma_i^m} \nabla_s \phi_k^{m,i} \cdot \nabla_s \phi_l^{m,i} \, \mathrm{d}\mathcal{H}^2, \qquad \vec{A}_{kl}^i := A_{kl}^i \, \vec{Id}_1,$$

where we recall that $\{\{\phi_k^{m,i}\}_{k=1}^{K_i}\}_{i=1}^{I_S}$ is the standard basis of $\widehat{W}^h(\Gamma^m)$ and $\pi^m := (\pi_1^m, \ldots, \pi_{I_S}^m)$: $C(\Gamma^m, \mathbb{R}) \to \widehat{W}^h(\Gamma^m)$ is the standard interpolation operator at the nodes $\{\{\vec{q}_k^{m,i}\}_{k=1}^{K_i}\}_{i=1}^{I_S}$. Then on introducing the matrices

$$M := \mathrm{diag}(M^1, \ldots, M^{I_S}), \quad A := \mathrm{diag}(A^1, \ldots, A^{I_S}),$$
$$\vec{A} := \mathrm{diag}(\vec{A}^1, \ldots, \vec{A}^{I_S}), \quad \vec{N} := \mathrm{diag}(\vec{N}^1, \ldots, \vec{N}^{I_S}),$$

where $M, A : \mathbb{R}^K \to \mathbb{R}^K$, $\vec{A} : (\mathbb{R}^3)^K \to (\mathbb{R}^3)^K$ and $\vec{N} : \mathbb{R}^K \to (\mathbb{R}^3)^K$, the system of equations (4.6a,b) can be written as: Find $(\delta \vec{X}^{m+1}, \kappa^{m+1}) \in \underline{\mathbb{X}} \times \mathbb{R}^K$ such that

$$\begin{pmatrix} M & -\frac{1}{\tau_m} \vec{N}^T \vec{\mathcal{P}} \\ \vec{\mathcal{P}} \vec{N} & \vec{\mathcal{P}} \vec{A} \vec{\mathcal{P}} \end{pmatrix} \begin{pmatrix} \kappa^{m+1} \\ \delta \vec{X}^{m+1} \end{pmatrix} = \begin{pmatrix} 0 \\ -\vec{\mathcal{P}} \vec{A} \vec{\mathcal{P}} \vec{X}^m \end{pmatrix}. \tag{5.5}$$

Here, with the obvious abuse of notation, $\kappa^{m+1} = (\kappa_1^{m+1}, \ldots, \kappa_{I_S}^{m+1})^T$ with $\kappa_i^{m+1} = ([\kappa_i^{m+1}]_1, \ldots, [\kappa_i^{m+1}]_{K_i})$, $i = 1 \to I_S$, and $\delta \vec{X}^{m+1} = (\delta \vec{X}_1^{m+1}, \ldots, \delta \vec{X}_{I_S}^{m+1})^T$ with $\delta \vec{X}_i^{m+1} = ([\delta \vec{X}_i^{m+1}]_1, \ldots, [\delta \vec{X}_i^{m+1}]_{K_i})$, $i = 1 \to I_S$, are the vectors of coefficients with respect to the standard basis $\{\{\phi_k^{m,i}\}_{k=1}^{K_i}\}_{i=1}^{I_S}$ of κ^{m+1} and $\vec{X}^{m+1} - \vec{X}^m$ in (4.6a,b), respectively.

Similarly, the system (4.7a,b) can be written as: Find $(\delta \vec{X}^{m+1}, \kappa^{m+1}) \in \underline{\mathbb{X}} \times \mathbb{X}$ such that

$$\begin{pmatrix} \mathcal{K} A \mathcal{K} & -\frac{1}{\tau_m} \mathcal{K} \vec{N}^T \vec{\mathcal{P}} \\ \vec{\mathcal{P}} \vec{N} \mathcal{K} & \vec{\mathcal{P}} \vec{A} \vec{\mathcal{P}} \end{pmatrix} \begin{pmatrix} \kappa^{m+1} \\ \delta \vec{X}^{m+1} \end{pmatrix} = \begin{pmatrix} 0 \\ -\vec{\mathcal{P}} \vec{A} \vec{\mathcal{P}} \vec{X}^m \end{pmatrix}. \tag{5.6}$$

5.1   *Schur complement approach*

As M is nonsingular, we can reformulate (5.5) as

$$\kappa^{m+1} = \frac{1}{\tau_m} M^{-1} \vec{N}^T \vec{\mathcal{P}} \delta \vec{X}^{m+1}, \tag{5.7a}$$
$$(\vec{\mathcal{P}} \vec{A} \vec{\mathcal{P}} + \frac{1}{\tau_m} \vec{\mathcal{P}} \vec{N} M^{-1} \vec{N}^T \vec{\mathcal{P}}) \delta \vec{X}^{m+1} = -\vec{\mathcal{P}} \vec{A} \vec{\mathcal{P}} \vec{X}^m. \tag{5.7b}$$

Similarly, (5.6) can be solved by applying a Schur complement approach and then solving for $\delta \vec{X}^{m+1} \in \underline{\mathbb{X}}$:

$$\vec{\Pi} \vec{\mathcal{P}} (\vec{A} + \frac{1}{\tau_m} \vec{N} \mathcal{K} S \mathcal{K} \vec{N}^T) \vec{\mathcal{P}} \vec{\Pi} \delta \vec{X}^{m+1} = -\vec{\Pi} \vec{\mathcal{P}} \vec{A} \vec{\mathcal{P}} \vec{X}^m. \tag{5.8}$$

Here S is the inverse of $\mathcal{K} A \mathcal{K}$ on the space $(\ker \mathcal{K} A \mathcal{K})^\perp$. Also $\vec{\Pi} : (\mathbb{R}^3)^K \to \mathcal{R}^\perp$ is the orthogonal projection onto $\mathcal{R}^\perp$, where $\mathcal{R} := \mathrm{span}\{\vec{\mathcal{P}} \vec{N} \mathcal{K} e_i : i = 1 \to I_{EV}\} \equiv \{\vec{\mathcal{P}} \vec{N} \mathcal{K} v : v \in \ker \mathcal{K} A \mathcal{K}\} \subset \underline{\mathbb{X}}$ with $\{e_i\}_{i=1}^{I_{EV}}$ being a basis of the space $E = \ker A \cap \mathbb{X}$. In practice we always found that $I_{EV} = \dim(E)$ is equal to the number of volumes enclosed by the given surface cluster; e.g. $I_{EV} = 2$ for a double bubble, $I_{EV} = 3$ for a triple bubble and so on. This is the natural generalization to surface clusters of the result proved for curve networks in the plane; see [7].

The Schur complement systems (5.7b) and (5.8) can be solved with a (preconditioned) conjugate gradient solver. Here we used a simple diagonal preconditioner as considered in [9, p. 314] for the two-dimensional case. Where necessary, the solution of $\mathcal{K} A \mathcal{K} y = x$ in order to compute $S x$ can be obtained with an (inner loop) CG solver without a projection, as the right hand side vector x always satisfies the necessary compatibility condition, i.e. $x \in (\ker \mathcal{K} A \mathcal{K})^\perp$. See [45] for a justification of using a CG solver for a positive semidefinite system.

REMARK 5.2   The approximation (4.28a–c) can be solved by the following lagged iteration. Let $\lambda_i^{m+1,0} = \lambda_i^m$ for $m = 0 \to M - 1$, where we set $\lambda_i^0 = 0$, $i = 1 \to 3$. Then for $j \geqslant 0$ find $\vec{X}^{m+1,j+1} \in \underline{V}^h(\Gamma^m)$ and $\kappa^{m+1,j+1} \in \widehat{W}^h(\Gamma^m)$ such that

$$\left\langle \frac{\vec{X}^{m+1,j+1} - \vec{X}^m}{\tau_m}, \chi \vec{\nu}^m \right\rangle_m^h - \langle \kappa^{m+1,j+1} - \lambda^{m+1,j}, \chi \rangle_m^h = 0 \quad \forall \chi \in \widehat{W}^h(\Gamma^m), \qquad (5.9a)$$

$$\langle \kappa^{m+1,j+1} \vec{\nu}^m, \vec{\eta} \rangle_m^h + \langle \nabla_s \vec{X}^{m+1,j+1}, \nabla_s \vec{\eta} \rangle_m = 0 \quad \forall \vec{\eta} \in \underline{V}^h(\Gamma^m); \qquad (5.9b)$$

and then find $\lambda_i^{m+1,j+1} \in \mathbb{R}$, $i = 1 \to 3$, such that $\lambda^{m+1,j+1} \in W^h(\Gamma^m)$ and

$$\int_{\Gamma_1^m} (\kappa_1^{m+1,j+1} - \lambda_1^{m+1,j+1}) \, \mathrm{d}\mathcal{H}^2 = \int_{\Gamma_2^m} (\kappa_2^{m+1,j+1} - \lambda_2^{m+1,j+1}) \, \mathrm{d}\mathcal{H}^2$$

$$= \int_{\Gamma_3^m} (\kappa_3^{m+1,j+1} - \lambda_3^{m+1,j+1}) \, \mathrm{d}\mathcal{H}^2. \qquad (5.9c)$$

The iteration is stopped once $\sum_{i=1}^3 |\lambda_i^{m+1,j+1} - \lambda_i^{m+1,j}|$ is sufficiently small, upon which we set $(\vec{X}^{m+1}, \kappa^{m+1}, \lambda^{m+1}) = (\vec{X}^{m+1,j+1}, \kappa^{m+1,j+1}, \lambda^{m+1,j+1})$. Clearly, (5.9a,b) can be written as (5.5) with a slightly different right hand side, and so it can be solved with the correspondingly adapted Schur approach (5.7b).

5.2   Anisotropic schemes

In the case $r = (1, \ldots, 1)$, when the approximations (4.8a,b) and (4.9a,b) are linear, the anisotropic equivalents of (5.5) and (5.6) are given by

$$\begin{pmatrix} M_\beta & -\frac{1}{\tau_m} \vec{N}^T \vec{\mathcal{P}} \\ \vec{\mathcal{P}} \vec{N} & \vec{\mathcal{P}} \vec{A}_\gamma \vec{\mathcal{P}} \end{pmatrix} \begin{pmatrix} \kappa_\gamma^{m+1} \\ \delta \vec{X}^{m+1} \end{pmatrix} = \begin{pmatrix} 0 \\ -\vec{\mathcal{P}} \vec{A}_\gamma \vec{\mathcal{P}} \vec{X}^m \end{pmatrix} \qquad (5.10)$$

and

$$\begin{pmatrix} \mathcal{K} A_\beta \mathcal{K} & -\frac{1}{\tau_m} \mathcal{K} \vec{N}^T \vec{\mathcal{P}} \\ \vec{\mathcal{P}} \vec{N} \mathcal{K} & \vec{\mathcal{P}} \vec{A}_\gamma \vec{\mathcal{P}} \end{pmatrix} \begin{pmatrix} \kappa_\gamma^{m+1} \\ \delta \vec{X}^{m+1} \end{pmatrix} = \begin{pmatrix} 0 \\ -\vec{\mathcal{P}} \vec{A}_\gamma \vec{\mathcal{P}} \vec{X}^m \end{pmatrix}, \qquad (5.11)$$

with the obvious definitions of M_β, A_β and $\vec{A}_\gamma$. Similarly, the schemes (4.12a,b) and (4.13a,b) in the linear case $r = (1, \ldots, 1)$ can be formulated as follows. We define the orthogonal projection $\vec{\mathcal{P}}_\partial : (\mathbb{R}^3)^K \to \mathbb{X}_\partial$ onto the Euclidean space associated with $\underline{V}_\partial^h(\Gamma^m)$, where, on recalling (2.26) and (4.11), we note that $\vec{\mathcal{P}}_\partial$ can be decomposed into the projection $\vec{\mathcal{P}}$ and independent local projections of the form $\vec{Id} - |\nabla F(\vec{q})|^{-2} \nabla F(\vec{q}) \otimes \nabla F(\vec{q})$ for all the vertices $\vec{q} \in \mathcal{B}_k^m$, where in general $\vec{q} \notin \partial \mathcal{D}$. Then the system (4.13a,b) can be reformulated as: Find $(\delta \vec{X}^{m+1}, \kappa^{m+1}) \in \mathbb{X}_\partial \times \mathbb{X}$ such that

$$\begin{pmatrix} \mathcal{K} A_\beta \mathcal{K} & -\frac{1}{\tau_m} \mathcal{K} \vec{N}^T \vec{\mathcal{P}}_\partial \\ \vec{\mathcal{P}}_\partial \vec{N} \mathcal{K} & \vec{\mathcal{P}}_\partial \vec{A}_\gamma \vec{\mathcal{P}}_\partial \end{pmatrix} \begin{pmatrix} \kappa_\gamma^{m+1} \\ \delta \vec{X}^{m+1} \end{pmatrix} = \begin{pmatrix} 0 \\ -\vec{\mathcal{P}}_\partial \vec{A}_\gamma \vec{X}^m \end{pmatrix}, \qquad (5.12)$$

and similarly for (4.12a,b). The Schur complement approaches (5.7b) and (5.8) are then easily generalized to the anisotropic setting.

In the truly nonlinear case, i.e. when $r_i > 1$ for some $i = 1 \to I_S$, a lagged fixed point type iteration can be employed, where linear systems of the form e.g. (5.11) need to be solved at each iteration step. See [12] for analogous details in the case of a single closed hypersurface.

6. Numerical results

In this section we present several numerical simulations of evolving surface clusters in $\mathbb{R}^3$. We stress that all of the presented experiments were performed without any remeshing. In fact, in practice the initial mesh quality is maintained or even improved on by the intrinsically induced tangential motion of our schemes. A more detailed discussion of this property in the single closed hypersurface case can be found in [10], while excellent mesh properties for fully anisotropic surface energies in the closed surface case have been presented in [12].

Throughout this section we use essentially uniform time steps, i.e. $\tau_m = \tau$, $m = 0 \to M - 2$, and $\tau_{M-1} = T - t_{m-1}$. For later purposes, we define

$$\vec{X}(t) := \frac{t - t_{m-1}}{\tau_{m-1}} \vec{X}^m + \frac{t_m - t}{\tau_{m-1}} \vec{X}^{m-1}, \quad t \in [t_{m-1}, t_m], \ m \geqslant 1.$$

Finally, we note that we implemented the approximations within the finite element toolbox ALBERTA (see [63]), where in particular we made use of new submesh tools recently presented in [49]. ALBERTA is a freely available library with data structures and functions for adaptive finite element simulations in one, two, and three space dimension, written in the programming language ANSI-C. All of the presented computations were run on a standard Linux desktop PC.

6.1 *Isotropic flows*

First we present numerical simulations for isotropic surface energy densities, i.e. $\gamma_i(\vec{p}) = \varsigma_i |\vec{p}|$, $\varsigma_i > 0$, $i = 1 \to I_S$. Hence the free energy (2.12) reduces to

$$E_\gamma(\Gamma) = \sum_{i=1}^{I_S} \varsigma_i |\Gamma_i|. \tag{6.1}$$

Unless otherwise stated, we set $\sigma = (\varsigma_1, \ldots, \varsigma_{I_S}) = (1, \ldots, 1)$. For the presented computations we employ the schemes (4.12a,b) and (4.13a,b) with $\beta \equiv (1, \ldots, 1)$. Here we recall that in the absence of intersections with an external boundary $\partial \mathcal{D}$ these schemes collapse to (4.8a,b) and (4.9a,b), respectively.

6.1.1 *Double bubbles.* In the first experiment, we start off with a partition of the unit ball into two half balls. Under the isotropic equal energy density surface diffusion flow this evolves to a standard double bubble, as shown in Figure 5. The discretization parameters for this experiment are $K = 3267$, $J = 6240$, $\tau = 10^{-3}$ and $T = 1$; and the maximum observed relative volume
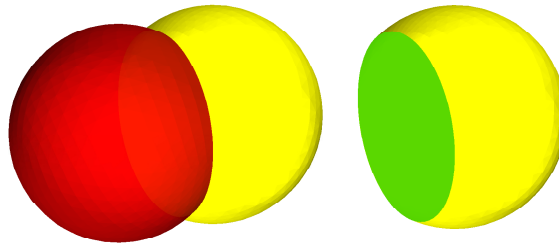

FIG. 5. Plots of Γ^M and (Γ_2^M, Γ_3^M).

loss was $e^M_{\mathrm{vol}} = 0.11\%$; recall Remark 4.2. For this simple evolution of a partitioned unit ball to a symmetric standard double bubble, we in addition investigated the effect of refining the discretization parameters h and τ on the relative volume loss, the error in the discrete energy of the numerical steady state solution compared to the true surface area of the standard double bubble, as well as on the observed triple junction angles. To this end, we define the following quantities. Let e^M_{vol} denote the maximum relative volume loss of the two volumes enclosed by Γ^M, relative to the volumes enclosed by Γ^0. Moreover, let $e^M_{\mathrm{area}} := \left| |\Gamma^M| - |\Gamma^\star| \right|$, where $\Gamma^\star$ denotes the symmetric double bubble enclosing two volumes of $2\pi/3$ each, and so a simple calculation yields $|\Gamma^\star| = 4^{1/3}3\pi \approx 14.96$. In addition, let $\theta^M := (\theta^M_1, \theta^M_2, \theta^M_3)$ denote the average angles that the elements of the polygonal surfaces of Γ^M make along the triple junction line $\mathcal{T}^M_1$. That is, for each element $\sigma^{M,1}_{j_1}$ of Γ^M_1 that has an edge which lies on $\mathcal{T}^M_1$, we find the element $\sigma^{M,2}_{j_2} \subset \Gamma^M_2$ that shares this edge with $\sigma^{M,1}_{j_1}$, and then compute the angle between their two respective normals. This is repeated for all elements along the triple junction line, and the average is denoted by θ^M_3. Similarly, θ^M_1 is the average angle between the surfaces Γ^M_2 and Γ^M_3, and analogously for θ^M_2. Finally, we denote by e^M_{angle} the maximal deviation from $120°$ for any of the angles between two elements along the triple junction line $\mathcal{T}^M_1$, between any two surfaces. For different values of K, and setting $\tau = 10^{-3}3267K^{-1}$, we report on these error quantities in Table 1. We observe that, similarly to the two-dimensional results obtained in [7, Tables 4 and 5], the errors in volume, surface area and triple junction angles become smaller, as the discretization parameters decrease. Here we recall that as the force balance conditions (2.4b) are approximated weakly in our formulation, true $120°$ contact angles cannot be expected on the discrete level. But the observed discrete angles approach $120°$ as $h \to 0$. The same behaviour can be observed for our approximation (4.28a–c) for the volume preserving mean curvature flow. The corresponding numerical results are shown in Table 2, where we note once again that all of the measured quantities appear to be approximated consistently.

TABLE 1

Quantities e^M_{vol}, e^M_{area}, θ^M, e^M_{angle} for the surface diffusion experiment with $T = 1$.

K	e^M_{vol}	e^M_{area}	θ^M	e^M_{angle}
243	0.518%	5.0803e-01	(109.0, 142.0, 109.0)	34.7
867	0.253%	1.4459e-01	(114.3, 131.4, 114.3)	17.6
3267	0.113%	4.1503e-02	(117.1, 125.8, 117.1)	8.8
12675	0.048%	1.2371e-02	(118.5, 122.9, 118.5)	4.4

TABLE 2

Quantities e^M_{vol}, e^M_{area}, θ^M, e^M_{angle} for the conserved mean curvature flow experiment with $T = 1$.

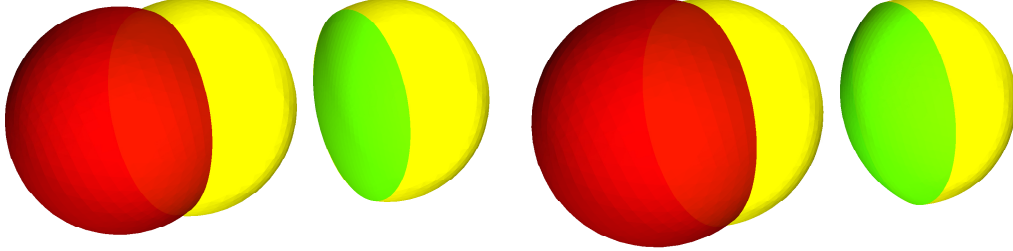| K	e^M_{vol}	e^M_{area}	θ^M	e^M_{angle}
243	0.031%	4.5878e-01	(108.4, 143.1, 108.4)	36.7
867	0.014%	1.1955e-01	(114.0, 132.0, 114.0)	18.6
3267	0.004%	2.9544e-02	(117.0, 126.0, 117.0)	9.2
12675	0.001%	6.6432e-03	(118.5, 123.0, 118.5)	4.6

FIG. 6. Plots of Γ^M and (Γ_2^M, Γ_3^M) for $\sigma = (1, 1, 1.5)$ (left) and $\sigma = (1, 1, 1.75)$ (right).
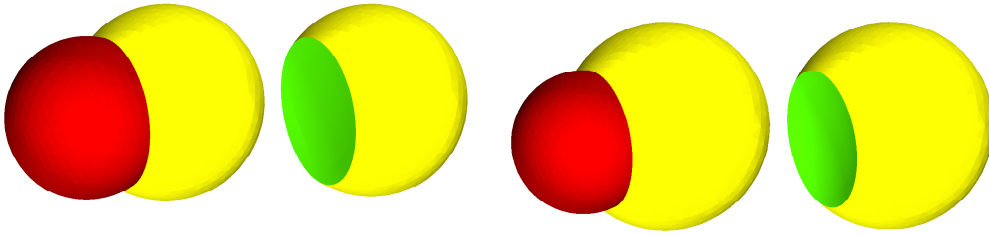

FIG. 7. Plots of Γ^M and (Γ_2^M, Γ_3^M) for enclosed volume ratios of 1/2 (left) and 1/4 (right).

In the next experiments, with all other parameters the same as in Figure 5, we choose $\sigma = (1, 1, 1.5)$ and $\sigma = (1, 1, 1.75)$. The results are in Figure 6. As expected, the higher weighting of the surface area of the surface Γ_3 in the free energy (6.1) leads to this surface shrinking relative to the other two surfaces Γ_1 and Γ_2. The effect becomes more pronounced for larger choices of ς_3. Moreover, we repeat the experiment in Figure 5 for the equal energy case $\sigma = (1, 1, 1)$ for a nonequal volume double bubble setup. Keeping all the discretization parameters as before, we simulate the surface diffusion flow for two clusters that are given as the union of a half ball and a half ellipsoid. The relative enclosed volume ratios for the two flows are 1/2 and 1/4, and the numerical steady state solutions can be seen in Figure 7.

In addition, we show two experiments for unstable double bubbles, also called torus bubbles; see e.g. [42, Fig. 7] for an illustration. Here $I_S = 4$ and $I_T = 2$. The initial surface cluster is given by the union of two half spheres and a torus, the latter defined by the equation

$$(R - [x_1^2 + x_2^2]^{1/2})^2 + x_3^2 = r^2 \qquad (6.2)$$

with $R = 2$ and $r = 1$. Hence the volume relation of the torus/dumbbell volumes is 1.28. The discretization parameters are $K = 4802$, $J = 9216$, $\tau = 10^{-3}$ and $T = 1$. The maximum relative volume loss for this experiment was 0.08%. See Figure 8 for the results. We note that the final solution at time $T = 1$, which is close to being a numerical steady state, is an approximation of a so called unstable double bubble, which before the proof of the double bubble conjecture was a possible theoretical candidate for a surface area minimizing constellation. Here we recall that the double bubble conjecture states that for two given volumes, the standard double bubble has least possible surface area among all the surfaces enclosing and separating these two volumes. Here the standard double bubble is made up of three constant mean curvature surfaces, meeting along a common circle at an angle of 120 degrees; cf. Figures 5 and 6 for some examples. The conjecture for volumes in $\mathbb{R}^3$ has been proved only relatively recently in [48], while the corresponding conjecture
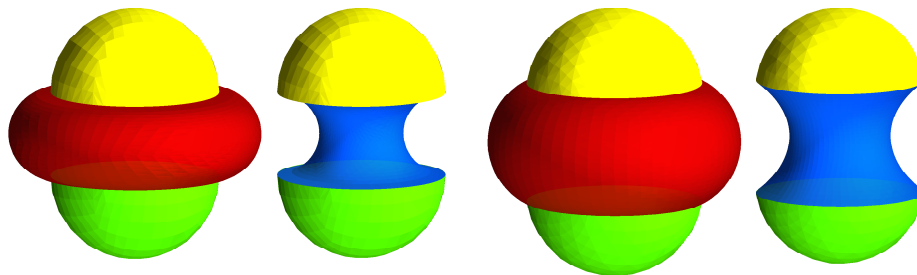
FIG. 8. Plots of Γ^m and $(\Gamma_1^m, \Gamma_2^m, \Gamma_4^m)$ at times $t_m = 0, 1$.
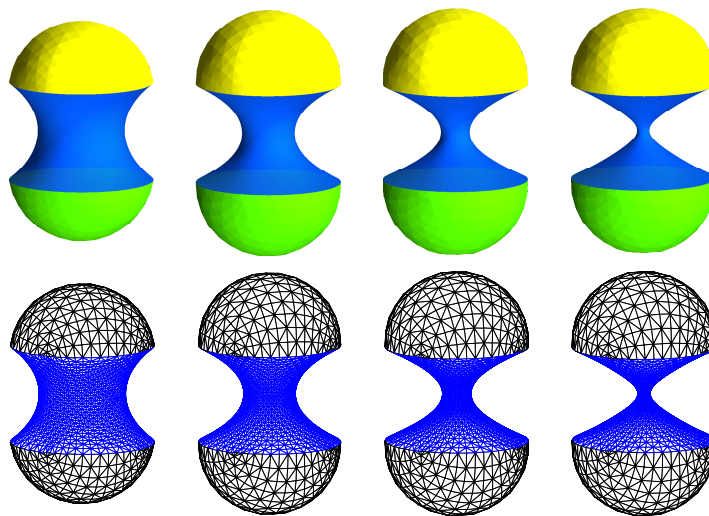
FIG. 9. Plots of $(\Gamma_1^m, \Gamma_2^m, \Gamma_4^m)$ at times $t_m = 1, 25, 26.5, 26.6$. Below the corresponding triangulations.

for triple bubbles in $\mathbb{R}^3$ still remains open. We refer to the previously mentioned review article [53] for more details. In fact, if we continue the simulation in Figure 8 for long enough, then the above mentioned instability becomes evident also in our numerical approximation. As expected, and in agreement with corresponding phase field computations in e.g. [59, Fig. 13], the inner wall of the
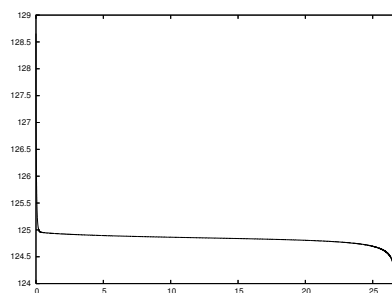
FIG. 10. A plot of $|\Gamma|$ over time.
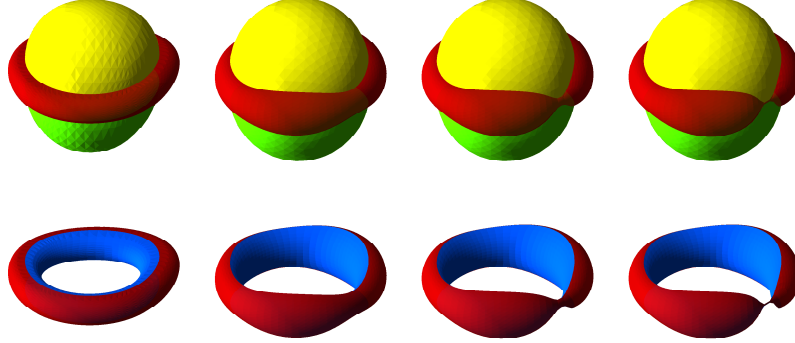
FIG. 11. Plots of Γ^m and (Γ_3^m, Γ_4^m) at times $t_m = 0, 0.75, 0.9, 0.91$.
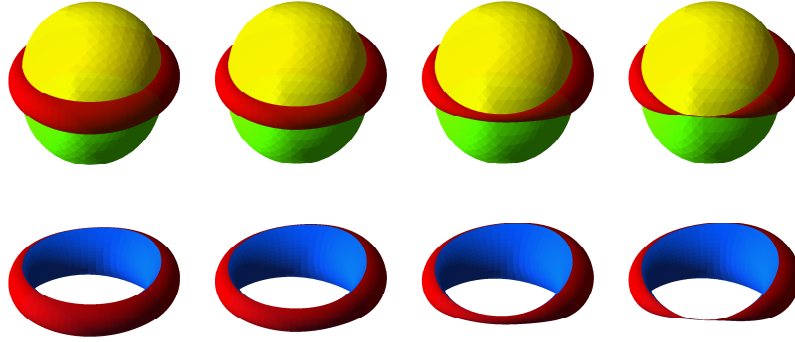
FIG. 12. Plots of Γ^m and (Γ_3^m, Γ_4^m) at times $t_m = 0.5, 0.7, 0.8, 0.815$.

torus bubble tries to pinch, which would lead to three separately enclosed volumes. These results are shown in Figure 9, together with the corresponding triangulations. Of course, this change of topology goes beyond the parametric formulation employed in this paper and our finite element approximation can only integrate until just before the rupture, which in this case occurs at around time $t = 26.61$. A plot of the free energy $|\Gamma|$ over time can be seen in Figure 10. In addition, we show a simulation for a torus bubble that is not rotationally symmetric, and where the torus part of the double bubble is relatively smaller compared to the previous experiment. Here the initial cluster was obtained by starting with a torus bubble as before, but now in (6.2) setting $R = 2$ and $r = 0.5$, followed by two slight stretchings of this cluster obtained by applying the transformations

$$\vec{\mathcal{G}}_1(\vec{z}) := \begin{cases} (z_1 e^{-0.1 z_1}, z_2, z_3), & z_1 < 0, \\ \vec{z}, & z_1 \geqslant 0, \end{cases} \quad \text{and} \quad \vec{\mathcal{G}}_2(\vec{z}) := \begin{cases} (z_1, z_2 e^{-0.05 z_2}, z_3), & z_2 < 0, \\ \vec{z}, & z_2 \geqslant 0, \end{cases}$$

respectively. This resulted in a volume relation of the torus/dumbbell volumes of 0.25. The results of the surface diffusion flow for this torus bubble are shown in Figure 11, where the discretization parameters are $K = 5314$, $J = 10240$ and $\tau = 10^{-3}$. We observe that in this evolution the instability leads to a slightly different behaviour. In particular, it results in the thinning of the toroidal ring at one point. Eventually the thinning would lead to the ring tearing apart, and it appears that this change of topology would occur at around time $t = 0.91$.

A slightly different behaviour can be observed for the volume preserving mean curvature flow. To demonstrate this, we repeated the last experiment with the same initial data and the same discretization parameters for our approximation (4.28a–c); see Figure 12 for the numerical results. Once again, the torus bubble eventually pinches off, but this time the pinching is caused by a uniform thinning of the ring on one side, while it gains in dimension on the opposite side, in agreement with corresponding phase field computations in e.g. [33, Fig. 8]. This is in contrast to the very local behaviour caused by the fourth order flow in Figure 11.

6.1.2   *Triple bubbles.*   We first show an experiment for the mean curvature flow. The initial surfaces are given by a partitioning of the unit ball into three equal segments, leading to three curved surfaces and three flat ones, so that $I_S = 6$ and $I_T = 4$. The four triple junction lines meet at two quadruple junction points. The discretization parameters are $K = 6534$, $J = 12288$, $\tau = 10^{-4}$ and $T = 0.15$. We note that, if continued, the cluster will shrink to a point, as is to be expected for mean curvature flow. In this numerical experiment this happens at around time 0.178. The results are shown in Figure 13.
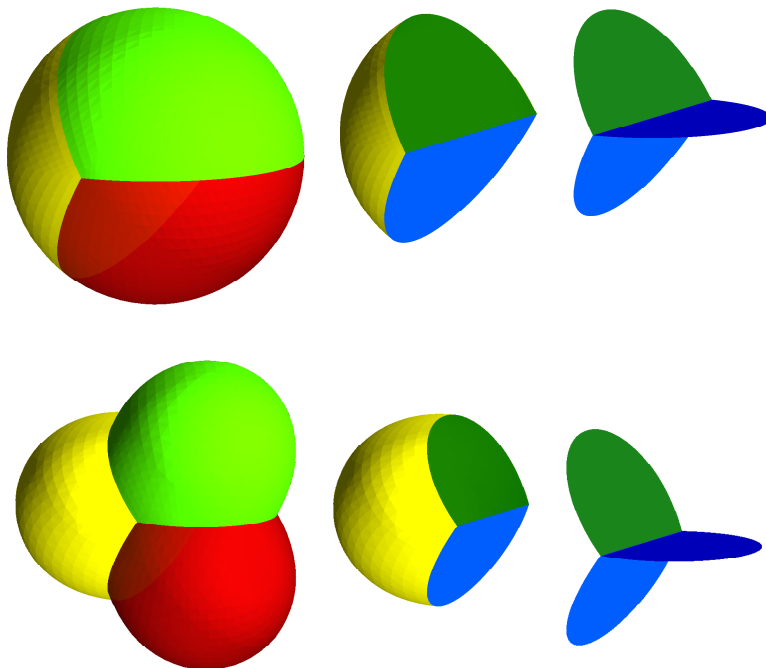
FIG. 13. Plots of Γ^m, $(\Gamma_1^m, \Gamma_4^m, \Gamma_5^m)$ and $(\Gamma_4^m, \Gamma_5^m, \Gamma_6^m)$ for $m = 0, M$ (scaled for $m = M$).

We also present computations for a surface diffusion flow. With the same initial surface cluster as before, and the same discretization parameters, we integrate the flow until time $T = 1$. At this stage the solution has reached a numerical steady state, which approximates the well known standard triple bubble. Here we recall that the corresponding conjecture that this is indeed the surface area minimizing way to separate three given volumes is still an open problem; although a proof for the planar case has recently been given in [75]. The maximum observed relative volume loss for this
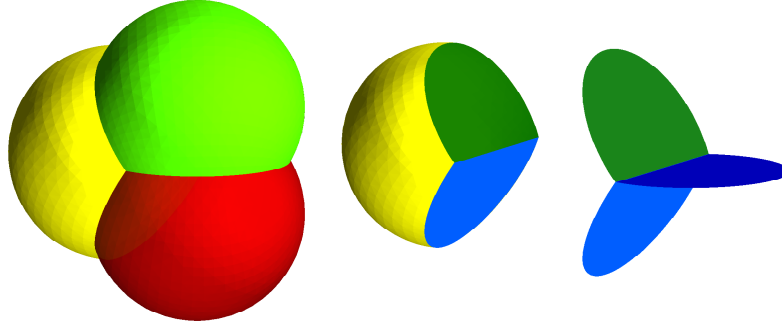
FIG. 14. Plots of Γ^M, $(\Gamma_1^M, \Gamma_4^M, \Gamma_5^M)$ and $(\Gamma_4^M, \Gamma_5^M, \Gamma_6^M)$.

computation was 0.03%. See Figure 14 for the results. In order to underline the conjecture that the standard triple bubble is the unique global minimizer among all triple bubbles, we also present a numerical simulation for a nonstandard triple bubble that enclosed the same volumes as the bubble in Figure 14. To this end, we choose a cluster with $I_S = 5$ and $I_T = 2$ that consists of three adjacent cubes with side length $(4\pi/9)^{1/3}$. For the discretization parameters $K = 4292$, $J = 8192$, $\tau = 10^{-4}$ and $T = 1$ we present the evolution in Figure 15. For the numerical steady state solution in Figure 15 we observe a discrete energy of $|\Gamma^M| \approx 16.56$, while the final solution in Figure 14 has $|\Gamma^M| \approx 16.38$, in agreement with the triple bubble conjecture.
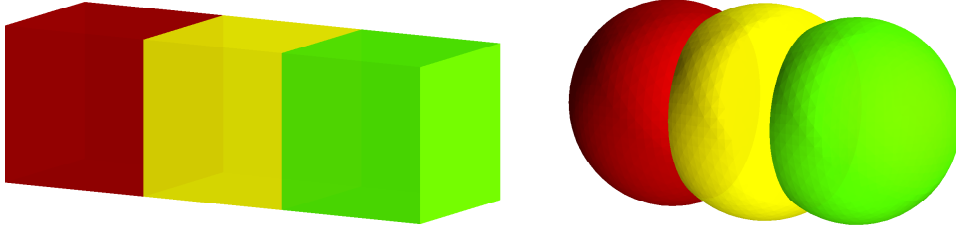
FIG. 15. Plots of Γ^0 and Γ^M.

In the next experiments, we choose the same initial data as in Figure 14 but let $\sigma = (1.25, 1, 1, 1, 1, 1)$ and $\sigma = (1.5, 1, 1, 1, 1, 1)$. The results are in Figure 16, where the discretization parameters are the same as before. As expected, and similarly to the results shown in Figure 6, we observe that for increasing ς_1 the relative area of the surface Γ_1 shrinks, compared to the remaining surfaces Γ_i, $i = 2 \to 6$. A similar behaviour can be observed for the weighting $\sigma = (1, 1, 1, 1, 1, 1.5)$ (see Figure 17), where now the area of the surface Γ_6 relatively shrinks, compared to other surfaces. It is interesting to note that for the numerical steady state in Figure 17, we observe a discrete energy of $E_\gamma(\Gamma^M) \approx 16.70$ (recall (6.1)), which is larger than the value $|\Gamma^M| \approx 16.56$ observed in Figure 15. Of course, the interface Γ_6, which would separate the left and right volumes, is not present in the latter experiment, and so here $E_\gamma(\Gamma^M) = |\Gamma^M|$ for the given surface energy weights. Hence we conjecture that for three equal volumes and the given weights, the unique surface area minimizer is given by a caterpillar triple bubble as shown in Figure 15.
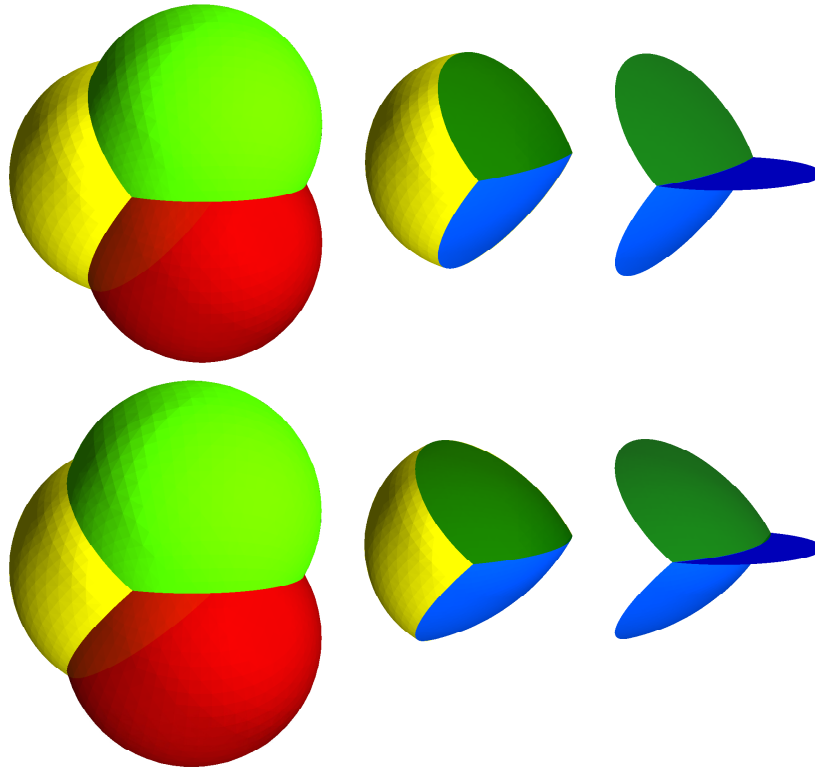
FIG. 16. Plots of Γ^M, $(\Gamma_1^M, \Gamma_4^M, \Gamma_5^M)$ and $(\Gamma_4^M, \Gamma_5^M, \Gamma_6^M)$ for $\varsigma_1 = 1.25$ (top) and $\varsigma_1 = 1.5$ (bottom).
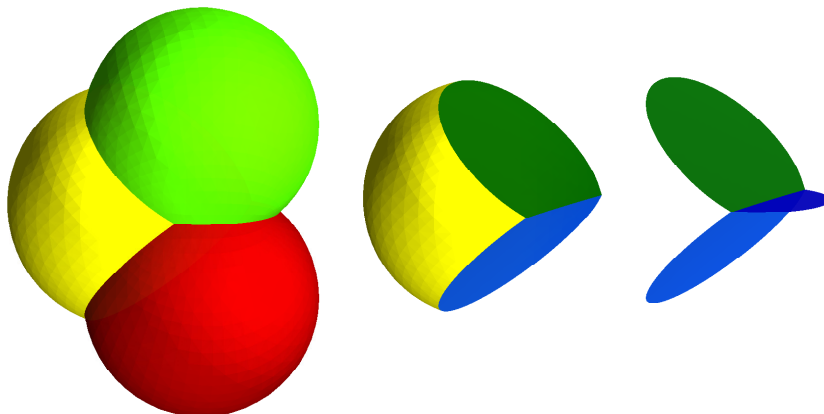

FIG. 17. Plots of Γ^M, $(\Gamma_1^M, \Gamma_4^M, \Gamma_5^M)$ and $(\Gamma_4^M, \Gamma_5^M, \Gamma_6^M)$ for $\varsigma_6 = 1.5$.

6.1.3 *Quadruple bubbles.* Here we report on two experiments for quadruple bubbles, when four volumes are enclosed by the surface cluster. The first cluster consists of $I_S = 9$ surfaces meeting at $I_T = 8$ triple junction lines, which in turn meet at four different quadruple junction points. Here we note that two triple junction lines arise from the intersection of Γ_2, Γ_3 and Γ_6; that is, the light green, the light blue and the brown surface in Figure 18. We start with a configuration made up of two unit cubes and two cuboids, with each cuboid having twice the volume of a unit cube. The discretization parameters are $K = 7305$, $J = 13824$, $\tau = 10^{-4}$ and $T = 1$. The results for the approximation (4.7a,b) can be seen in Figure 18. We conjecture that the numerical steady state displayed in Figure 18 is an approximation of a stable cluster of constant mean curvature surfaces, which is a local surface area minimizer for this non-equal volume quadruple bubble constellation. In fact, the solution in Figure 18 looks very similar to quadruple bubbles observed in real life (see e.g. [43, Fig. 2e]).
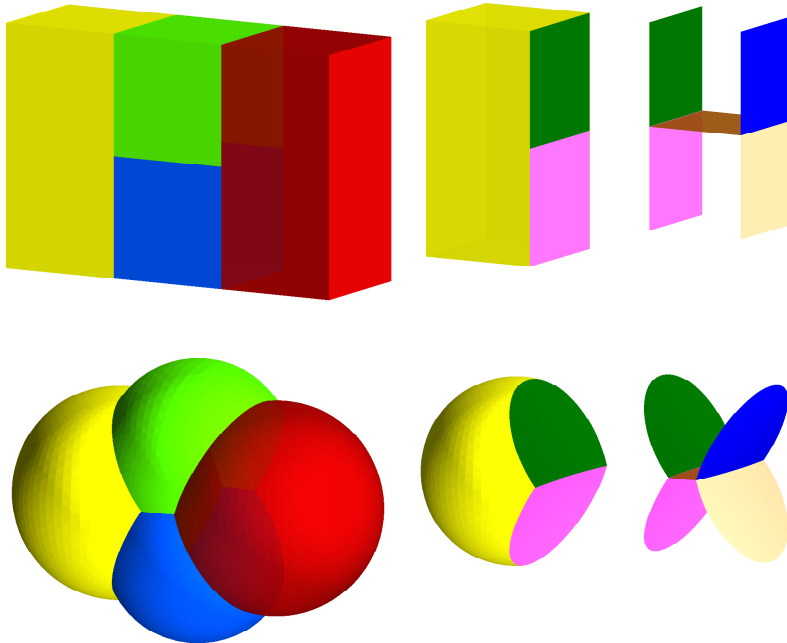

FIG. 18. Plots of Γ^m, $(\Gamma_1^m, \Gamma_5^m, \Gamma_7^m)$ and $(\Gamma_5^m, \Gamma_6^m, \Gamma_7^m, \Gamma_8^m, \Gamma_9^m)$ for $m = 0, M$.

Here we recall that the conjectured unique minimizer over all quadruple bubbles is the so-called standard quadruple bubble, or 4-bubble, as displayed in [28, Fig. 3]. The conjecture can be found in [66] and more details about the standard 4-bubble are given in [3]. Next we include a simulation for the surface diffusion flow towards such a standard quadruple bubble, and compare the final surface area to the value obtained for the solution in Figure 18. To this end, we start the evolution with a cluster that is topologically equivalent to the standard bubble, i.e. the cluster consists of $I_S = 10$ surfaces meeting at $I_T = 10$ triple junction lines, which in turn meet at five different quadruple junction points. The initial volumes are given by two unit cubes, by a cuboid of dimension $1 \times 2 \times 1$, and by a cuboid of dimension $2 \times 2 \times 1/2$. Hence overall the separated volumes are the same as in
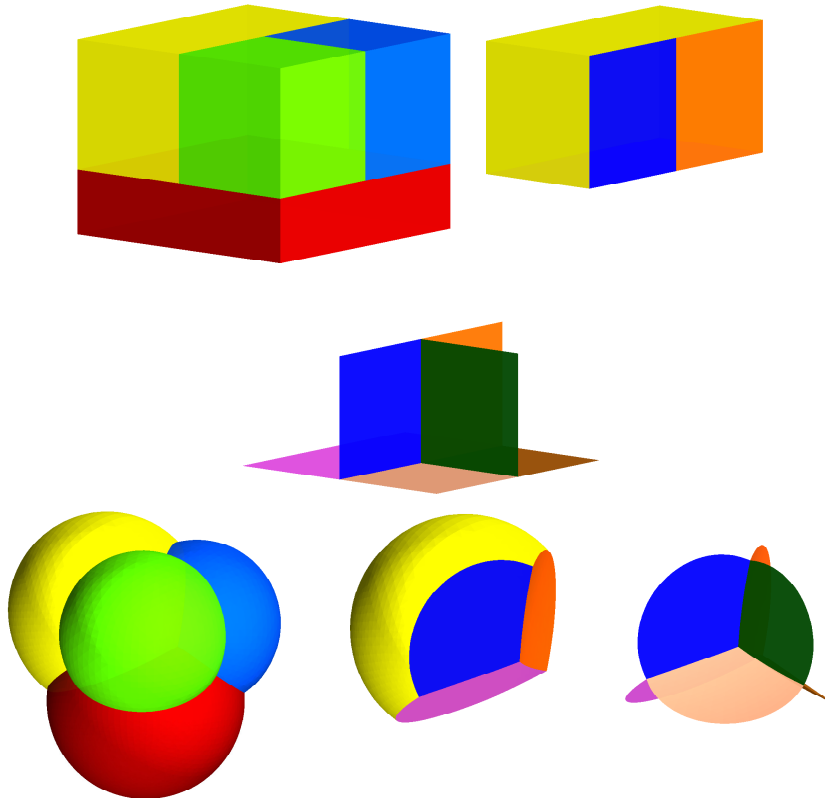
FIG. 19. Plots of Γ^m, $(\Gamma_1^m, \Gamma_2^m, \Gamma_3^m, \Gamma_7^m)$ and $(\Gamma_2^m, \Gamma_3^m, \Gamma_5^m, \Gamma_7^m, \Gamma_8^m, \Gamma_9^m)$ for $m = 0, M$.

Figure 18. The discretization parameters for this simulation are $K = 8378$, $J = 15872$, $\tau = 10^{-4}$, $T = 1$; and the numerical results can be seen in Figure 19. We note that the numerical steady state displayed in Figure 19 has a total surface area of $|\Gamma^M| \approx 21.75$, which as expected is smaller than the value $|\Gamma^M| \approx 22.08$ for the solution in Figure 18. A plot of the free energy $|\Gamma|$ over time for both experiments can be seen in Figure 20.
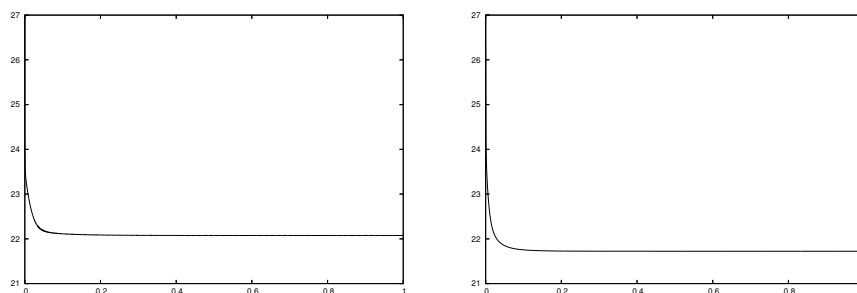

FIG. 20. A plot of $|\Gamma|$ over time for the nonstandard quadruple bubble (left) and for the standard quadruple bubble (right).

6.1.4 *Surfaces attached to an external boundary.* The first experiment is for a surface that is attached to the boundary of $\mathcal{D} := \mathbb{R}^2 \times (0, \infty)$. Starting with an initial surface in the shape of a unit cube, the surface evolves into a half sphere under flow by surface diffusion, as expected; see the left of Figure 21. The discretization parameters are $K = 5185$, $J = 10240$, $\tau = 10^{-3}$ and $T = 1$. For the remaining experiments we consider surfaces attached to the lower and upper boundary of the slabs $\mathcal{D} = \mathbb{R}^2 \times (0, \varrho)$, where either $\varrho = 4$ or 8. The surface diffusion flow for the surface defined by

$$\Gamma(0) = \bigcup \{r(x_3)\mathbb{S}^1 \times \{x_3\} : x_3 \in [0, \varrho]\}, \quad \text{where} \quad r(x_3) = 1 + \alpha \cos(2\pi x_3/\varrho), \tag{6.3}$$

with $\varrho = 4$ and $\alpha = 0.5$, can be seen on the right of Figure 21, where the discretization parameters are $K = 4160$, $J = 8192$, $\tau = 10^{-3}$ and $T = 2$. This time, we observe that the surface evolves to a cylinder. We note that all of the experiments in this subsection illustrate surface area minimizers for a fixed enclosed volume inside the slabs $\mathcal{D} = \mathbb{R}^2 \times (0, \varrho)$, with $\varrho = 4$ or 8. Here we recall that inside such slab domains the isoperimetric problem is solved, with the surface area minimizing surfaces being either half spheres or cylinders; see e.g. [5]. Moreover, in the next two experiments in this subsection we start with two different initial surfaces attached to the boundary of the slab $\mathcal{D} = \mathbb{R}^2 \times (0, 8)$, i.e. $\varrho = 8$. First we start with a triangulation of a cuboid of dimension $1 \times 1 \times 8$ inside $\mathcal{D}$, and this evolves to a cylinder. In fact, as this surface is constant in the x_3-direction the flow is essentially one dimensional, i.e. it corresponds to a square evolving to a circle. However, if we start with a perturbed cylinder inside $\mathcal{D}$, where we choose (6.3) with $\alpha = 0.25$, then we observe pinch-off and the flow does not converge to a cylinder, which in this case is unstable; see [5]. Instead, the flow wants to separate the surface into two surfaces, which would each evolve into a half sphere. Of course, as mentioned before, such a change of topology is beyond the parametric formulation and hence, without a heuristically defined reparameterization, our finite element approximation can only integrate until just before the pinch-off, which in this case occurs at around time $t = 1.487$. The discretization parameters are $K = 4128$, $J = 8192$, $\tau = 10^{-3}$, and the results can be seen in Figure 22.

We also consider simulations for surfaces attached to a curved boundary, and here we initially consider the unit ball with boundary $\partial\mathcal{D} = \mathbb{S}^2$. As the initial surface $\Gamma(0)$ we choose a flat hyperplane at height $x_3 = \alpha$ inside the unit ball, so that the ball is partitioned into two volumes. For the resulting volume ratios we choose the values 1, $1/2$, $1/4$ and $1/8$, which corresponds to $\alpha = 0$ and $\alpha \approx 0.226, 0.426, 0.585$, respectively. We show numerical approximations of the steady state solutions for the surface diffusion flows starting from these initial conditions in Figure 23, where the discretization parameters are $K = 4225$, $J = 8192$, $\tau = 10^{-3}$ and $T = 0.2$. As the boundary $\partial\mathcal{D}$ is curved, we cannot expect $\mathcal{B}_1^{m+1} \subset \partial\mathcal{D}$ in these experiments. The observed maximal distance of any vertex in $\mathcal{B}_1^M$ to $\partial\mathcal{D}$ for the four experiments was $e_\partial^M = 0$, 5.7×10^{-4}, 2.8×10^{-3} and

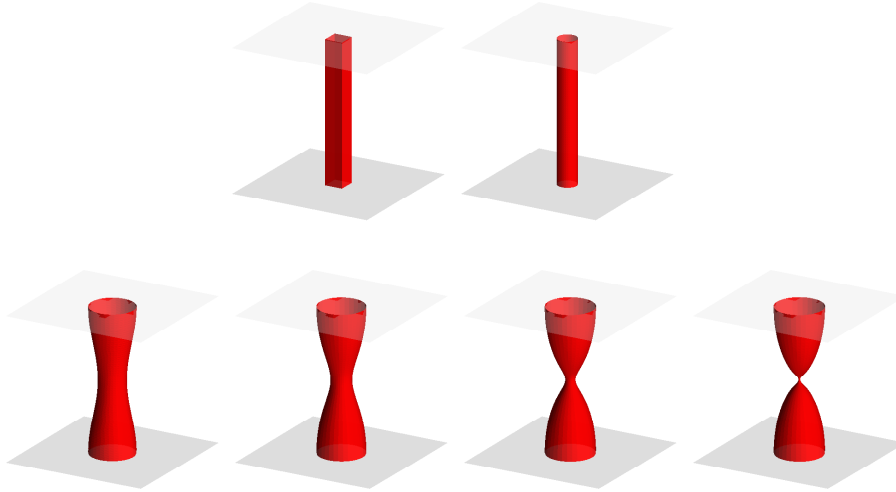Fig. 21. Plots of Γ^0 and Γ^M.

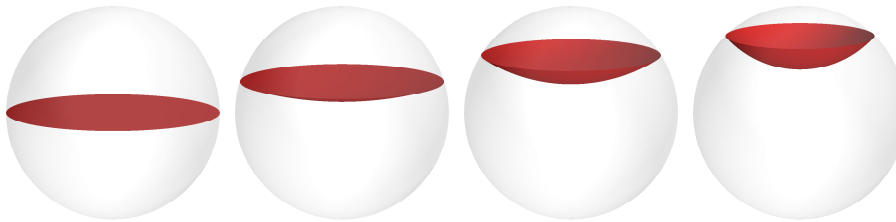FIG. 22. Plots of Γ^0 and Γ^M (top) and plots of Γ^m for $t_m = 0, 1, 1.45, 1.48$ (bottom).

FIG. 23. Plots of Γ^M for relative volume ratios $1, 1/2, 1/4$ and $1/8$.
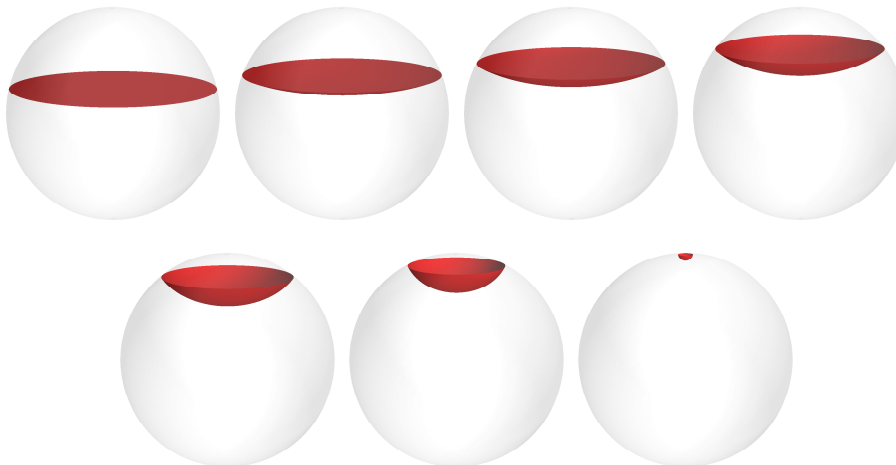

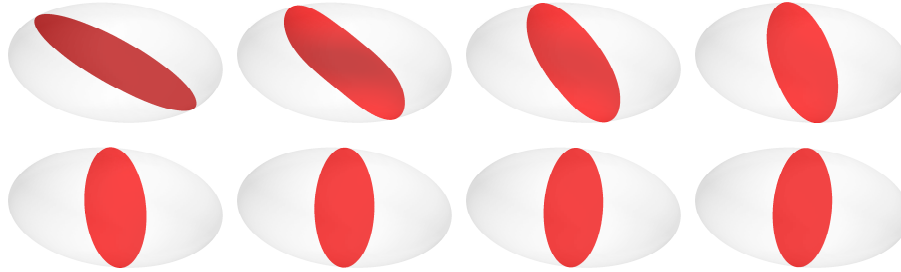FIG. 24. Plots of Γ^m for $t_m = 0, 0.1, \ldots, 0.4, 0.45, 0.5$.

FIG. 25. Plots of Γ^m for $t_m = 0, 0.1, \ldots, 0.7$.

8.5×10^{-3}, respectively. A simulation for the mean curvature flow of the initial configuration with $\alpha \approx 0.226$ can be seen in Figure 24, where we kept all the discretization parameters as before. Here we observed an extinction time close to $t = 0.5$.

Finally, we present the evolution of a surface attached to an ellipsoid. The dimensions of the ellipsoid are $2 \times 1 \times 1$, and the initial surface $\Gamma(0)$ is given by a hyperplane that makes an angle of $25°$ with the (x_1, x_2)-plane. For the discretization parameters $K = 8321$, $J = 16384$, $\tau = 5 \times 10^{-3}$ and $T = 0.7$ we show the numerical results in Figure 25. As expected, under the surface diffusion flow the surface aligns itself with the (x_2, x_3)-plane, where it assumes the area minimizing shape of a unit disk. For this experiment, the maximal distance of a boundary line vertex to $\partial\mathcal{D}$ was $e_\partial^M = 8.9 \times 10^{-3}$.

6.2 Anisotropic flows

In what follows we present numerical results for fully anisotropic evolution equations for surface clusters. Here we employ our schemes (4.12a,b) and (4.13a,b), where we recall that in the absence of intersections with an external boundary $\partial\mathcal{D}$ these schemes collapse to (4.8a,b) and (4.9a,b), respectively.

Unless otherwise stated, we choose the constant mobility $\beta = (1, \ldots, 1)$ and set $\gamma = (\gamma_1, \ldots, \gamma_1)$, where γ_1 is chosen of the form (2.15) with (2.17).

6.2.1 *Anisotropic mean curvature flow.*   Similarly to [65], it can be proven that for an anisotropy that is symmetric with respect to the x_3-axis and for the anisotropic mobility $\beta = \gamma$, an exact solution to (2.19) with $I_S = 1$ for a single hypersurface touching the boundary of $\mathcal{D} := \mathbb{R}^2 \times (0, \infty)$ is given by

$$\Gamma(t) = \{\vec{q} \in \mathbb{R}^3 : \gamma_1^*(\vec{q}) = \sqrt{1-4t}\} \cap \overline{\mathcal{D}}, \tag{6.4}$$

i.e. shrinking (upper) halves of boundaries of Wulff shapes; recall (2.16). Using (6.4) we now perform a convergence test for our approximation (4.12a,b) with $\beta = \gamma$. An exact solution to (2.19) with $I_S = 1$ and $\beta = \gamma$ defined by (2.15) with $L_1 = 1$ and $G_1^{(1)} = \text{diag}(1, \varepsilon_1^2, \varepsilon_1^2)$, on noting (2.16) and (6.4), is given by

$$\vec{x}_1(\cdot, t) = (1 - 4t)^{1/2}[G_1^{(1)}]^{1/2}\vec{\text{id}}_{\mathbb{S}^2_{\geqslant 0}}, \quad t \in [0, \overline{T}), \quad \overline{T} = 0.25;$$

where $\vec{\text{id}}_{\mathbb{S}^2_{\geqslant 0}}$ is the identity function on the upper unit sphere $\Omega \equiv \mathbb{S}^2_{\geqslant 0} \subset \mathbb{R}^3$. For $\varepsilon_1 =$

TABLE 3

Absolute errors $\|\vec{X} - \vec{x}\|_{L^\infty}$ for the test problem, with $T = \frac{1}{2}\overline{T} = \frac{1}{8}$ and $T = \overline{T} - \tau$, respectively.

K	$\varepsilon_1 = 0.5$			$\varepsilon_1 = 0.1$		
	$h_{\vec{X}^0}$	$T = \frac{1}{2}\overline{T}$	$T = \overline{T} - \tau$	$h_{\vec{X}^0}$	$T = \frac{1}{2}\overline{T}$	$T = \overline{T} - \tau$
289	2.7470e-01	7.8899e-03	1.0094e-01	2.7076e-01	4.6355e-03	1.0020e-01
1089	1.3957e-01	2.2296e-03	7.6033e-02	1.3801e-01	1.5169e-03	7.6160e-02
4225	7.0067e-02	5.8183e-04	4.9572e-02	6.9339e-02	4.0686e-04	4.9487e-02
16641	3.5069e-02	1.5238e-04	3.0130e-02	3.4711e-02	1.2193e-04	3.4094e-02

0.5 and $\varepsilon_1 = 0.1$ we report on the error $\|\vec{X} - \vec{x}\|_{L^\infty}$ in Table 3. Here we always compute the error $\|\vec{X} - \vec{x}\|_{L^\infty} := \max_{m=1 \to M} \|\vec{X}(t_m) - \vec{x}(\cdot, t_m)\|_{L^\infty}$, where $\|\vec{X}(t_m) - \vec{x}(\cdot, t_m)\|_{L^\infty} := \max_{k=1 \to K_1} \{\min_{\vec{y} \in \Omega} |\vec{X}_1^m(\vec{q}_k^1) - \vec{x}_1(\vec{y}, t_m)|\}$ between $\vec{X}$ and the true solution on the interval $[0, T]$ by employing a Newton method. We used $\tau = 0.125 h_{\vec{X}^0}^2$ and either $T = \frac{1}{2}\overline{T}$ or $T = \overline{T} - \tau$, where $h_{\vec{X}^0} := \max_{i=1 \to I_S} \max_{j=1 \to J_i} \text{diam}(\vec{X}_i^0(\sigma_j^i))$. We note that the experiments indicate that the convergence rate for the error away from the singularity is $O(h^2)$, and up to the singularity at time $\overline{T}$ is of order less than $O(h)$, which corresponds to the results obtained for the closed hypersurface case in [12]. In Figure 26, we present the evolution for the case $K = 4225$ and $\varepsilon_1 = 0.5$. We note that for the convergence experiments in Table 3 the condition (4.14) was satisfied exactly throughout. As noted earlier, in this case this is to be expected since $\partial\mathcal{D}$ is flat.
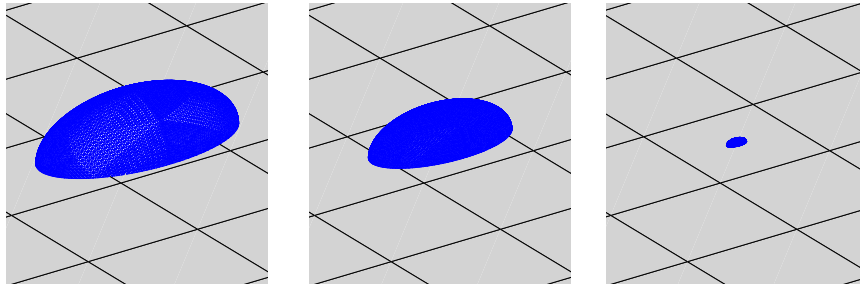

FIG. 26. Plots of $\vec{X}(t)$ at times $t = 0, \frac{1}{2}\bar{T}, \bar{T} - \tau$.

6.2.2 *Anisotropic surface diffusion.* For the anisotropy as displayed on the left of Figure 2, i.e. for the regularized l^1-norm

$$\gamma_1(\vec{p}) = \sum_{j=1}^{3} [\varepsilon_1^2 |\vec{p}|^2 + p_j^2 (1 - \varepsilon_1^2)]^{1/2}, \tag{6.5}$$

we repeat the experiment in Figure 5, now for the anisotropic flow. Here we choose $\varepsilon_1 = 10^{-1}$ and $\varepsilon_1 = 10^{-2}$ in (6.5). The discretization parameters for the two experiments are $K = 3267$, $J = 6240$ and $\tau = 10^{-3}$, $T = 1$. See Figure 27 for the results, where we note once again that our
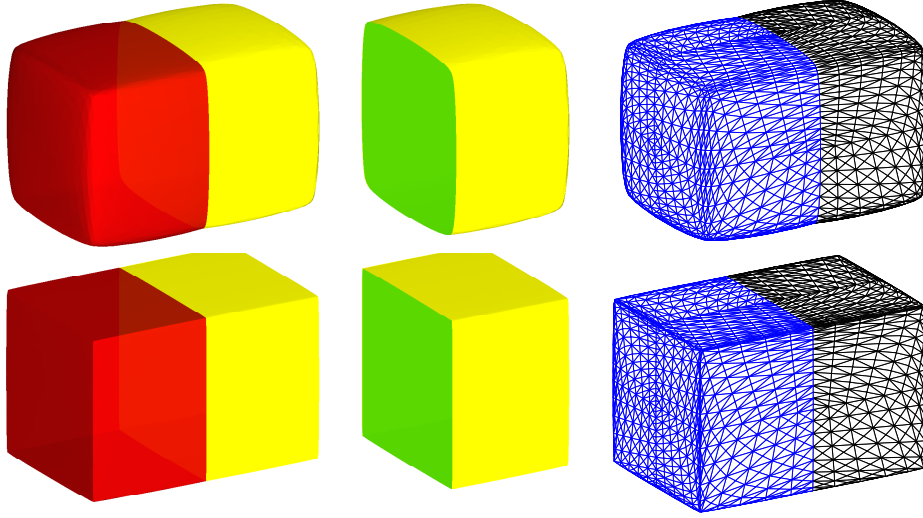
FIG. 27. Plots of Γ^M, (Γ_2^M, Γ_3^M) and the triangulations of Γ^M for $\varepsilon_1 = 10^{-1}$ (top) and $\varepsilon_1 = 10^{-2}$ (bottom).
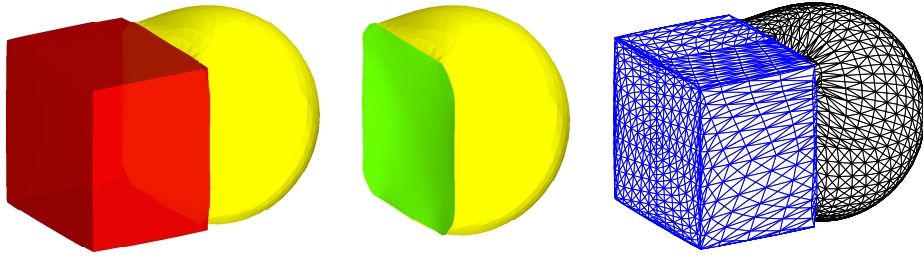

FIG. 28. Plots of Γ^M, (Γ_2^M, Γ_3^M) and the triangulations of Γ^M.

scheme produces good quality meshes throughout. In addition, we observe that our finite element approximation can easily handle these almost crystalline surface energies, which suggests that it can be used to numerically study possible energy minimizing configurations of e.g. salt crystals, as discussed in e.g. [55, 74].

Moreover, we repeated the experiment in Figure 27 but used an isotropic surface energy density $\gamma_2 = \gamma_3 = |\cdot|$ for the surfaces Γ_2 and Γ_3, while γ_1 is given by (6.5) with $\varepsilon_1 = 10^{-2}$. The numerical results for this simulation are shown in Figure 28.

The next experiment is for the setup as in Figure 14, but now for the anisotropic surface energy densities γ_i all chosen as on the right of Figure 2. With the same discretization parameters as in Figure 14, we obtained the results as displayed in Figure 29.

In the remainder, we present some computations for the anisotropic surface diffusion flow of a single surface attached to the boundary of $\mathcal{D} := \{\vec{q} \in \mathbb{R}^3 : q_3 > 0\}$. As initial surface we choose a unit half sphere attached to $\partial\mathcal{D}$. The discretization parameters are $K = 4225$, $J = 8256$, $\tau = 10^{-3}$ and $T = 1$. The results for the choices $\gamma_1(\vec{p}) = |\vec{p}|$, as well as the two anisotropies displayed in Figure 3 are shown in Figure 30. As expected, the initial surfaces evolve to upper halves of Wulff
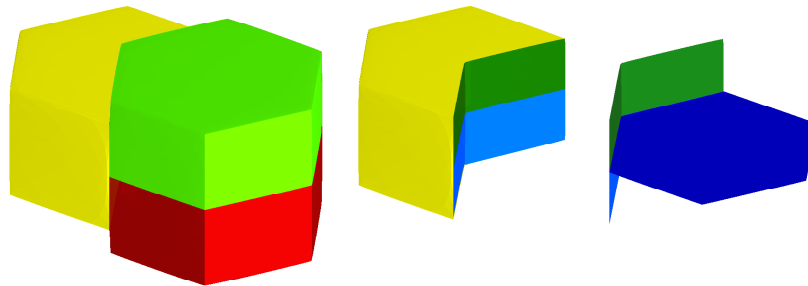
FIG. 29. Plots of Γ^M, $(\Gamma_1^M, \Gamma_4^M, \Gamma_5^M)$ and $(\Gamma_4^M, \Gamma_5^M, \Gamma_6^M)$.
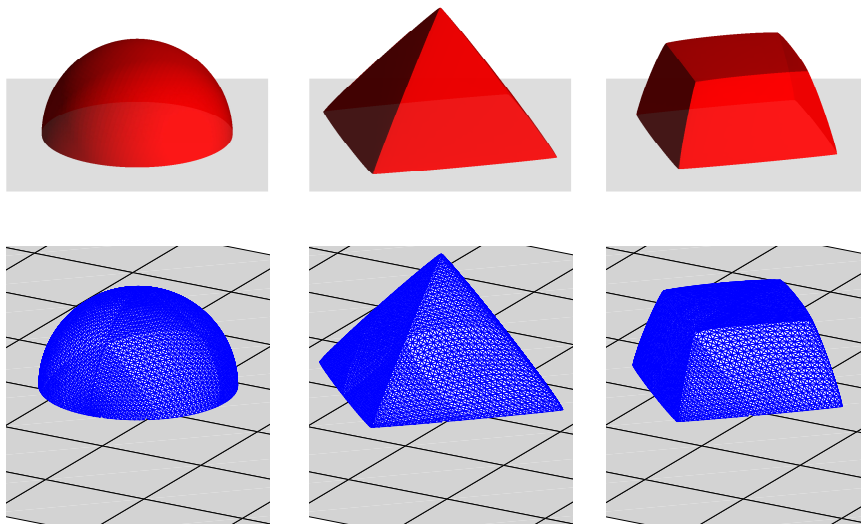
FIG. 30. Plots of Γ^M for different anisotropies, with the triangulations given below.

shapes. We note that the last example has clear resemblances with shapes observed in the laboratory for epitaxial thin film growth; see e.g. [73, Fig. 5.12]. We also remark that in epitaxial thin film growth the equilibrium state is given as a stationary solution of an anisotropic surface energy and that surface diffusion is the main transport mechanism in this context. Hence the flow (2.20) is a relevant equation for surface evolution in thin film growth, although more general models take elastic effects into account, see e.g. [40].

REFERENCES

1. ALMGREN, F., & TAYLOR, J. E. Soap bubble clusters. *Forma* **11** (1996), 199–207.   Zbl 1017.49502   MR 1487207
2. ALMGREN, F. J., Jr. Existence and regularity almost everywhere of solutions to elliptic variational problems with constraints. *Mem. Amer. Math. Soc.* **4** (1976).   Zbl 0327.49043 MR 0420406

3. AMILIBIA, A. M. Existence and uniqueness of standard bubble clusters of given volumes in $\mathbb{R}^N$. *Asian J. Math.* **5** (2001), 25–31. Zbl 1018.53005 MR 1868162

4. ANGENENT, S., & GURTIN, M. E. Multiphase thermomechanics with interfacial structure. 2. Evolution of an isothermal interface. *Arch. Ration. Mech. Anal.* **108** (1989), 323–391. Zbl 0723.73017 MR 1013461

5. ATHANASSENAS, M. A variational problem for constant mean curvature surfaces with free boundary. *J. Reine Angew. Math.* **377** (1987), 97–107. Zbl 0604.53003 MR 0887402

6. BARRETT, J. W., GARCKE, H., & NÜRNBERG, R. On the variational approximation of combined second and fourth order geometric evolution equations. *SIAM J. Sci. Comput.* **29** (2007), 1006–1041. Zbl 1148.65074 MR 2318696

7. BARRETT, J. W., GARCKE, H., & NÜRNBERG, R. A parametric finite element method for fourth order geometric evolution equations. *J. Comput. Phys.* **222** (2007), 441–462. Zbl 1112.65093 MR 2298053

8. BARRETT, J. W., GARCKE, H., & NÜRNBERG, R. A phase field model for the electromigration of intergranular voids. *Interfaces Free Bound.* **9** (2007), 171–210. Zbl 1132.35082 MR 2314058

9. BARRETT, J. W., GARCKE, H., & NÜRNBERG, R. Numerical approximation of anisotropic geometric evolution equations in the plane. *IMA J. Numer. Anal.* **28** (2008), 292–330. Zbl 1145.65069 MR 2401200

10. BARRETT, J. W., GARCKE, H., & NÜRNBERG, R. On the parametric finite element approximation of evolving hypersurfaces in $\mathbb{R}^3$. *J. Comput. Phys.* **227** (2008), 4281–4307. Zbl 1145.65068 MR 2406538

11. BARRETT, J. W., GARCKE, H., & NÜRNBERG, R. Parametric approximation of Willmore flow and related geometric evolution equations. *SIAM J. Sci. Comput.* **31** (2008), 225–253. Zbl pre05680058 MR 2460777

12. BARRETT, J. W., GARCKE, H., & NÜRNBERG, R. A variational formulation of anisotropic geometric evolution equations in higher dimensions. *Numer. Math.* **109** (2008), 1–44. Zbl 1149.65082 MR 2377611

13. BARRETT, J. W., GARCKE, H., & NÜRNBERG, R. Finite element approximation of coupled surface and grain boundary motion with applications to thermal grooving and sintering. Preprint No. 11/2009, Univ. Regensburg.

14. BARRETT, J. W., GARCKE, H., & NÜRNBERG, R. Finite element approximation of a phase field model for multicomponent surface diffusion. In preparation.

15. BELLETTINI, G., CHERMISI, M., & NOVAGA, M. Crystalline curvature flow of planar networks. *Interfaces Free Bound.* **8** (2006), 481–521. Zbl 1103.74017 MR 2283923

16. BETOUNES, D. E. Kinematics of submanifolds and the mean curvature normal. *Arch. Ration. Mech. Anal.* **96** (1986), 1–27. Zbl 0615.53011 MR 0853973

17. BRAKKE, K. A. *The Motion of a Surface by its Mean Curvature*. Math. Notes 20, Princeton Univ. Press, Princeton, NJ (1978). Zbl 0386.53047 MR 0485012

18. BRAKKE, K. A. The surface evolver. *Experiment. Math.* **1** (1992), 141–165. Zbl 0769.49033 MR 1203871

19. BRONSARD, L., GARCKE, H., & STOTH, B. A multi-phase Mullins–Sekerka system: matched asymptotic expansions and an implicit time discretisation for the geometric evolution problem. *Proc. Roy. Soc. Edinburgh Sect. A* **128** (1998), 481–506. Zbl 0924.35199 MR 1632810

20. BRONSARD, L., & REITICH, F. On three-phase boundary motion and the singular limit of a vector-valued Ginzburg–Landau equation. *Arch. Ration. Mech. Anal.* **124** (1993), 355–379. Zbl 0785.76085 MR 1240580

21. CAHN, J. W. Stability, microstructural evolution, grain growth, and coarsening in a two-dimensional two-phase microstructure. *Acta Metall.* **39** (1991), 2189–2199.

22. CAHN, J. W., HOLM, E. A., & SROLOVITZ, D. J. Modeling microstructural evolution in two-dimensional two-phase microstructures. *Mater. Sci. Forum* **94–96** (1992), 141–158.

23. COX, S. J., & GRANER, F. Three-dimensional bubble clusters: Shape, packing, and growth rate. *Phys. Rev. E* **69** (2004), 031409.

24. DECKELNICK, K., DZIUK, G., & ELLIOTT, C. M. Error analysis of a semidiscrete numerical scheme for diffusion in axially symmetric surfaces. *SIAM J. Numer. Anal.* **41** (2003), 2161–2179. Zbl 1058.65097 MR 2034610

25. DEPNER, D., GARCKE, H., & KOHSAKA, Y. Mean curvature flow of surface clusters. In preparation.

26. DZIUK, G., An algorithm for evolutionary surfaces. *Numer. Math.* **58** (1991), 603–611. Zbl 0714.65092 MR 1083523

27. DZIUK, G. Convergence of a semi-discrete scheme for the curve shortening flow. *Math. Models Methods Appl. Sci.* **4** (1994), 589–606. Zbl 0811.65112 MR 1291140

28. FISCHER, F. Four-bubble clusters and Menelaus' theorem. *Amer. J. Phys.* **70** (2002), 986–991. MR 1933590

29. FOISY, J., ALFARO, M., BROCK, J., HODGES, N., & ZIMBA, J. The standard double soap bubble in $\mathbb{R}^2$ uniquely minimizes perimeter. *Pacific J. Math.* **159** (1993), 47–59. Zbl 0738.49023 MR 1211384

30. FONSECA, I., & MÜLLER, S. A uniqueness proof for the Wulff theorem. *Proc. Roy. Soc. Edinburgh Sect. A* **119** (1991), 125–136. Zbl 0752.49019 MR 1130601

31. GARCKE, H., & NESTLER, B. A mathematical model for grain growth in thin metallic films. *Math. Models Methods Appl. Sci.* **10** (2000), 895–921. Zbl pre01882736 MR 1771511

32. GARCKE, H., NESTLER, B., & STINNER, B. A diffuse interface model for alloys with multiple components and phases. *SIAM J. Appl. Math.* **64** (2004), 775–799. Zbl 1126.82025 MR 2068122

33. GARCKE, H., NESTLER, B., STINNER, B., & WENDLER, F. Allen–Cahn systems with volume constraints. *Math. Models Methods Appl. Sci.* **18** (2008), 1347–1381. Zbl 1147.49036 MR 2439843

34. GARCKE, H., NESTLER, B., & STOTH, B. On anisotropic order parameter models for multi-phase systems and their sharp interface limits. *Phys. D* **115** (1998), 87–108. Zbl 0936.82010 MR 1616772

35. GARCKE, H., NESTLER, B., & STOTH, B. A multiphase field concept: numerical simulations of moving phase boundaries and multiple junctions. *SIAM J. Appl. Math.* **60** (1999), 295–315. Zbl 0942.35095 MR 1740846

36. GARCKE, H., & NOVICK-COHEN, A. A singular limit for a system of degenerate Cahn–Hilliard equations. *Adv. Differential Equations* **5** (2000), 401–434. Zbl 0988.35019 MR 1750107

37. GARCKE, H., & WIELAND, S. Surfactant spreading on thin viscous films: nonnegative solutions of a coupled degenerate system. *SIAM J. Math. Anal.* **37** (2006), 2025–2048. Zbl 1102.35056 MR 2213404

38. GURTIN, M. E. *Thermomechanics of Evolving Phase Boundaries in the Plane*. Oxford Math. Monogr., Oxford Univ. Press, New York (1993). Zbl 0787.73004 MR 1735282

39. GURTIN, M. E. *Configurational Forces as Basic Concepts of Continuum Physics*. Appl. Math. Sci. 137, Springer, New York (2000). Zbl 0951.74003 MR 1735282

40. GURTIN, M. E., & JABBOUR, M. E. Interface evolution in three dimensions with curvature-dependent energy and surface diffusion: interface-controlled evolution, phase transitions, epitaxial growth of elastic films. *Arch. Ration. Mech. Anal.* **163** (2002), 171–208. Zbl 1053.74005 MR 1912105

41. HASS, J., HUTCHINGS, M., & SCHLAFLY, R. The double bubble conjecture. *Electron. Res. Announc. Amer. Math. Soc.* **1** (1995), 98–102. Zbl 0864.53007 MR 1369639

42. HASS, J., & SCHLAFLY, R. Double bubbles minimize. *Ann. of Math. (2)* **151** (2000), 459–515. Zbl 0970.53008 MR 1765704

43. HAYASHI, T., & CARTHEW, R. W. Surface mechanics mediate pattern formation in the developing retina. *Nature* **431** (2004), 647–652.

44. HERRING, C., Surface tension as a motivation for sintering. In: *The Physics of Powder Metallurgy*, W. E. Kingston (ed.), McGraw-Hill, New York (1951), 143–179.

45. HESTENES, M. R., Pseudoinverses and conjugate gradients. *Comm. ACM* **18** (1975), 40–43. MR 0366018

46. HILDEBRANDT, S., & TROMBA, A. *Mathematics and Optimal Form*. Scientific American Library, New York (1985). MR 0854269

47. HOFFMAN, D. W., & CAHN, J. W. A vector thermodynamics for anisotropic surfaces: I. Fundamentals and application to plane surface junctions. *Surface Sci.* **31** (1972), 368–388.

48. HUTCHINGS, M., MORGAN, F., RITORÉ, M., & ROS, A. Proof of the double bubble conjecture. *Ann. of Math. (2)* **155** (2002), 459–489. Zbl 1009.53007 MR 1906593

49. KÖSTER, D., KRIESSL, O., & G. SIEBERT, K. Design of finite element tools for coupled surface and volume meshes. *Numer. Math. Theory Methods Appl.* **1** (2008), 245–274. Zbl 1174.65539 MR 2460010

50. KRAYNIK, A. M., REINELT, D. A., & VAN SWOL, F. Structure of random foam. *Phys. Rev. Lett.* **93** (2004), 208301.

51. LAWLOR, G., & MORGAN, F. Paired calibrations applied to soap films, immiscible fluids, and surfaces or networks minimizing other norms. *Pacific J. Math.* **166** (1994), 55–83. Zbl 0830.49028 MR 1306034

52. MORGAN, F. Soap bubbles in $\mathbb{R}^2$ and in surfaces. *Pacific J. Math.* **165** (1994), 347–361. Zbl 0820.53002 MR 1300837

53. MORGAN, F. Colloquium: Soap bubble clusters. *Rev. Modern Phys.* **79** (2007), 821–827. MR 2346329

54. MORGAN, F. *Geometric Measure Theory: a Beginner's Guide*. 4th ed., Elsevier/Academic Press, Amsterdam (2009). Zbl 1179.49050 MR 2455580

55. MORGAN, F., FRENCH, C., & GREENLEAF, S. Wulff clusters in $\mathbb{R}^2$. *J. Geom. Anal.* **8** (1998), 97–115. Zbl 0934.49024 MR 1704570

56. MULLINS, W. W. Theory of thermal grooving. *J. Appl. Phys.* **28** (1957), 333–339.

57. MULLINS, W. W. The effect of thermal grooving on grain boundary motion. *Acta Metall.* **6** (1958), 414–427.

58. NESTLER, B., WENDLER, F., SELZER, M., STINNER, B., & GARCKE, H. Phase-field model for multiphase systems with preserved volume fractions. *Phys. Rev. E* **78** (2008), 011604.

59. NÜRNBERG, R. Numerical simulations of immiscible fluid clusters. *Appl. Numer. Math.* **59** (2009), 1612–1628. Zbl 1162.76030 MR 2512281

60. PAN, J. Modelling sintering at different length scales. *Int. Mater. Rev.* **48** (2003), 69–85.

61. POZZI, P. Anisotropic mean curvature flow for two dimensional surfaces in higher codimension: a numerical scheme. *Interfaces Free Bound.* **10** (2008), 539–576. Zbl 1158.65076 MR 2465273

62. RUUTH, S. J. Efficient algorithms for diffusion-generated motion by mean curvature. *J. Comput. Phys.* **144** (1998), 603–625. Zbl 0946.65093 MR 1638032

63. SCHMIDT, A., & SIEBERT, K. G. *Design of Adaptive Finite Element Software: The Finite Element Toolbox ALBERTA*. Lecture Notes in Comput. Sci. Engrg. 42, Springer, Berlin (2005). Zbl 1068.65138 MR 2127659

64. SMITH, C. S. Grains, phases, and interfaces: an interpretation of microstructure. *Trans. Amer. Inst. Mining Met. Engrg.* **175** (1948), 15–51.

65. SONER, H. M. Motion of a set by the curvature of its boundary. *J. Differential Equations* **101** (1993), 313–372. Zbl 0769.35070 MR 1204331

66. SULLIVAN, J. M., & MORGAN, F. Open problems in soap bubble geometry. *Int. J. Math.* **7** (1996), 833–842. Zbl 0867.53009 MR 1417788

67. SUTTON, A. P., & W. BALLUFFI, R. *Interfaces in Crystalline Materials*. Clarendon Press, Oxford (1995).

68. TAYLOR, J. E. The structure of singularities in soap-bubble-like and soap-film-like minimal surfaces. *Ann. of Math. (2)* **103** (1976), 489–539. Zbl 0335.49032 MR 0428181

69. TAYLOR, J. E. Mathematical models of triple junctions. *Interface Sci.* **7** (1999), 243–249.

70. TAYLOR, J. E. A variational approach to crystalline triple-junction motion. *J. Statist. Phys.* **95** (1999), 1221–1244. Zbl 0952.74015 MR 1712448

71. TAYLOR, J. E., & CAHN, J. W. Linking anisotropic sharp and diffuse surface motion laws via gradient flows. *J. Statist. Phys.* **77** (1994), 183–197. Zbl 0844.35044

72. TAYLOR, J. E., CAHN, J. W., & HANDWERKER, C. A. Geometric models of crystal growth. *Acta Metall. Mater* **40** (1992), 1443–1474.

73. VENABLES, J. A. *Introduction to Surface and Thin Film Processes*. Cambridge Univ. Press, Cambridge (2000).

74. WECHT, B., BARBER, M., & TICE, J. Double crystals. *Acta Cryst. Sect. A* **56** (2000), 92–95. MR 1743539

75. WICHIRAMALA, W. Proof of the planar triple bubble conjecture. *J. Reine Angew. Math.* **567** (2004), 1–49. Zbl 1078.53010 MR 2038304

76. WULFF, G. Zur Frage der Geschwindigkeit des Wachstums und der Auflösung der Kristallflächen. *Z. Krist.* **34** (1901), 449–530.

77. ZHAO, H.-K., MERRIMAN, B., OSHER, S., & WANG, L. Capturing the behavior of bubbles and drops using the variational level set approach. *J. Comput. Phys.* **143** (1998), 495–518. Zbl 0936.76065 MR 1631196